ABSTRACT

Title of dissertation: QUANTUM OPTICS WITH OPTOMECHANICAL SYSTEMS IN THE LINEAR AND NONLINEAR REGIME: WITH APPLICATIONS IN FORCE SENSING AND ENVIRONMENTAL ENGINEERING

XUNNONG XU, Doctor of Philosophy, 2016

Dissertation directed by: Prof. Jacob M. Taylor
Joint Quantum Institute, University of Maryland

Optomechanical system, a hybrid system where mechanical and optical degrees of freedom are mutually coupled, is a new platform for studying quantum optics. In a typical optomechanical setup, the cavity is driven by a large amplitude coherent sate of light to enhance the effective optomechanical coupling. This system can be linearized around its classical steady state, and many interesting effects arise from the linearized optomechanical interaction, such as the dynamical modification of the properties of the mechanical resonator and the modulation of the amplitude and phase of the light coming out the of cavity. When the single-photon optomechanical coupling is comparable to the optical and mechanical loss, we must also keep the nonlinear interactions in the hamiltonian, which make it possible to study optomechanically induced nonlinear phenomena such as photon-blockade, Kerr nonlinearity, etc.

In this thesis, we study quantum optics with optomechanical systems both in the linear and nonlinear regime, with emphasis on its applications in force sensing and environmental engineering. We first propose a mirror-in-the-middle system and show that when driving near optomechanical instability, the optomechanical interaction will generate squeezed states of the output light. This system can be used to detect weak forces far below the standard quantum limit. Subsequently, we find that this particular driving scheme can also lead to enhanced optomechanical nonlinearity in a certain regime and by measuring the output field appropriately. We study the photon-blockade effect and discuss the conditions for maximum photon antibunching. We then focus on thermal noise reduction for mechanical resonators, by designing a system of two coupled resonators whose damping is primarily clamping loss. We show that optomechanical coupling to the clamping region enables dynamical control over the coupled mechanical resonator. This leads to the counterintuitive outcome: increasing optical power simultaneously reduces the temperature and linewidth of the mechanical mode, in contrast to direct optomechanical cooling. We also consider the Brillouin scattering induced optomechanical interaction in ring wave-guide resonators where phonon scattering via impurities is present. We find that it is possible to realize chiral transport behavior of phonons by modifying the phonon environment with optomechanics. We study a simple few-mode theory and it can explain experimental data well. Finally, we study a continuum multi-mode theory and calculate the phonon Green's function using a diagrammatic perturbative expansion, showing that a decrease in the phonon diffusion constant is possible with increasing optical pump power.

QUANTUM OPTICS WITH OPTOMECHANICAL SYSTEMS IN THE LINEAR AND NONLINEAR REGIME: WITH APPLICATIONS IN FORCE SENSING AND ENVIRONMENTAL ENGINEERING

by

Xunnong Xu

Dissertation submitted to the Faculty of the Graduate School of the
University of Maryland, College Park in partial fulfillment
of the requirements for the degree of
Doctor of Philosophy
2016

Advisory Committee:
Prof. Jay D. Sau, Chair
Prof. Jacob M. Taylor, Co-Chair/Advisor
Prof. Mohammad Hafezi
Prof. Edo Waks
Prof. Victor Yokovenko

Dedication

Dedicated to my parents

for their endless love and encouragement.

Acknowledgments

First of all, I would like to thank my advisor, Prof. Jacob Taylor, for the continuous support of my Ph.D study. His immense knowledge in physics, his creativity in coming up with new ideas and his energy in deriving equations and coding have always impressed me. I always consider him as a model when doing my research. His curiosity teaches me how to expand my knowledge and his sense of humor makes me feel that science could also be a lot of fun. His guidance helped me in all the time of research and writing of this thesis. Jake has also been very patient and considerate, in terms of both scientific research and personal life. I could not have imagined having a better advisor and mentor for my Ph.D study at Maryland.

Besides my advisor, I would like to thank Prof. Jay Sau for coming to my candidacy talk two years ago and for the challenging questions and helpful comments, and now for chairing my committee. I would like to thank Prof. Mohammad Hafezi for providing guidance in my research and for the insightful discussions about my projects in our previous group meetings. Mohammad has always been a funny and nice person, and I enjoyed playing ping pong with him. I would also like to thank Prof. Edo Waks and Prof. Victor Yokovenko for being on my committee and for providing feedback for my thesis.

My thanks also go to Michael Gullans, who helped me a lot in the last three years. I spend a lot of time discussing research with him, and his knowledge in quantum optics is extremely helpful for me. Michael is also a very good friend and elder brother to me. I enjoyed talking with him about personal life and also

thank him for inviting me to his house party. I want to thank Thomas Purdy, whose expertise in optomechanics experiment shows me how a real device works differently from a theoretical model. I also want to thank my collaborators at Illinois for introducing me the measurement and data analysis of our experiment.

I would like to thank my fellow group members and friends Prabin Adhikari, Haitan Xu, Dvir Kafri, Vanita Srinivasa, Chiao-Hsuan Wang, Stephen Ragole, Andrew Glaudell and Jianxin Chen for the stimulating discussions of physics and for the exchange of ideas of scientific career, and for all the fun we have had in the last few years. I also want to thank many other JQI friends, Yi-Hsieh Wang, Mathew Ranchu, Yidan Wang, Xiao Li, Zhexuan Gong, Mohammad Maghrebi, Bin Cao, Alireza Seif Tabrizi, Guanyu Zhu, Fangli Liu, Jiehang Zhang for talking about science and life, playing ping pong, and having so much fun together. My thanks also go to other friends I made in Maryland, including my former roommates Ruiliang Bai, Yuwei Cui, Haiqing Zhao, and my classmates Xu Jiang and Yong Zhao. Without these friends, I can not imagine how boring my PhD life would be.

Last but not the least, I would like to thank my family in China: my parents for their endless love even though I am far away from home for many years, my sister for supporting me spiritually, and my uncle for advices and encouragement.

Table of Contents

List of Figures

Chapter 1: Introduction

Light, in the language of modern quantum physics, has a particle-wave duality. In both the particle theory and the wave theory, it is possible to show that there is a pressure exerted on a surface that is exposed to light. Back in 1619, Johannes Kepler put forward the concept of radiation pressure to explain why the tail of a comet always points away from the Sun [1]. In the work of James Clark Maxwell on electromagnetism [2], he shows the property of momentum of light and thus that light can also exert pressure on a surface. The first measurement of the pressure of light on a solid body was made by Pyotr Lebedev in 1901 [3], which also became the first quantitative confirmation of Maxwell's theory. In the 21st century, the study of radiation pressure induced effects [4–7], especially in the context of quantum physics, is still very important for many purposes, such as ultra-sensitive measurement, as in Laser Interferometer Gravitational-Wave Observatory (LIGO) [8], and exploring the modification and control of mechanical motion with light field, for instance, optomechanical cooling [9–11], the generation of optomechanical entanglement [12] and quantum coherent state transfer [13, 14].

On the other hand, we have also seen dramatic progress in atomic, molecular and optical (AMO) physics in the past two decades, such as the optical cooling and

trapping of neutral atoms [15] to nano-Kelvins to form Bose-Einstein condensates (BEC) [16,17], the trapping of charged ions for quantum information processing [18], and the study of cavity quantum electrodynamics (cavity QED) [19] and circuit quantum electrodynamics (circuit QED) [20]. The quest for achieving quantum control has now been extended to macroscopic objects and their "classical" degrees of freedom, namely mechanical motion. This is useful for controlling thermal noise for mechanics-based devices and thus improving ultimate sensitivity limits, as in the case of LIGO, where even thermal motion of the end mirrors can cover the signal from gravitational waves. Another important application is in quantum information storage and processing, as mechanical resonators are relatively easy to fabricate and to scale up.

The pressure of light when acting on a mechanical object can lead to the so-called "optomechanical coupling" between optical degrees of freedom and mechanical degrees of freedom. In a typical optomechanical setup, such as a Fabry-Perot cavity with one freely vibrating end mirror, the motion of the end mirror is modified due to the presence of the radiation pressure, and the amplitude and phase of light coming out the of cavity is also modulated at the same time because of the change in cavity length due to mirror motion. Understanding and using this type of mutual coupling, especially in the quantum regime where the coupling is stronger than optical/mechanical damping and thermal dephasing is negligible, in the hybrid optical-mechanical system, are the main goals of the field of quantum optomechanics. In recent years, quantum optomechanics has received substantial theoretical and experimental interest [21–24], as evidenced by advances such as ground state cooling

of mechanical resonator [25–27], the generation of squeezed states of light [28–30] and the study of single-photon nonlinear optics in various optomechanical platforms [31–36].

1.1 Optomechanical coupling

Before the formal description of a typical optomechanical system and the introduction of the concept of optomechanical coupling, let us look at some real optomechanical devices built in labs, as shown in Fig. 1.1 below. Optical cavities and

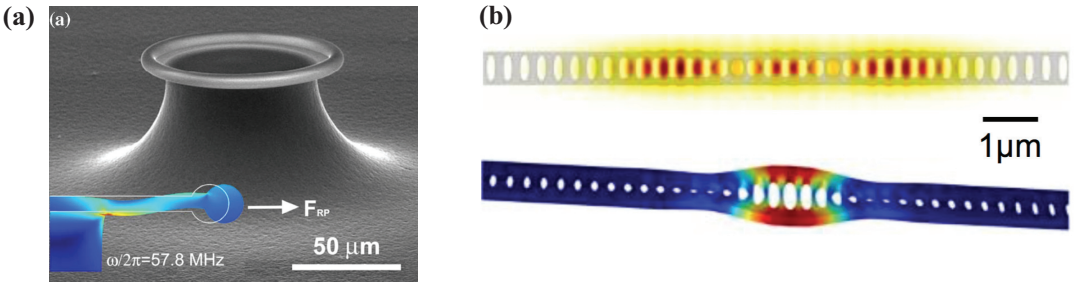

Figure 1.1: (a) Optomechanical microdisk cavity [37] and (b) Optomechanical photonic/phononic crystal [38].

mechanical resonators are the two basic ingredients for a typical optomechanical system. In Fig. 1.1(b), the waveguide is modified to provide both an optical cavity and also a mechanical resonator, where optical fields and mechanical motion, in the form of breathing modes or other deformations, interact with the optical boundary conditions.

The optical fields are usually electromagnetic fields (ranging from microwave to telecom to infrared to visible light) confined in cavities. Because of the boundary

condition set by the cavity, there are many resonant modes that are separated in frequency and also have different mode profiles. In the language of quantum optics, the electric field in a cavity (as a particle in a box) can be written in the following second-quantized form [39–41]:

$$\mathbf{E}(\mathbf{r},t) = \sum_{\mathbf{k}} \hat{e}_{\mathbf{k}} \epsilon_{\mathbf{k}} a_{\mathbf{k}} e^{-i\omega_{\mathbf{k}} t + i\mathbf{k}r} + \text{h.c.}, \tag{1.1}$$

where $\mathbf{k}$ is the wavevector, $\hat{e}_{\mathbf{k}}$ is the polarization, V is the volume of the cavity, $\epsilon_{\mathbf{k}} = \sqrt{\frac{\hbar\omega_{\mathbf{k}}}{\epsilon_0 V}}$ is the quantum strength of the electric field, and $a_{\mathbf{k}}$ is the annihilation operator. For a specific cavity mode with frequency ω_c, there is also a corresponding loss rate κ, because EM fields may leak out of the cavity or be absorbed by the cavity medium. The quality factor of this mode is thus defined as $Q_c = \omega_c/\kappa$.

The other part of the story is the mechanical resonator. In the simplest scenario, it is just a cavity mirror that is attached to a spring such that it is free to oscillate. The motion of the cavity mirror is characterized its displacement x from equilibrium position x_0 and its corresponding conjugate momentum p, which can be further described by a single quantum harmonic oscillator using annihilation operator a and creation operator $a^\dagger$. More generally, however, the dynamics of a mechanical resonator is described by a space- and time- dependent displacement field $\mathbf{u}(\mathbf{r},\mathbf{t})$ in the framework of continuum mechanics. If one is interested in the equation of motion for the global amplitude $x(t)$ of the motion, one can utilize a suitably normalized dimensionless mode function $\mathbf{u}(\mathbf{r},\mathbf{t})$, such that the displacement field would be $x(t) = \mathbf{u}(\mathbf{r},\mathbf{t})$. Then the temporal evolution of $u(r,t)$ can be described by the canonical simple equation of motion of a harmonic oscillator of effective mass

m:

$$m\frac{d^2x(t)}{dt^2} + m\gamma\frac{dx(t)}{dt} + m\omega_m^2 x(t) = F_{\text{ext}}(t) \tag{1.2}$$

where ω_m is the mechanical resonant frequency, γ is the mechanical damping rate, and $F_{\text{ext}}(t)$ is the total external force acting on the mechanical resonator. The mechanical quality factor $Q_m = \omega_m/\gamma$.

A generic optomechanical system consists of an optical cavity where light bunches back and forth between the end mirrors, while one end mirror is attached to a spring and is free to oscillate, as shown in the Fig. 1.2 below:

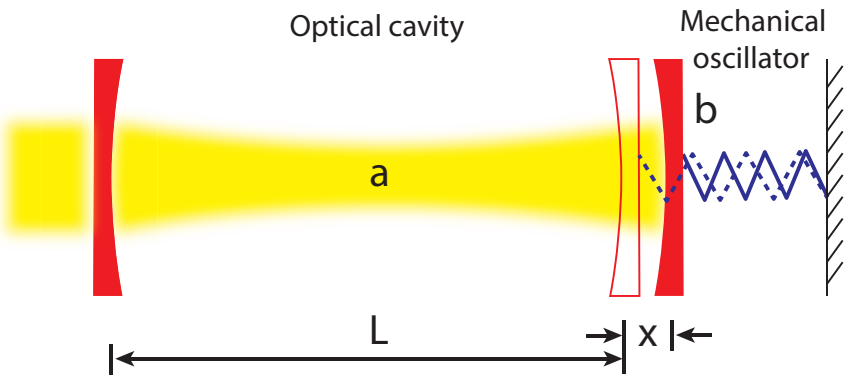

Figure 1.2: A typical optomechanical system where one end mirror of an optical cavity is attached to a spring and thus can oscillate as a harmonic oscillator. The displacement of the mechanical oscillator changes the total length of optical cavity, which further leads to a shift in the resonant frequency of the optical mode.

We can now calculate the radiation pressure exerted on the right end mirror by the light fields, or photons inside the cavity. The photons get reflected by the moving end mirror and transfer twice of its momentum $\hbar k$ to the mirror per round

trip time τ_c, so the total radiation pressure is given by:

$$F_{\rm rad} = 2\hbar k \frac{a^\dagger a}{\tau_c} = 2\hbar \frac{\omega_c}{c} \frac{a^\dagger a}{2L/c} = \hbar \frac{\omega_c}{L} a^\dagger a. \tag{1.3}$$

The work done by the photons is $W = F_{\rm rad} x$, and the change in the total photon energy is thus $dE = -W$, which translates into the interaction energy

$$H_{\rm int} = -\hbar\omega_c \frac{x}{L} a^\dagger a. \tag{1.4}$$

Alternatively, we can also find that the energy of the photons as

$$H = \hbar\omega_c(x) a^\dagger a = \hbar \frac{\omega_c}{1 + x/L} a^\dagger a \approx \hbar\omega_c (1 - x/L) a^\dagger a, \tag{1.5}$$

so the interaction energy

$$H_{\rm int} = -\hbar\omega_c \frac{x}{L} a^\dagger a = -\hbar\omega_c \frac{x_{\rm zpf}}{L} a^\dagger a (b + b^\dagger) = -\hbar g_0 a^\dagger a (b + b^\dagger). \tag{1.6}$$

which is the same as the previous expression. The single-photon optomechanical coupling rate is $g_0 = \omega_c x_{\rm zpf}/L$, which quantifies the interaction strength between a single photon and a single phonon. A full quantum mechanical description of the quantum dynamics of the vacuum field coupled with an oscillating boundary (mirror) in a one-dimensional cavity is presented in [42].

1.2 Brownian motion and input-output formalism

Mechanical resonators and optical fields are open systems that subject to noise, which is fluctuation and dissipation introduced by the environment due to exchange of energy and momentum through friction or cavity loss. This can be described by the interaction between the mode of interest and an continuum of environmental

degrees of freedom, as in the Caldeira-Leggett model [43], which eventually leads to damping and dephasing of the mode of interest. These dissipative phenomena are also related to the concept of Brownian motion, which was studied by Einstein in one of his 1905 papers [44]. A Brownian particle of mass m experiences random kicks from surrounding particles, which leads to friction, with coefficient γ, as shown in Fig. 1.3.

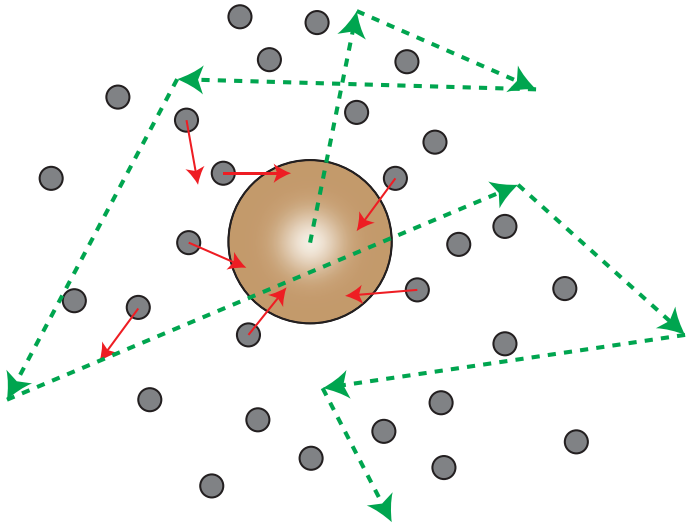

Figure 1.3: Brownian motion of a particle (large circle) as a result of random scattering with surrounding small particles (small circle).

The equations of motion of the Brownian particle are:

$$\dot{x} = p/m, \tag{1.7a}$$

$$\dot{p} = -\gamma p + \xi(t), \tag{1.7b}$$

where $\xi(t)$ is a random force because of the random kicks. This is the Langevin equations for Brownian motion. The effects of the fluctuating force can be summarized by giving its first and second moments, as time averages over an infinitesimal

time interval:

$$\langle \xi(t) \rangle = 0, \qquad \langle \xi(t)\xi(t') \rangle = 2B\delta(t - t'). \tag{1.8}$$

We can integrate the p equation and get

$$p(t) = e^{-\gamma t}p(0) + \int_0^t \mathrm{d}t' e^{-\gamma(t-t')}\xi(t') \tag{1.9}$$

The first term gives the exponential decay of the initial momentum, and the second term gives the extra momentum produced by the random noise. Assuming that the random force $\xi(t)$ is not correlated with the initial momentum of the Brownian particle, and using the correlation function in the equation above, we can calculate the mean squared momentum over this classical noise as

$$\left\langle p^2(t) \right\rangle = e^{-2\gamma t}p^2(0) + \frac{B}{\gamma}(1 - e^{-2\gamma t}) \tag{1.10}$$

In the long time limit ($t \to \infty$), the exponentials drop out, and this quantity approaches B/γ. Alternatively, we can find mean squared momentum using the equal partition theorem $p^2/2m = k_B T/2$, since the Brownian particle must be in a thermal equilibrium state at long times. This leads to the relation

$$B = m\gamma k_B T. \tag{1.11}$$

This result is known as the fluctuation-dissipation theorem [45]. It relates the strength of the random noise or fluctuating force to the magnitude of the friction or dissipation. It expresses the balance between friction, which tends to drive any system to a completely "dead" state, and noise, which tends to keep the system "alive." This balance is required to have a thermal equilibrium state at long times.

We now consider a system of a single-mode field with frequency ν and annihilation operator a interacting with a reservoir of a large number of degrees of freedom with closely spaced frequency ν_k and annihilation operator b_k, which is quite similar to Brownian motion. The system-reservoir hamiltonian, under the rotating-wave approximation (RWA) is [39]:

$$H = \hbar\nu a^\dagger a + \sum_k \hbar\nu_k b_k^\dagger b_k + \hbar\sum_k g_k(b_k^\dagger a + a^\dagger b_k) \tag{1.12}$$

The Heisenberg equations of motion are

$$\dot{a} = -i\nu a - i\sum_k g_k b_k, \tag{1.13a}$$

$$\dot{b}_k = -i\nu_k b_k - ig_k a, \tag{1.13b}$$

We first integrate the reservoir equation

$$b_k(t) = e^{-i\nu_k t}b_k(0) - ig_k\int_0^t \mathrm{d}t' e^{-i\nu_k(t-t')}a(t') \tag{1.14}$$

and then substitute this solution into the field equation

$$a = -i\nu a - \sum_k g_k^2\int_0^t \mathrm{d}t' e^{-i\nu_k(t-t')}a(t') - i\sum_k g_k e^{-i\nu_k t}b_k(0) \tag{1.15}$$

As in the Wigner-Weisskopf theory of spontaneous emission [46], the summation over k yields a δ function and thus

$$\sum_k g_k^2\int_0^t \mathrm{d}t' e^{-i\nu_k(t-t')}a(t') \approx \frac{\kappa}{2}a(t) \tag{1.16}$$

with $\kappa = 2\pi g^2(\nu)D(\nu)$. We can further define

$$a_{\mathrm{in}}(t) = -\frac{1}{2\pi}\sum_k g_k e^{-i\nu_k t}b_k(0) \tag{1.17}$$

This input field may be shown to satisfy the commutation relations $\left[a_{\text{in}}(t), a_{\text{in}}^{\dagger}(t')\right] = \delta(t-t')$. Then the equation for a becomes:

$$\dot{a} = -i\nu a - \frac{\kappa}{2}a + \sqrt{\kappa}a_{\text{in}}. \tag{1.18}$$

Similarly, we can also find a solution by specifying a final condition rather than an initial condition for the b_k fields [41]. This is related to the reservoir fields leaving the cavity instead of coming inside the cavity. The cavity output field a_{out} is related to the input field and fields inside the cavity by

$$a_{\text{in}} + a_{\text{out}} = \sqrt{\kappa}a, \tag{1.19}$$

which is essentially the boundary condition for optical fields, as shown in figure below.

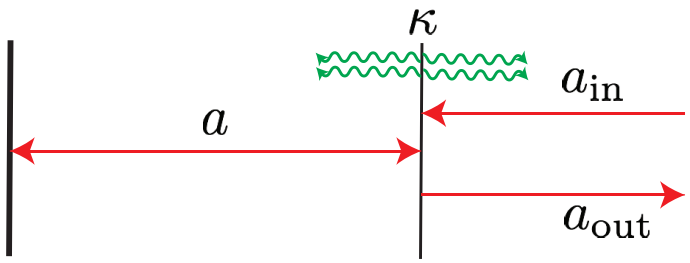

Figure 1.4: Input-output representation of a single-sided cavity.

1.3 Optomechanical cooling and heating

The hamiltonian for an optomechanical system is given by

$$H = \hbar\omega_c a^{\dagger}a + \hbar\omega_m b^{\dagger}b - \hbar g_0 a^{\dagger}a(b + b^{\dagger}) \tag{1.20}$$

The optical cavity is usually driven at certain laser frequency ω_L that is near the cavity resonance, with detuning $\Delta = \omega_L - \omega_c$. Because of the interaction, the cavity field a can be split into a "classical" coherent state with amplitude $\alpha = \langle a \rangle$ and quantum fluctuations:

$$a = \alpha + \delta a \tag{1.21}$$

We can move to the frame rotating with the driving frequency by applying a unitary transformation $U = \exp(-i\omega_L a^\dagger a t)$ to the hamiltonian and replace the cavity field with the above expression $a^\dagger a \rightarrow (\alpha^* + \delta a^\dagger)(\alpha + \delta a)$. In the first term of the hamiltonian, the $|\alpha|^2$ term is a constant and can be neglected immediately, while the term proportional to α cancels a term in the driving hamiltonian. In the last term of the hamiltonian, the $|\alpha|^2$ term can be removed by shifting the position of the mechanical oscillator, and the $\delta a^\dagger \delta a$ term is neglected because it is of second order in the quantum fluctuations. The hamiltonian thus becomes

$$\tilde{H} = -\hbar\Delta\delta a^\dagger \delta a + \hbar\omega_m b^\dagger b - \hbar g_0(\alpha^*\delta a + \alpha\delta a^\dagger)(b + b^\dagger). \tag{1.22}$$

Without loss of generality, we can assume α to be real, which can be done by choosing an appropriate phase of the driving laser. So we get a linearized interaction hamiltonian of the form:

$$H_{\text{int}} = -\hbar g_0 \alpha(\delta a + \delta a^\dagger)(b + b^\dagger) = -\hbar g(\delta a + \delta a^\dagger)(b + b^\dagger) \tag{1.23}$$

where we defined the pump enhanced optomechanical coupling strength $g = g_0\alpha$. The diagram for this interacting system is shown below.

The linearized hamiltonian gives us a simple way to understand the dynamics of the coupled optomechanical system, since it is always possible to exactly solve

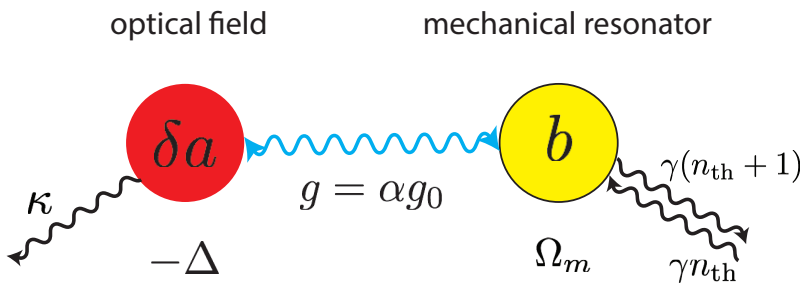

Figure 1.5: Linearized interaction between optical field and mechanical motion.

the linear dynamics, in principle. However, it is also very helpful to look at certain special cases of the hamiltonian, e.g. $\Delta = \pm\omega_m$, where we can make the rotating wave approximation to simplify the interaction hamiltonian. When $\Delta = -\omega_m$ (red-detuned laser), the beam splitter term $-\hbar g(\delta a b^\dagger + \delta a^\dagger b)$ becomes resonant while the two-mode squeezing term $-\hbar g(\delta a^\dagger b^\dagger + \delta a b)$ is rotating at frequency $2\omega_m$ so can be neglected in the sideband resolved regime when $\omega_m \gg \kappa$ and in longer time scales. The physical meaning of the beam splitter interaction is that a cavity photon is created from the driving photon by absorbing a phonon, and vice versa. Similarly, when $\Delta = \omega_m$ (blue-detuned laser), the two-mode squeezing term $-\hbar g(\delta a^\dagger b^\dagger + \delta a b)$ becomes resonant, which means a cavity photon a is created and a phonon are created from the driving photon at the same time, and vice versa. This parmetric/squeezing process is illustrated in the Fig. 1.6.

The analysis is very similar to the laser cooling (heating) of trapped ions. Actually, we can easily solve the dynamics by writing down the Heisenberg-Langevin equations of the optical and mechanical degrees of freedom. Instead of using operator b, we now use the x and p, since it is more appropriate describe the "classical"

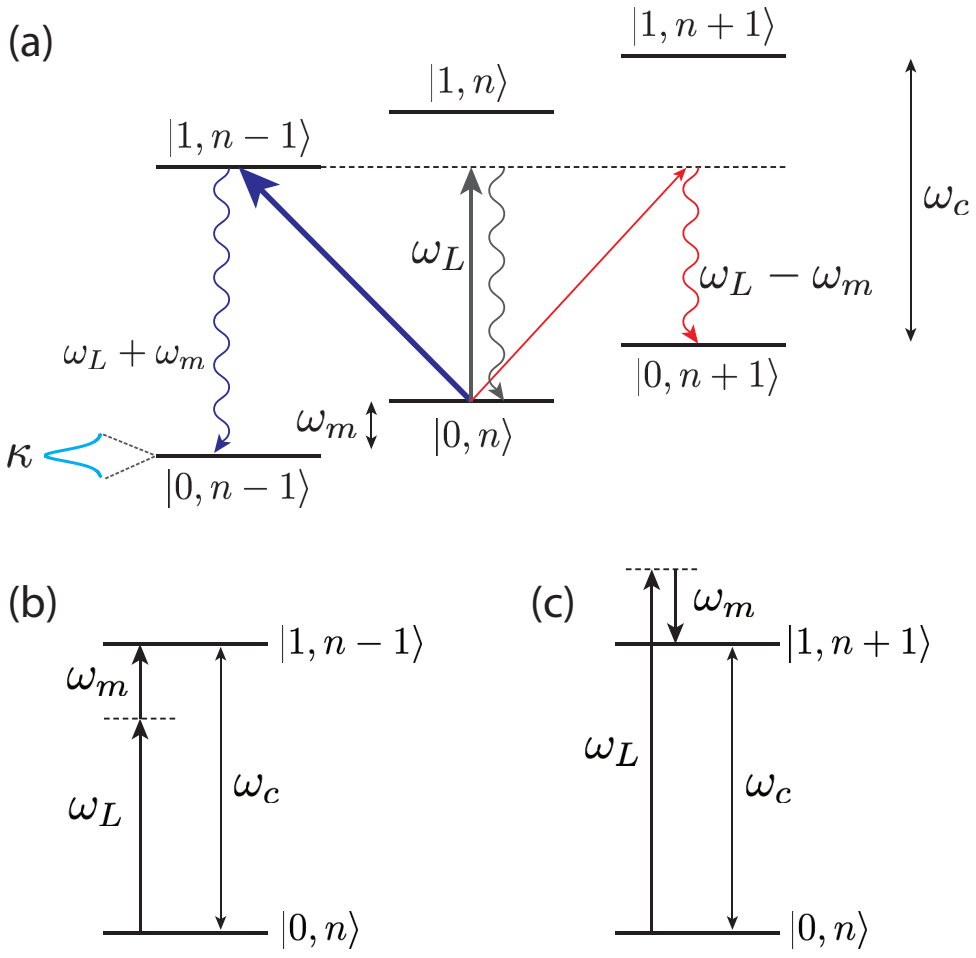

Figure 1.6: (a) Energy levels of optomechanical system and transitions when the driving laser frequency is red-detuned $\Delta = -\omega_m$ from the cavity resonance. The blue transition is from the beam-splitter interaction and is resonant, while the red-transition is from the two-mode squeezing interaction and is off resonance. (b) Phonon absorption process from beam-splitter interaction when $\Delta = -\omega_m$, and (c) Phonon creation process from two-mode squeezing interaction when $\Delta = \omega_m$.

dynamics of the mechanical motion. The equations of motion follows:

$$\dot{a} = i\Delta a - \frac{\kappa}{2}a + iGx + \sqrt{\kappa}a_{\rm in}, \tag{1.24a}$$

$$\dot{x} = p/m \tag{1.24b}$$

$$\dot{p} = -m\omega_m^2 x - \gamma p + G(a + a^\dagger) + F_{\rm in}. \tag{1.24c}$$

The p equations is simply the Brownian motion with an additional optical bath without the rotating wave approximation. Moving to frequency domain, we can find the modified susceptibility of the mechanical oscillator:

$$\chi^{-1}(\omega) = m\left\{\omega_m^2 - \omega^2 - i\gamma\omega + 2g^2\omega_m\left[\frac{1}{(\Delta+\omega) + i\kappa/2} + \frac{1}{(\Delta-\omega) - i\kappa/2}\right]\right\} \tag{1.25}$$

where ω is the Fourier frequency.

The g^2 term shows the modifications to the resonance frequency and damping rate of the mechanical oscillator because of the linearized coupling to optical fields, with

$$\omega_m^{\rm eff}(\omega) = \omega_m + \frac{g^2\omega_m}{\omega}\left[\frac{\Delta+\omega}{(\Delta+\omega)^2 + \kappa^2/4} + \frac{\Delta-\omega}{(\Delta-\omega)^2 + \kappa^2/4}\right] \tag{1.26a}$$

$$\gamma^{\rm eff}(\omega) = \gamma + \frac{g^2\omega_m}{\omega}\left[\frac{\kappa}{(\Delta+\omega)^2 + \kappa^2/4} - \frac{\kappa}{(\Delta-\omega)^2 + \kappa^2/4}\right] \tag{1.26b}$$

For example, when near the original resonance frequency $\omega = \omega_m$ and $\Delta = -\omega_m$, we get $\omega_m^{\rm eff} = \omega_m - g^2/2\omega_m$ and $\gamma^{\rm eff} = \gamma + 4g^2/\kappa$, which is the optical spring effect [47, 48] and the broadening of the mechanical linewidth, which eventually leads to the cooling of the mechanical oscillator [25–27].

1.4 Quantum measurements and force sensing

In classical physics, the dynamics of an object is deterministic, which can be described by Hamilton's equations of motion, and thus there is a definite trajectory in phase space given the initial condition. The continuous measurement of the position and momentum is possible, in principle. A fundamental difference between quantum physics and classical physics is the Heisenberg uncertainty relation: there is no definite trajectory for the motion of an object. This means that the uncertainties of a pair of conjugate variables, such as position and momentum, are bounded by the Planck's constant:

$$\Delta x \cdot \Delta p \geq \hbar/2 \tag{1.27}$$

We now consider the following scenario [49]: we want to continuously monitor the position of particle. We first make a position measurement of the particle by shining a photon onto it with frequency ν, wavelength $\lambda = c/\nu$ and a corresponding momentum $p = \hbar\nu/c$. Suppose at time t_1, we measure the particle's position with an error $\Delta x^1_{\text{measure}}$, then the corresponding perturbation of its motion is given by $\Delta P_{\text{perturb}} = \hbar/2\Delta x^1_{\text{measure}}$. After a time $\tau = t_2 - t_1$, the perturbation in momentum will lead to an extra uncertainty in the position $\Delta x_{\text{add}} = \Delta P_{\text{perturb}}\tau/m$. The momentum of the particle is inferred from these two position measurements at different times: $P = m\frac{x_2 - x_1}{\tau}$. The total error is thus given by

$$\Delta P = \frac{m}{\tau}\left[(\Delta x^1_{\text{measure}})^2 + (\Delta x^2_{\text{measure}})^2 + (\Delta x_{\text{add}})^2\right]^{1/2} \tag{1.28}$$

This leads to

$$\Delta P \geq \Delta P_{\mathrm{SQL}} = \sqrt{\hbar m/2\tau} \tag{1.29}$$

Similarly, the standard quantum limit for position is

$$\Delta x \geq \Delta x_{\mathrm{SQL}} = \sqrt{\hbar \tau/2m} \tag{1.30}$$

For force measurement, if the force lasts for a time τ_F, then

$$F \geq \frac{\Delta P_{\mathrm{SQL}}}{\tau_F} = \frac{1}{\tau_F}\sqrt{\hbar m/2\tau} \tag{1.31}$$

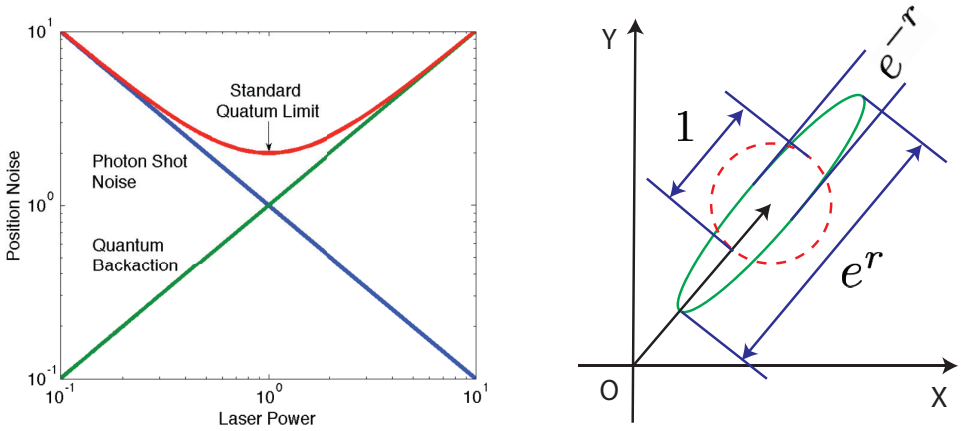

Figure 1.7: Uncertainty introduced by a quantum measurement sets a fundamental limit on the precision of a measurement process. (a) The standard quantum limit for force sensing using optical cavity. (b) A squeezed state (green ellipse) has less uncertainty in one quadrature than a coherent state (red circle).

If we are going to measure the position of a mechanical oscillator using an optomechanical system by analyzing the amplitude and phase of the optical fields coming out of the cavity, then there are two limits on the measurement precision: photon shot noise and quantum backaction. The photon shot noise could be reduced

by increasing optical pumping power, since it is related to the phase measurement precision, and is thus inversely proportional to the average photon number in the cavity: $\Delta\theta \propto 1/\sqrt{n}$. But at the same time, this introduces additional quantum fluctuations to the position of the mechanical oscillator, since the radiation pressure is increasing as the photon number fluctuation increases: $\Delta n \propto \sqrt{n}$. A compromise of these two noise leads to the corresponding standard quantum limit for position measurement precision [21], and it is reached when these two noise are equal. As shown in Fig. 1.7.

To achieve measurement sensitivity below the standard quantum limit, we may use non-classical states of light to perform the measurement, for example, squeezed states. With squeezing light, the variance (uncertainty) in one quadrature can be made smaller than that of a classical coherent state by a factor of e^{-r}, while the variance in the other quadrature is larger by at least a factor of e^{r}, where is the squeezing parameter, such that the Heisenberg uncertainty relation holds. If the information we want to measure is encoded in this particular quadrature, then it is possible to beat the sensitivity set by the standard quantum limit.

1.5 Optomechanical nonlinearities

There are some important concepts in classical nonlinear optics [50], such as sum frequency generation, four-wave mixing, Kerr effect (intensity-dependent refractive index), etc. In general, the optical response of these effects can be described by their corresponding nonlinear material polarization, in addition to the usual linear

term:

$$\tilde{P}(t) = \epsilon_0 \left[\chi^{(1)} \tilde{E}(t) + \chi^{(2)} \tilde{E}^2(t) + \chi^{(3)} \tilde{E}^3(t) + \cdots \right] \tag{1.32}$$

The different types of nonlinearity are summarized in the following equations:

$$\text{sum frequency generation:} \quad P(\omega_1 + \omega_2) = 2\epsilon_0 \chi^{(2)} E_1 E_2 \tag{1.33a}$$

$$\text{four-wave mixing:} \quad P(\omega_1 + \omega_2 - \omega_3) = 6\epsilon_0 \chi^{(3)} E_1 E_2 E_3^* \tag{1.33b}$$

$$\text{Kerr effect:} \quad P^{\mathrm{NL}}(\omega) = 3\epsilon_0 \chi^{(3)}(\omega + \omega - \omega) \left| E(\omega) \right|^2 E(\omega) \tag{1.33c}$$

These can also be written in the language of quantum physics, using some effective interaction hamiltonian

$$H = \hbar g (a_3 a_1^\dagger a_2^\dagger + \text{h.c.}) \tag{1.34a}$$

$$H = \hbar g (a_3 a_4 a_1^\dagger a_2^\dagger + \text{h.c.}) \tag{1.34b}$$

$$H = \hbar \chi^{(3)} (a^\dagger a)^2 \tag{1.34c}$$

In optomechanics, quantum nonlinearity at the single quanta level is only important when the singe-photon optomechanical coupling rate g_0 is comparable to the mechanical damping rate γ and the optical loss rate κ. We identify two regimes:

- Strong coupling regime: $g = \alpha g_0 > \gamma, \kappa$. In this regime, we will be able to see interesting quantum dynamics above classical dynamics. Another important parameter is the "$Q \cdot f$" product, which is a direct measure for the degree of decoupling from the thermal environment. Specifically, $Q_m \cdot f = Q_m \cdot \omega_m / 2\pi > k_B T/\hbar$ is the condition for neglecting thermal decoherence (dephasing) over one mechanical period, since we have $\omega_m > \bar{n}\gamma$ in this case.

- Single-photon strong coupling regime: $g_0 > \gamma, \kappa$. In this regime, higher order nonlinear interactions between mechanical and optical degrees of freedom are not negligible. Again, the "$Q \cdot f$" product is crucial in order to neglect thermal decoherence.

One major implication of strong single-photon nonlinearity is the nonlinear energy shift of photon energies, because of an effective photon-photon interaction. This eventually leads to the photon-blockade effect [32], which is of great importance in making single-photon source for quantum computation and also in quantum nonlinear optics. Suppose there is an effective third-order nonlinearity $H = \omega_0 a^\dagger a - g_{\rm nl}(a^\dagger a)^2$ in the system, the energy levels become $E_n = H\,|n\rangle = n\omega_0 - n^2 g_{\rm nl}$, as shown below: When driving the system with a laser with frequency $\omega_L = \omega_0 - g_{\rm nl}$, it will excites the ground state $|0\rangle$ to the first excited state $|1\rangle$, but the subsequent excitation from the first excited state $|1\rangle$ to the second excited state $|2\rangle$ will be off-resonant by an amount $2g_{\rm nl}$ because of the nonlinear frequency shift $-n^2 g_{\rm nl}$ for different levels. If the nonlinearity is strong enough compared to the optical linewidth, $g_{\rm nl} \geq \kappa$, then it will make the $|2\rangle$ state less populated, and the system is mostly in the one photon state $|1\rangle$, as shown in Fig. 1.8. This effective "two-level" system can be used as a qubit or single photon transistor for quantum information processing purposes.

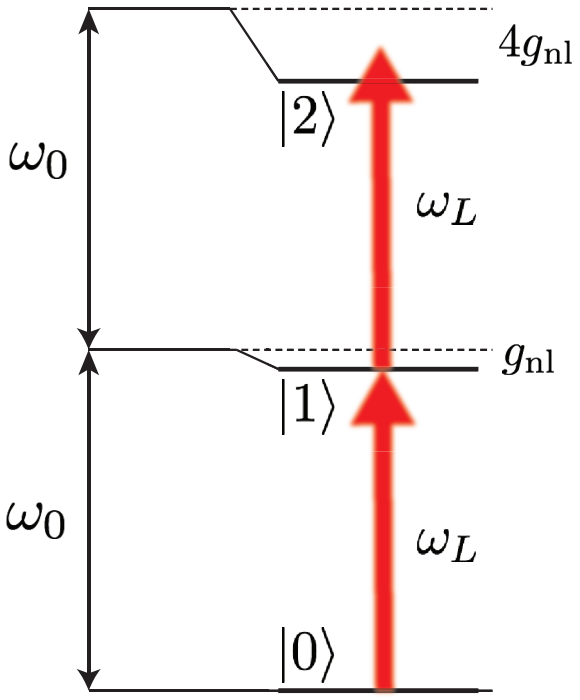

Figure 1.8: Energy level for a system with Kerr nonlinearity. The non-equal-distance energy shift makes the second photon excitation off resonance when the first photon excitation is on resonance.

1.6 Outline of the thesis

The outline of this thesis is as follows. In Chapter 2, we propose a coupled two-mode mirror-in-the-middle optomechanical system and show that when driving the cavity near optomechanical instability, the optomechanical interaction will generate squeezed states of the output light, by an amount determined by the strength of the driving field. Taking into other type of noise and the quantum efficiency of detectors into account, we estimate the maximum amount of squeezing to be 23 dB. This system could be used to detect weak forces far below the standard quantum limit. Subsequently, in Chapter 3, we find that this particular driving scheme can also lead to enhanced optomechanical nonlinearity in certain regime by measuring the output field appropriately. We discuss the photon-blockade mechanism and present numerical simulations for the two-photon correlation functions. We also discuss the feasibilities of our scheme and do a case study in optomechanical crystals. In Chapter 4, we focus on thermal noise reduction for mechanical resonators, by designing a system of two coupled resonators whose damping is primarily clamping loss limited. We show that optomechanical coupling to the clamping region enables dynamical control over the coupled mechanical resonator. This leads to the counter-intuitive outcome: increasing optical power simultaneously reduces the temperature and linewidth of the mechanical mode, in contrast to direct optomechanical cooling. In Chapter 5, we consider the Brillouin scattering induced optomechanical interaction in microsphere wave-guide resonators where phonon scattering via impurities is also present. We find that it is possible to realize chiral transport behavior of

phonons by modifying the phonon environment with optomechanics, recovering the result of Chapter 4 in a chiral system. Inspired by our theoretical work, our collaborators did an experiment and observed signatures of phonon chiral transport, the details of which is given in Appendix D. We also come up with a simple few-mode theory and it can explain experimental data well. Finally, in Chapter 6, we study a continuum multi-mode theory and calculate the phonon Green's function using a diagrammatic perturbation expansion, showing that chiral transport of phonons is possible in a large bandwidth, and the numerical result also suggests a decrease in the phonon diffusion constant with increasing optical pump power.

Chapter 2: Squeezing in a coupled two-mode optomechanical system for force sensing below the standard quantum limit

2.1 Introduction

Dramatic progress in coupling mechanics to light [21–23, 51] suggests that such devices may be used in a wide variety of settings to explore quantum effects in macroscopic systems. Furthermore, such systems can be exquisitely sensitive to small perturbations, such as forces induced either by acceleration as in accelerometer [52] or by, e.g., coupling to surfaces or fields as in atomic force microscopy [53]. For such force measurements, a high quality factor (Q_m) mechanical oscillator acts as a test mass, transducing a force into a time-dependent displacement of the oscillator [4, 49]. By using interferometric techniques to monitor the position of the oscillator, one can infer the force via optical signals. However, the radiation pressure coupling between the mechanical mode and optical mode has three consequences: photon shot noise, quantum backaction and dynamical backaction [21, 54]. The dynamical backaction modifies the oscillator dynamics [47] and makes laser cooling [10, 55] or amplification of phonons [56] in the mechanical system possible. Photon shot noise and quantum backaction, the former decreases with increasing input laser

power while the latter increases with increasing input laser power, introduce two sources of noise on the displacement readout of the oscillator motion. An optimal compromise between these two noise sources leads to the standard quantum limit (SQL) in force sensing [49].

The SQL, however, is itself not a fundamental limit. By using squeezed states of light [57], employing quantum nondemolition (QND) measurement [58, 59], or by cavity detuning [60], the SQL can be surpassed. In this work, we show that in a coupled two-mode optomechanical system, if we drive it appropriately, the interaction between cavity photons and the mechanical oscillator will generate squeezed states of the output light. Measuring an appropriate quadrature of the output light field, we would get fewer fluctuations than that of the vacuum state, which makes it possible to detect weak forces far below the SQL. Therefore, no squeezed state of light input is needed, which makes it easier to realize in experiment. Furthermore, compared with [59], we do not have to modulate the optomechanical coupling strength to realize single quadrature QND measurement. Finally, since we pump and probe different resonant optical modes, the effective optomechanical coupling is enhanced, and thus the pump power for achieving the best sensitivity is lowered substantially.

2.2 Model: coupled two-mode cavity optomechanics

We consider a high finesse Fabry-Pérot cavity with a dielectric mirror in the middle [61, 62] [Fig. 2.1(a)]. The end mirrors of the FP cavity are fixed, while

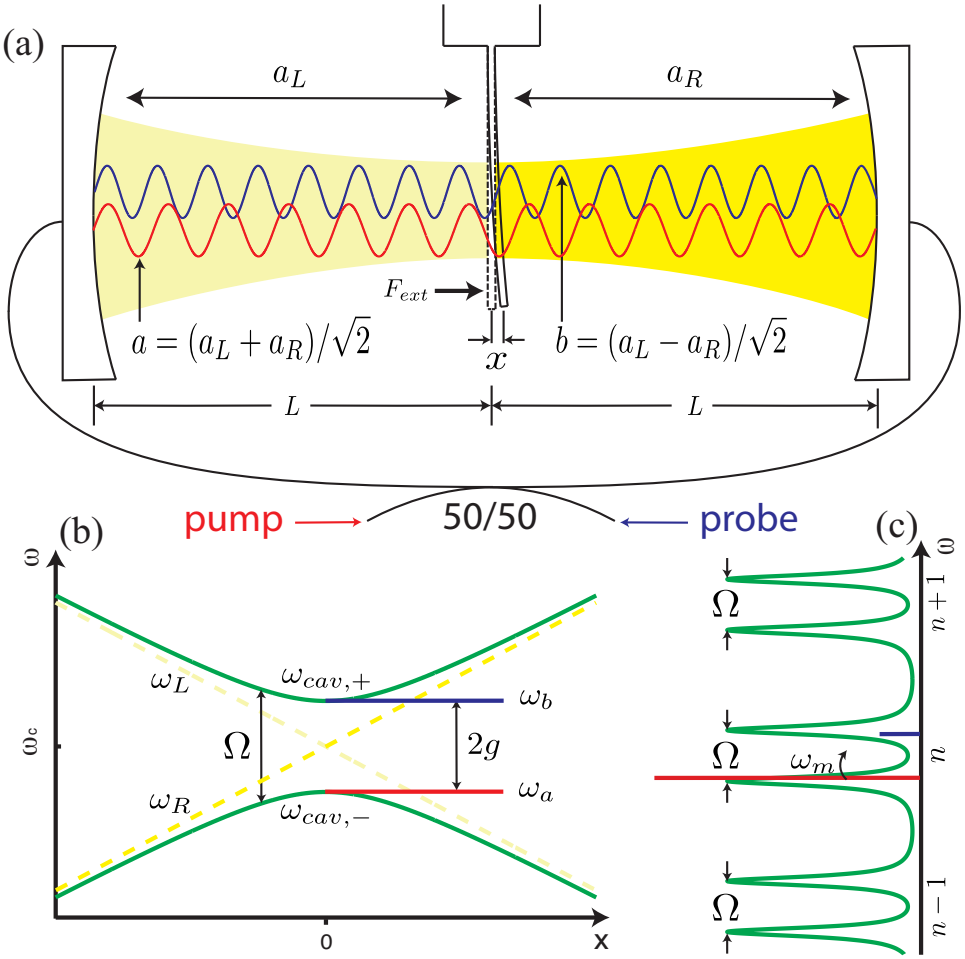

Figure 2.1: (a) A symmetric mirror-in-the-middle optomechanical system comprising a Fabry-Perot cavity of length $2L$ with a high reflectivity mirror mounted in the middle and coupled to a mechanical oscillator. Displacements of the middle mirror (via mechanical oscillations) couple the two normal modes a (red) and b (blue) as the left-right symmetry is broken. (b) Normal mode frequencies $\omega_{cav,\pm}$ (green) as a function of middle mirror displacement x. (c) Transmission spectrum of the three-mirror cavity, showing pairs of normal modes. We drive mode a strongly (long red line) and detect mode b (short blue line).

the middle mirror can vibrate along the optical axis of the cavity at a mechanical frequency ω_m with effective mass m. With the presence of the middle mirror, the FP cavity is divided into two sub-cavities, denoted by left (L) cavity and right (R) cavities. The middle mirror has a nonzero transmission, which allows the exchange of light between these two subcavities and thus leads to an effective coupling between the left and right cavity modes [63]. Further, the coupling will shift the resonant frequencies of two coupled cavity modes and leads to the so-called normal mode splitting effect [64, 65].

Following [62, 66], the normal mode splitting in the presence of the middle mirror can be calculated by assuming a transfer matrix with a high reflectivity r_d. For simplicity, we assuming the middle membrane to be exactly at the middle point of the FP cavity initially, dividing the cavity into two subcavities with the same length L, and the normal mode splitting when the middle mirror is at a new position x is given by $\Omega = \frac{c}{L}\arccos(|r_d|\cos(2kx))$ [Fig. 2.1(b)], where r_d is complex amplitude reflectivity of the middle mirror, k is the wave vector of the incoming field and x is the displacement from the middle point of the FP cavity.

The hamiltonian of the cavity fields in this three-mirror system is

$$H_{\text{opt}} = \hbar(\omega_c + fx)a_L^\dagger a_L + \hbar(\omega_c - fx)a_R^\dagger a_R - \hbar g(a_L^\dagger a_R + a_R^\dagger a_L), \qquad (2.1)$$

where ω_c is the resonance frequency of the subcavities with the middle mirror exactly in the middle ($x = 0$), $f = (\partial\omega_{cav}/\partial x)|_{x=0}$ is the shift of cavity resonant frequency per unit length evaluated at $x = 0$, and $a_L(a_R)$ is the left (right) cavity mode annihilation operator. Here only the linear order frequency shift is considered, since

the displacement x is much smaller than the cavity length L. The last term describes the coupling between left/right cavity modes with strength g. In the high reflectivity limit ($|r_d| \to 1$), $g = |t_d|c/2L$ and $f = -\omega_c/L$, where t_d is the amplitude transmission coefficient and c is the speed of light in vacuum.

2.3 Heisenberg-Langevin equations and system dynamics

We look only in a narrow spectral range around a nominal pair of normal modes $a = (a_L + a_R)/\sqrt{2}$ and $b = (a_L - a_R)/\sqrt{2}$. We also drive mode a strongly at frequency ω_L and move to the rotating frame with respect to the pump laser [39]. The cavity field is coupled to fields outside the cavity through the ends mirrors, while we assume the mechanical oscillator is coupled to a thermal bath through clamping losses. The classical and quantum fluctuations of the environmental degrees of freedom will introduce damping to the cavity field and mechanical oscillator [40, 41], as required by the fluctuation-dissipation theorem [45]. In the Markovian approximation, the Heisenberg-Langevin equations for mechanical and optical degrees of freedom are, in the high temperature limit, as follows:

$$\dot{x} = p/m, \tag{2.2a}$$

$$\dot{p} = -m\omega_m^2 x - \gamma p + \frac{\hbar\omega_c}{L}(a^\dagger b + b^\dagger a) + F_{in}, \tag{2.2b}$$

$$\dot{a} = -i(\Delta_c - g)a - \kappa a + i\frac{\omega_c}{L}bx + E + \sqrt{2\kappa}a_{in}, \tag{2.2c}$$

$$\dot{b} = -i(\Delta_c + g)b - \kappa b + i\frac{\omega_c}{L}ax + \sqrt{2\kappa}b_{in}. \tag{2.2d}$$

In the equations above, γ is the damping of the mechanical oscillator, κ is the damping of the cavity, and $\Delta_c = \omega_c - \omega_L$ is the cavity detuning. E is the pump

strength which is related to input laser power P_{in} and cavity damping κ by $|E| = \sqrt{P_{in}\kappa/\hbar\omega_L}$. a_{in}, b_{in} are the vacuum fluctuations of the two cavity modes. F_{in} is the force acting on the oscillator, and it has two parts: an external force F_{ext} acting on the oscillator, which is also the force to be detected [Fig. 2.1(a)]; the Brownian stochastic force, or thermal fluctuating force F_{th}, which leads to damping of the oscillator.

The steady state of the system is $\langle x\rangle = 0$, $\langle p\rangle = 0$, $\langle b\rangle = \beta = 0$, $\langle a\rangle = \alpha = E/[i(\Delta_c - g) + \kappa]$. Following [67,68], we linearize the equations of motion around the steady state and study the stability of this solution by applying the Routh-Hurwitz criterion [69], which at positive effective detuning $\Delta = \Delta_c + g > 0$ is simplified to a constraint on pump strength,

$$\alpha^2 < m\omega_m^2 L^2(\kappa^2 + \Delta^2)/2\hbar\Delta\omega_c^2 = \alpha_0^2. \tag{2.3}$$

This suggests that the steady state we found is the only stable solution at low power. Writing x, p, a, b in terms of steady state values ($\langle x\rangle$, etc.) and fluctuations ($\tilde{x}$, etc.), and neglecting terms of order $\frac{\omega_c}{L}\tilde{b}\tilde{x}$, $\frac{\omega_c}{L}\tilde{a}\tilde{x}$, $\frac{\hbar\omega_c}{L}\tilde{a}\tilde{b}$, then the fluctuation of mode a decouple, and the equations of motion become

$$\dot{x} = p/m, \tag{2.4a}$$

$$\dot{p} = -m\omega_m^2 x - \gamma p + \hbar G(b + b^\dagger) + F_{in}, \tag{2.4b}$$

$$\dot{b} = -i\Delta b - \kappa b + iGx + \sqrt{2\kappa}b_{in}, \tag{2.4c}$$

where we choose α to be real and define the effective optomechnical coupling $G = \omega_c\alpha/L$. For convenience, we have removed the tilde of the fluctuating variables. We

find that the pumped, coupled two-mode model is reduced to an effective single-mode model [70], where the cavity consist of a fixed partial transmitting mirror and movable perfect reflecting mirror and the optomechanical coupling strength is determined by α.

We then define the quadratures of mode b as $X = (b+b^\dagger)/\sqrt{2}$, $Y = (b-b^\dagger)/i\sqrt{2}$, move to frequency domain by Fourier transform, and solve a set of linear equations. We find

$$x(\omega) = \chi(\omega)F_{in}(\omega) + \chi(\omega)\frac{2\hbar G\sqrt{\kappa}}{(\kappa - i\omega)^2 + \Delta^2}\left[(\kappa - i\omega)X_{in}(\omega) + \Delta Y_{in}(\omega)\right], \tag{2.5}$$

where $\chi(\omega)$ is the susceptibility of the optomechanical system to force,

$$\chi(\omega) = \left\{ m\left[\omega_m^2 - \omega^2 - i\gamma\omega - \frac{2\hbar G^2\Delta/m}{(\kappa - i\omega)^2 + \Delta^2}\right]\right\}^{-1}. \tag{2.6}$$

From the expression above, we immediately identify an effective, frequency-dependent mechanical resonant frequency ω_m' and an effective damping γ' which are shifted from the original ones. The shift in resonant frequency is the "optical spring" effect [47], while the shift in damping leads to cooling or heating of the oscillator, depending on the sign of detuning [21, 22]. The cavity field fluctuations enter the equation of motion for oscillator Eq. (2.5) as an additional fluctuations force, which is identified as the shot noise fluctuations of radiation pressure force.

2.4 Force detection sensitivity

Within the input-output formalism [41], the output field quadratures we measure are related to the field quadratures inside the cavity by $X_{out}(\omega) = \sqrt{2\kappa}X(\omega) - X_{in}(\omega)$ and $Y_{out}(\omega) = \sqrt{2\kappa}Y(\omega) - Y_{in}(\omega)$. We consider a homodyne measurement of the signal [41, 71]

$$\begin{aligned} S(\omega) &= \sin\theta X_{out}(\omega) + \cos\theta Y_{out}(\omega) \\ &= \chi_F(\omega)F_{in}(\omega) + \chi_X(\omega)X_{in}(\omega) + \chi_Y(\omega)Y_{in}(\omega), \end{aligned} \tag{2.7}$$

where θ is an experimentally adjustable phase, which determines the measured quadrature. Here the signal is written in terms of three inputs (force input F_{in}, quadrature fluctuations X_{in} and Y_{in}) and corresponding susceptibilities. The force and field susceptibilities are:

$$\chi_F(\omega) = \frac{2\sqrt{\kappa}G[\Delta\sin\theta + (\kappa - i\omega)\cos\theta]}{(\kappa - i\omega)^2 + \Delta^2}\chi(\omega) \tag{2.8a}$$

$$\begin{aligned} \chi_X(\omega) &= \frac{4\hbar\kappa G^2[\Delta\sin\theta + (\kappa - i\omega)\cos\theta](\kappa - i\omega)}{[(\kappa - i\omega)^2 + \Delta^2]^2}\chi(\omega) \\ &\quad + \frac{(\kappa^2 + \omega^2 - \Delta^2)\sin\theta - 2\kappa\Delta\cos\theta}{(\kappa - i\omega)^2 + \Delta^2}, \end{aligned} \tag{2.8b}$$

$$\begin{aligned} \chi_Y(\omega) &= \frac{4\hbar\kappa G^2[\Delta\sin\theta + (\kappa - i\omega)\cos\theta]\Delta}{[(\kappa - i\omega)^2 + \Delta^2]^2}\chi(\omega) \\ &\quad + \frac{2\kappa\Delta\sin\theta + (\kappa^2 + \omega^2 - \Delta^2)\cos\theta}{(\kappa - i\omega)^2 + \Delta^2}. \end{aligned} \tag{2.8c}$$

To calculate the sensitivity to the external force F_{ext}, we define the effective force noise

$$F(\omega) = \left.\frac{S(\omega)}{\partial S(\omega)/\partial F_{ext}}\right|_{F_{ext}=0}, \tag{2.9}$$

and its quantum noise spectral density is $S_{FF}(\omega) = \int d\omega' \langle F(\omega)F(\omega')\rangle$. The vacuum radiation input noise b_{in} is delta correlated and the thermal fluctuating force is approximated as white noise thus is also delta correlated, so we have

$$S_{FF}(\omega) = 2m\gamma k_B T + \frac{1}{2}\left|\frac{\chi_X(\omega) - i\chi_Y(\omega)}{\chi_F(\omega)}\right|^2, \tag{2.10}$$

and the square of the corresponding force detection sensitivity $\eta(\omega)$ is given by its symmetric part [54]: $\eta(\omega) = \frac{1}{2}[S_{FF}(\omega) + S_{FF}(-\omega)]$.

2.5 DC force sensing optimization

We now focus on the DC ($\omega = 0$) force sensing regime. To get the best sensitivity, we first optimize the function $\eta(\omega = 0) = S_{FF}(\omega = 0)$ for α and then optimize for θ. We find that for the optimal pump strength α_*^2, the second term goes to zero as $\Delta \sin\theta + \kappa\cos\theta \to 0$, which corresponds to a backaction free point. At first sight, it seems that χ_F approaches zero as $\Delta \sin\theta + \kappa\cos\theta \to 0$, and the sensitivity diverges. However, if we choose the pump strength appropriately, then not only can the divergence at $\theta_0 = -\arctan(\kappa/\Delta)$ be avoided, but also the sensitivity can achieve its optimal value. The optimal pump strength is given by

$$\alpha_*^2 = \alpha_0^2\left(1 - \frac{2\kappa}{\Delta}\frac{\Delta\sin\theta + \kappa\cos\theta}{\sqrt{\kappa^2 + \Delta^2}}\right), \tag{2.11}$$

where α_0 is the threshold pump strength defined in Eq. (2.3). At this point, the effective mechanical frequency $\omega_m' \to 0$ as $\theta \to \theta_0$, so χ_F is still finite. We then try to find out the behavior of the sensitivity near the critical angle θ_0. To ensure that the pump strength does not exceed the threshold value and that the effective

mechanical frequency is positive, we let the angle θ approaches θ_0 from the positive side, that is $\theta = \theta_0 + \delta\theta$, with $0 < \delta\theta \ll 1$. We note that, if θ approaches θ_0 from the negative side, we can replace the minus sign in Eq. (2.11) with a plus sign, and the result will be similar. In the vicinity of θ_0, the pump is approximated as

$$\alpha_*^2 = \alpha_0^2(1 - \frac{2\kappa}{\Delta}\delta\theta). \tag{2.12}$$

At the optimal pump strength and optimal angle, the total sensitivity is found:

$$\eta(\omega = 0) \approx 2m\gamma k_B T + \hbar m\omega_m^2 \left(\frac{\Delta}{4\kappa} + \frac{\kappa}{\Delta}\right)\xi^2, \tag{2.13}$$

with the dimensionless parameter ξ defined by $\xi = \delta\theta \cdot 2\kappa/\Delta$. This result implies that thermal noise limited detection can be achieved by choosing the critical angle θ_0 appropriately. The expense for achieving the best sensitivity is that we have to pump the system at a power close to the threshold value, thus increasing the possibility of destabilizing the system. The ultimate sensitivity for force detection is limited by how strong the thermal noise is and how close we can pump the system near its instability point. The result also suggests that we could further improve the sensitivity by choosing $\Delta = 2\kappa$. Then we look at the input laser power, and find that if $\Delta_c = g$, the power is minimized. Along with the condition $\Delta = 2\kappa$, we have $\Delta_c = g = \kappa$, and the optimal pump power is

$$P_{\text{opt}} \approx \frac{5}{4}(1 - \xi)m\omega_m^2 \left(\frac{L}{Q_c}\right)^2 \omega_c, \tag{2.14}$$

where $Q_c = \omega_c/\kappa$ is the quality factor of the cavity. Considering an optomechanical system with $m = 5.36 \times 10^{-10}$ Kg, $\omega_m = 2\pi \times 130$ kHz, cavity length $L = 2.50 \times 10^{-2}$ m, pumping laser wavelength $\lambda = 1.55$ μm, and cavity finesse of $F = 20000$

[72], we find that for $\xi = 0$, $P_{\rm opt} = 0.816$ mW, and the circulating power $P_{\rm cir} = P_{\rm opt}F/2\pi = 2.56$ W. The single photon optomechanical coupling $g_{\rm OM} = \omega_c x_{\rm ZPF}/L = 2\pi \times 8.77$ Hz, where $x_{\rm ZPF}$ is the zero point fluctuation of the displacement of the middle mirror. The force sensitivity is $\sqrt{\eta} \sim \sqrt{\hbar m \omega_m^2}\xi = \xi \times 1.94 \times 10^{-16}{\rm N}/\sqrt{\rm Hz}$. For small ξ, attonewton force sensitivity could be achieved with current devices.

2.6 Bandwidth for optimal performance

In practice, we need to understand the behavior of $\eta(\omega)$ at low but nonzero frequencies to determine the bandwidth for force detection. We note that at nonzero frequencies, the asymmetry of the quantum noise spectral density $S_{FF}(\omega)$ is very small, thus we could use the approximation $\eta(\omega) \approx S_{FF}(\omega)$. A full analysis of the bandwidth is only possible numerically, so here we present a simple but illuminating approximation method. The argument is the following: at nonzero frequencies, in order to keep the $\delta\theta$ dependence in Eq. (A.13), we require $|\omega \cos\theta| < \Delta \sin\theta + \kappa \cos\theta$, which is equivalent to

$$|\omega| < \frac{1}{2}\left[1 + \left(\frac{\Delta}{\kappa}\right)^2\right]\xi\kappa. \tag{2.15}$$

Thus the bandwidth is approximately $[1 + (\Delta/\kappa)^2]\,\xi\kappa$. Neglecting the thermal noise term, we plot the DC sensitivity for different values of ξ in Fig. 2.2(a), and the sensitivity at low signal frequencies for different values of κ, ξ, Δ/κ in Fig. 2.2(b), 2.2(c), 2.2(d) respectively. We find that the bandwidth shown in the numerical result is in good agreement with Eq. (2.15). Thus we could use this formula to estimate the bandwidth at low frequencies for a given set of parameters.

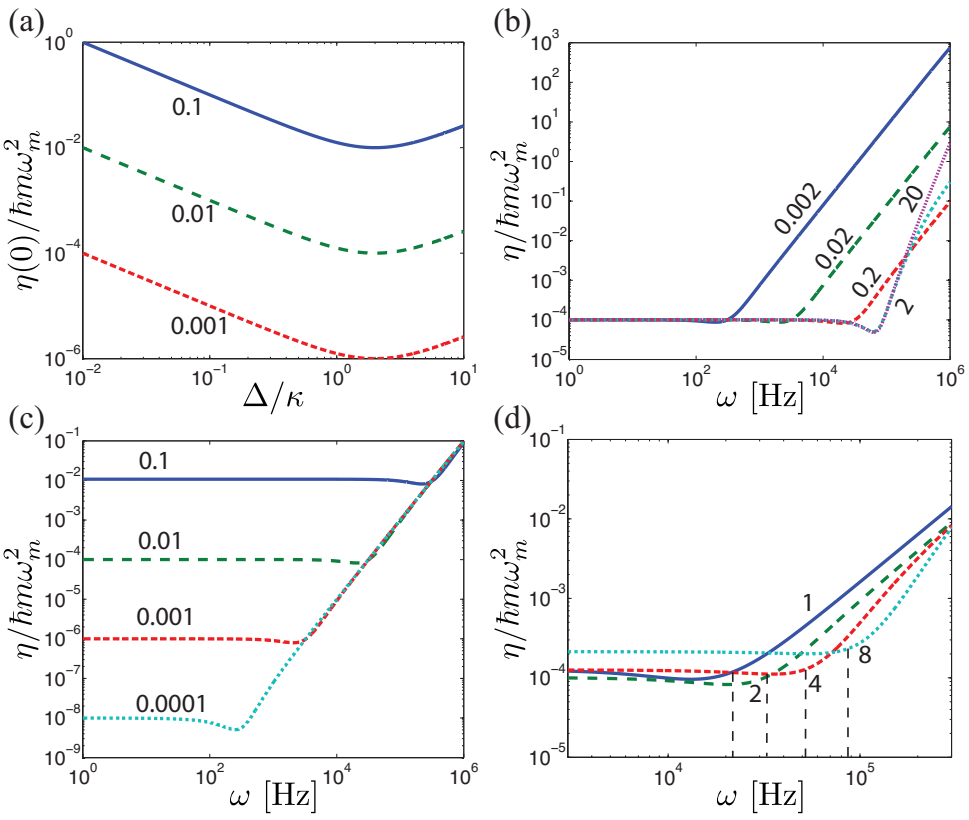

Figure 2.2: (a) Sensitivity at DC as a function of Δ/κ for different values of ξ (numerics shown in plot). At $\Delta/2\kappa$, the minimum value is achieved. In the following figures, we choose $\omega_m = 2\pi \times 10^6$ Hz, $\kappa = 0.2\omega_m$, $\Delta = 2\kappa$ and $\xi = 0.01$ as the base values to plot the sensitivity as a function of frequency. The bandwidth is the frequency range where the best sensitivity is maintained. (b) Bandwidth dependence on κ, where ω_m is fixed and κ varies and the ratio κ/ω_m is shown in plot. In the resolved sideband regime the bandwidth increases with κ linearly, while in the unresolved regime, it does not increase much. (c) Bandwidth dependence on ξ, which is approximately linear. (d) Bandwidth dependence on Δ/κ , where κ is fixed and Δ varies. The dependence is approximately in the form $\sqrt{1+(\Delta/\kappa)^2}$ and suggests a narrower bandwidth than our estimate Eq. (2.15).

2.7 Squeezing spectrum of the cavity output

Finally, we study the squeezing spectrum of the output signal $S(\omega)$, which is given by $\tilde{S}(\omega) = \int \mathrm{d}\omega' \langle S(\omega), S(\omega') \rangle$ [41, 73]. Using the noise correlation relations, we have

$$\tilde{S}(\omega) = 2m\gamma k_B T \left|\chi_F(\omega)\right|^2 + \frac{1}{2}\left|\chi_X(\omega) - i\chi_Y(\omega)\right|^2. \tag{2.16}$$

At DC, we can minimize it by choosing the optimal angle and pump strength, obtaining

$$\tilde{S} = \frac{n_{th}}{Q_m}\frac{\Delta}{\kappa}(1-\xi) + \frac{1}{2}\left[1 + \left(\frac{\Delta}{2\kappa}\right)^2\right]\xi^2. \tag{2.17}$$

where $n_{th} = k_B T/\hbar\omega_m$ is the number of thermal phonon and $Q_m = \omega_m/\gamma$ is the quality factor of the mechanical oscillator. For $\Delta = 2\kappa$, $\tilde{S} = 2(1-\xi)n_{th}/Q_m + \xi^2$. Nano-mechanical oscillators of high quality factor and low phonon number have now been fabricated by many groups, which makes it possible to reduce the thermal noise term to a very small value. By driving the system near the threshold ($\xi \to 0$), squeezing ($\tilde{S} < 1$) in the signal we measure could be realized. This is the optomechanical analog of the squeezing in the output field from an optical parametric oscillator (OPO) [39]. Similarly, choosing $\theta \to \pi/2 + \theta$, we calculate the squeezing spectrum of a signal $\pi/2$ out of phase and find that the optical noise term is proportional to $1/\xi^2$, which is consistent with the Heisenberg uncertainty relation.

In all the analysis above, however, we have not yet taken into account the quantum noise $X'_{in}(\omega)$ introduced when measuring the field quadrature $S(\omega)$. Considering a measurement efficiency $P < 1$, then the actual signal we measure is

$S'(\omega) = \sqrt{P}S(\omega) + \sqrt{1-P}X'_{in}(\omega)$. We find the modified sensitivity to be $\eta'(\omega) = \eta(\omega) + (1-P)/2P|\chi_F(\omega)|^2$. Assuming that the optimization at α_*^2 and θ_0 is still valid, then the sensitivity at DC is $\eta'(0) = \eta(0) + \hbar m\omega_m^2(1-P)/(1-\xi)\cdot\kappa/\Delta$, and the corresponding squeezing spectrum is $\tilde{S}' = \tilde{S} + (1-P)/2$, in the limit $P \to 1$. Thus, a homodyne measurement efficiency of 99% will limit the squeezing to 23 dB (decibel).

2.8 Conclusion

Our approach to squeezing for improved force sensing may also have direct application in related topics, including atomic force microscopy, magnetic resonance force microscopy, and even in quantum transduction via mechanics as recently suggested [74]. Furthermore, more complicated cavity mode structures, such as those of higher orbital angular momentum, may provide additional methods for achieving this outcome in single-side cavities, as the fundamentals of our approach are simply having two well isolated, near-by cavity modes that both interact with the mechanical degree of freedom.

Chapter 3: Quantum nonlinear optics near optomechanical instabilities

3.1 Introduction

Recent years have seen dramatic progress in realizing deterministic interactions between single photons, which has profound implications for future optical technologies [75–78]. The most striking success has been achieved with cavity quantum electrodynamics (cQED) [79–86], where photons inherent the saturation of a single two-level atom due to strong interactions between the atom and the cavity field. Alternative approaches have been explored based on slow-light-enhanced Kerr nonlinearites [87–89], single dye-molecules [90], strong photon interactions mediated by Rydberg atoms [91–94], enhanced nonlinearities in plasmonic systems [95,96] and atoms coupled to wave guides [97–100].

Optomechanical systems, where light and mechanical motion are coupled by radiation pressure [21, 24, 26, 27, 101–103], are a promising approach to realizing strong photon interactions. Unfortunately no experiment has yet managed to reach the single-photon strong coupling regime. Recently it was noted that, in the weak coupling regime, there are still signatures of optomechanical nonlinearity [33–35];

however, strong coupling is required to achieve significant nonlinear quantum effects and deterministic photon interactions with optomechanics [31, 32, 104, 105].

In this article, we show that it may not be necessary to reach the quantum strong coupling regime in order to obtain large single-photon nonlinearities. Instead, in two-mode optomechanical systems with strong side-band resolution, the nonlinearity can be enhanced to the single-photon level by driving the system near an instability. In particular, as the strength of the driving field increases, the frequency of one of the optomechanical normal modes approaches zero and the associated harmonic oscillator length becomes large [106]. The increased quantum fluctuations associated with this mode result in an enhanced nonlinear interaction. We show that when the mechanical mode is sideband resolved with respect to the cavity, the enhancement in the nonlinear coupling can exceed the dissipation by an amount scaling with the sideband resolution ω_m/κ, where ω_m is the mechanical frequency and κ is the cavity linewidth. We demonstrate that this results in enhanced photon-photon interactions by calculating the equal time, two-photon correlation function $g^{(2)}(0)$ for weakly incident probe light. The presence of anti-bunching $g^{(2)}(0) < 1$ in the cavity output field indicates the onset of photon blockade and, in this case, significant two-photon nonlinearity. We infer a new parameter $P = g_0^2\omega_m/\kappa^3$ (g_0 is single-photon optomechanical coupling), whose largeness is the relevant quantity for determining the strength of the nonlinearity. We find that in current devices based on optomechanical crystals, our approach could increase the observable antibunching by more than an order of magnitude.

In section 3.2, we describe the system using an effective hamiltonian and show

that after diagonalization, the nonlinear interaction is strongly enhanced. In section 3.3, we take dissipation into account using the master equation and determine the conditions for realizing strong quantum nonlinearity. Subsequently, in section 3.4, we discuss the photon-blockade mechanism and present numerical simulations for the two-photon correlation functions. In section 3.5, we discuss the feasibilities of our scheme and do a case study in optomechanical crystals.

3.2 Model

The system we consider is shown in Fig. 3.1(a). It consists of a high finesse optical cavity that has two spatially separated, degenerate optical modes (a_L, a_R) at frequency ω_c coupled at a rate J through a mirror with near perfect reflection [107]. Both optical modes are also coupled to a common mechanical mode (c) through radiation pressure with single-photon optomechanical coupling rate g_0. In the symmetric-antisymmetric mode basis $a = (a_L + a_R)/\sqrt{2}$, $b = (a_L - a_R)/\sqrt{2}$ the Hamiltonian is $(\hbar = 1)$:

$$H = (\omega_c - J)a^\dagger a + (\omega_c + J)b^\dagger b + \omega_m c^\dagger c - g_0(a^\dagger b + b^\dagger a)(c + c^\dagger). \quad (3.1)$$

In addition, there is also a dissipative interaction of the cavity and mechanical modes with their environment, with a conservative term $V = \sqrt{\kappa}(a_{\rm in}(t)a^\dagger + h.c.)$ and damping κ (described below). The two cavities are assumed to have identical damping rates.

In the presence of a strong drive $a_{\rm in}(t) = a_{\rm in} + \sqrt{\kappa}\,\alpha_{\rm p}e^{-i\omega t}$ there is an an effective linear coupling between the antisymmetric mode and the mechanical mode, and

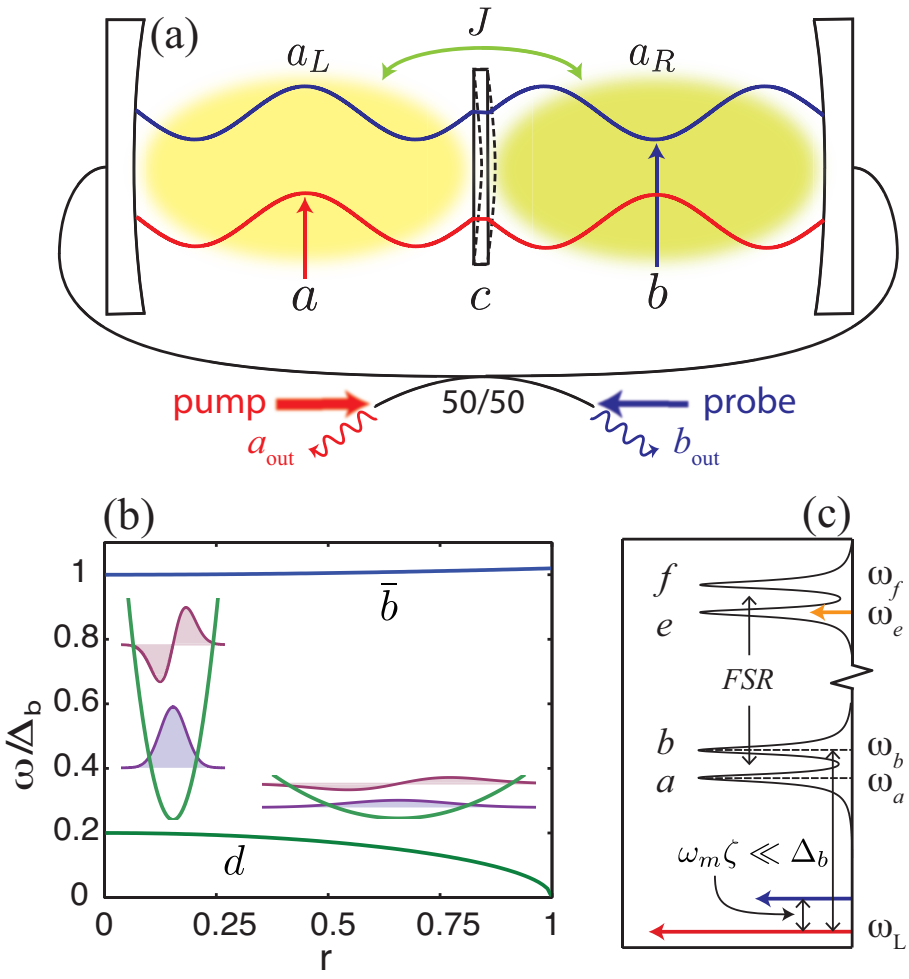

Figure 3.1: (a) Schematic of the coupled two-mode system. Displacements of the middle mirror (via mechanical oscillations) couple the symmetric mode a (red) and antisymmetric mode b (blue) as the left-right symmetry is broken. (b) Normal modes of the coupled harmonic oscillator bilinear hamiltonian for $\Delta_b = 5\omega_m$, with blue (green) line representing the higher (lower) energy branch $\bar{b}$ (d). As pump power increases, the energy of the lower branch decreases, the effective potential becomes flat and the associated harmonic oscillator length becomes larger. (c) Energy scales for the pump, probe and cooling modes.

also a residual nonlinear coupling between the mechanical mode and both optical modes. The Hamiltonian in the rotating frame for the pump displaced oscillator states ($a \to a + \alpha$) becomes [24]

$$H = \Delta_a a^\dagger a + \Delta_b b^\dagger b + \omega_m c^\dagger c - G_0(b + b^\dagger)(c + c^\dagger) - g_0(a^\dagger b + b^\dagger a)(c + c^\dagger) \quad (3.2)$$

where $\Delta_{a(b)}$ is the detuning of mode a (b) with respect to the pumping laser and $G_0 \equiv g_0\alpha = g_0\alpha_p\kappa/(\Delta_a - i\kappa/2)$ is the pump-enhanced linear coupling. By choosing an appropriate phase of the pump, we can make G_0 real. In what follows, we make the further assumptions that $\Delta_b \gg \omega_M$, such that the parameter $\eta \equiv \omega_m/\Delta_b$ is much smaller than 1. In this regime the hybridized polariton modes Eq. (3.4)-(3.5) retain mostly their original photonic or mechanical character, reducing the deleterious effect of optical loss on the 'mechanical' mode. We give the full expressions in Appendix B.

The first four terms in H are bilinear in the oscillator modes and can be diagonalized to give the normal modes (see Appendix B)

$$H_0 = \Delta_a a^\dagger a + (\Delta_b + \delta)\bar{b}^\dagger\bar{b} + \omega_m\zeta\, d^\dagger d, \quad (3.3)$$

with the normal mode frequencies given in terms of the parameters $\delta \approx r^2\omega_m\eta/2$ and $\zeta = \sqrt{1 - r^2}$ to first order in η. We defined the rescaled driving amplitude $r \equiv 2G_0/\sqrt{\omega_m\Delta_b}$. As $r \to 1$ the frequency of the lower branch goes to zero and the mode effectively becomes a free particle, leading to enhanced quantum fluctuations in this mode, as shown in Fig. 3.1(b). For $r > 1$, the normal mode frequency becomes imaginary signifying the onset of the instability. For $0 \leq r < 1$ and $\eta \ll 1$,

the normal mode operators are, surprisingly

$$\bar{b} \approx b - \frac{r}{2}\sqrt{\eta}(c + c^\dagger), \tag{3.4}$$

$$d \approx \frac{1}{2\sqrt{\zeta}}(c - c^\dagger) + \frac{\sqrt{\zeta}}{2}(c + c^\dagger) + \frac{r}{2}\sqrt{\eta}(b - b^\dagger). \tag{3.5}$$

In this regime, $\bar{b}$ is mostly optical while d is mostly mechanical, to $O(r\sqrt{\eta})$. Including the nonlinearity, we can reexpress the normal-ordered Hamiltonian to first order in η:

$$H = H_0 - \frac{g_0}{\sqrt{\zeta}}(a^\dagger\bar{b} + a\bar{b}^\dagger)(d + d^\dagger) - \frac{g_0}{\sqrt{\zeta}}\sqrt{\frac{\eta}{4\zeta}}(a + a^\dagger)(d^2 + d^{\dagger 2} + 2d^\dagger d). \tag{3.6}$$

Near the instability, $\zeta \ll 1$, the effective optomechanical coupling $g_0/\sqrt{\zeta}$ is strongly enhanced. This approach is distinct from simply choosing a low frequency mechanical oscillator to begin with because the mass and frequency of a mechanical oscillator (of the same shape and material) are usually related to each other by $\omega_m \propto \sqrt{1/m}$, so that the stiffness $m\omega_m^2$ remains constant. As a result, the optomechanical coupling g_0, which scales with the intrinsic position fluctuations $x_{\mathrm{zpf}} = \sqrt{\hbar/m\omega_m}$, will typically increase with frequency. This back-action induced softening has the benefits of combining small mass and low frequency, so the effective coupling can be enhanced substantially.

3.3 Nonlinear interactions and dissipations

In the normal mode basis, H contains five distinct nonlinear interactions:

$$\bar{b}^\dagger ad + h.c., \quad a^\dagger\bar{b}d + h.c., \quad a^\dagger dd + h.c., \quad add + h.c., \quad (a + a^\dagger)d^\dagger d. \tag{3.7}$$

When the frequency of the d mode is small, these nonlinear terms will destabilize the system towards large mode occupation, which, together, with the cavity induced decay will contaminate any few photon effects. To keep the system far in the stable regime, we require $g_0/\sqrt{\zeta}, g_0\sqrt{\eta/\zeta^2} \ll \omega_m\zeta$, which further constrains Δ_b and ζ. In addition, the mechanical mode must be close to the ground state, below we show how this can be achieved with optomechanical cooling for the normal mode when the heating rate $\gamma_\uparrow$ (defined below) is much less than κ. All together, to have a large effective single photon optomechanical nonlinearity we require

$$\gamma_\uparrow \ll \kappa \ll g_0/\sqrt{\zeta} \ll \omega_m\zeta. \tag{3.8}$$

This can be satisfied for large Δ_b and small $\gamma_\uparrow$ when

$$P \equiv \frac{g_0^2}{\kappa^2}\frac{\omega_m}{\kappa} \gg 1. \tag{3.9}$$

Thus the condition for single photon nonlinearities is relaxed from $g_0 \gg \kappa$ to $P \gg 1$.

To treat the dissipation we use the master equation for the density matrix ρ of the three-mode system

$$\dot{\rho} \;=\; -i[H,\rho] - \kappa\big(\mathcal{D}[a]+\mathcal{D}[b]\big)\rho - \gamma_m\big((\bar{n}_{\rm th}+1)\mathcal{D}[c]+\bar{n}_{\rm th}\mathcal{D}[c^\dagger]\big)\rho, \tag{3.10}$$

where $\mathcal{D}[A]\rho = 1/2\,\{A^\dagger A,\rho\} - A\rho A^\dagger$ for any operator A, γ_m is the mechanical heating rate, and $\bar{n}_{\rm th}$ is the thermal occupation of the mechanical mode in the absence of the coupling to the cavity. In the normal mode basis, the jump operator for the cavity and mechanical modes become $b \to \bar{b} + \sqrt{\eta/\zeta}\,\big(d+d^\dagger\big)/2$ and $c \to (d+d^\dagger)/2\sqrt{\zeta} + \sqrt{\zeta}(d-d^\dagger)/2$, respectively, implying that dissipation of both cavity mode b and mechanical mode c results in added noise on the d mode. Near the instability

$\zeta \ll 1$, the downward transitions (emission) and upward transitions (absorption) in the d mode occur at the respective rates

$$\gamma_\downarrow = \tfrac{\eta}{4\zeta}\kappa + \tfrac{\gamma_m}{4\zeta}(2\bar{n}_{\rm th} + 1 + 2\zeta), \tag{3.11}$$

$$\gamma_\uparrow = \tfrac{\eta}{4\zeta}\kappa + \tfrac{\gamma_m}{4\zeta}(2\bar{n}_{\rm th} + 1 - 2\zeta). \tag{3.12}$$

Since $\gamma_\downarrow - \gamma_\uparrow = \gamma_m \ll \gamma_\uparrow$, the absorption terms will tend to excite the d mode to high occupation numbers roughly given by $\bar{n}_d \sim \gamma_\uparrow/(\gamma_\downarrow - \gamma_\uparrow)$ [24].

A natural way to overcome this difficulty is to add optomechanical cooling to the d mode. As shown in Fig. 3.1(c), we consider using another pair of cavity modes e, f separated by the cavity free spectrum range (FSR) to induce sideband cooling of the d mode. Driving mode e enhances the coupling between mode f and the mechanical mode c by an amount α_e, the steady state amplitude of e. Moving to the optomechanical normal mode basis, we get the additional terms in the hamiltonian:

$$\Delta_e e^\dagger e + \Delta_f f^\dagger f - \frac{g_0}{\sqrt{\zeta}}\alpha_e(f + f^\dagger)(d + d^\dagger). \tag{3.13}$$

We see that the coupling is further enhanced by $1/\sqrt{\zeta}$ because of the increase of harmonic oscillator length. Similar to the usual single-mode optomechanical cooling, when $\Delta_f = \omega_m\zeta$, the d mode is cooled by the f mode [24] and the system quickly reaches steady state.

3.4 Photon-blockade and numerical simulations of $g^2(0)$

The nonlinear terms will have the strongest effect when one of the interactions in Eq. (3.7) is tuned into resonance. Here we focus on the resonant interaction

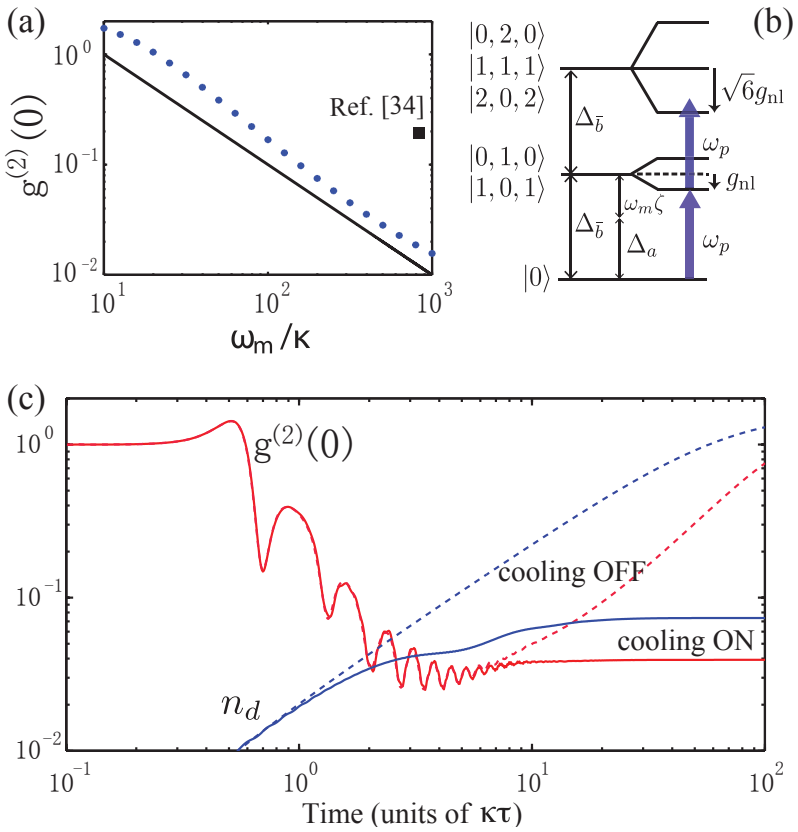

Figure 3.2: (a) Dotted line shows $g^2(0)$ of the $\bar{b}$ mode as a function of P with $g_0 = \kappa$ (so $P = \omega_m/\kappa$), $\alpha_e = 0.1$ and $\beta_{\bar{b}} = 0.02\kappa$. We restrict the mode occupations to be less than 4. When $P > 40$, $g^2(0)$ roughly scales as $1/P$ (black line). The black square represents the value of $g^2(0)$ obtained in Ref. [34] when $\omega_m/\kappa \to \infty$. For comparison, the $g^2(0)$ in Ref. [32], when $g_0 = \kappa$, increases linearly with P^2. (b)The level diagram of the system when the interaction $\bar{b}^\dagger ad$ becomes resonant. The probe field drives the lower energy state of the first excited state on resonance. (c) Evolution of the equal time, two-photon correlation function $g^{(2)}(0)$ (red lines) and the population in the d mode $n_d = \langle d^\dagger d \rangle$ (blue lines), after the probe field is turned on ($P = 500$, $g_0 = \kappa$, $\gamma_{\uparrow\downarrow} = \kappa/\sqrt{P}$ and $\beta_{\bar{b}} = 0.02\kappa$). Dotted lines show the result for $\alpha_e = 0$ indicating cooling on d is OFF, while solid lines are for $\alpha_e = 0.1$ indicating cooling is ON.

$\bar{b}^\dagger ad$, which has the resonance condition: $\Delta_{\bar{b}} = \Delta_a + \omega_m \zeta$ (Here $\Delta_{\bar{b}} = \Delta_b + \delta$ is the energy of the normal mode $\bar{b}$). In the occupation number basis $|n_a, n_{\bar{b}}, n_d\rangle$, the 2-fold degeneracy of the first excited state is broken by $g_{\rm nl}$ and the 3-fold degeneracy of the second excited state is broken by $\sqrt{6} g_{\rm nl}$ due to the 3-body interaction $\bar{b}^\dagger ad + \text{h.c.}$:

$$|0,1,0\rangle \xleftrightarrow{g_{\rm nl}} |1,0,1\rangle\,, \;\; \Delta\omega : \pm g_{\rm nl}$$

$$|0,2,0\rangle \xleftrightarrow{\sqrt{2} g_{\rm nl}} |1,1,1\rangle \xleftrightarrow{2 g_{\rm nl}} |2,0,2\rangle\,, \;\; \Delta\omega : 0, \pm\sqrt{6} g_{\rm nl}$$

with $g_{\rm nl} = g_0/\sqrt{\zeta}$. Since $\bar{b}$ has a strong overlap with the antisymmetric cavity mode, we can optically probe it as illustrated in Fig. 3.1(a). Similar to the Jaynes-Cummings nonlinearity in cQED system [79], when probing the $\bar{b}$ mode at frequency $\omega_p = \Delta_{\bar{b}} - g_{\rm nl}$ with strength $\beta_{\bar{b}}$, we can observe a photon-blockade effect because of the anharmonicity of the ladders, which is shown in Fig. 3.2(b). The signature of the photon blockade will be in the antibunching of the output light, i.e., when $g^{(2)}(0) < 1$, where $g^{(2)}(0)$ is the equal time, two-photon correlation function defined by

$$g^{(2)}(t) = \frac{\left\langle \bar{b}^\dagger(\tau)\bar{b}^\dagger(\tau+t)\bar{b}(\tau+t)\bar{b}(\tau)\right\rangle}{\left\langle \bar{b}^\dagger(\tau)\bar{b}(\tau)\right\rangle^2} \tag{3.14}$$

for a given evolution time τ. Fig. 3.2(a) shows that, for optimal parameters described below, the minimum value of $g^{(2)}(0) \sim 1/P$, thus the system exhibits a strong single photon nonlinearity even when $g_0 \lesssim \kappa$.

Fig. 3.2(c) shows the typical evolution of $g^{(2)}(0)$ with τ obtained from numerical simulation of the master equation. The initial condition has all modes in the vacuum state. Without cooling the system reaches a quasi-steady state with strong antibunching before it is eventually pumped to states with a finite population in d

as shown by the dashed blue line in Fig. 3.2(c). However, in the presence of cooling the d mode occupation remains small and the system reaches a steady state with strong antibunching.

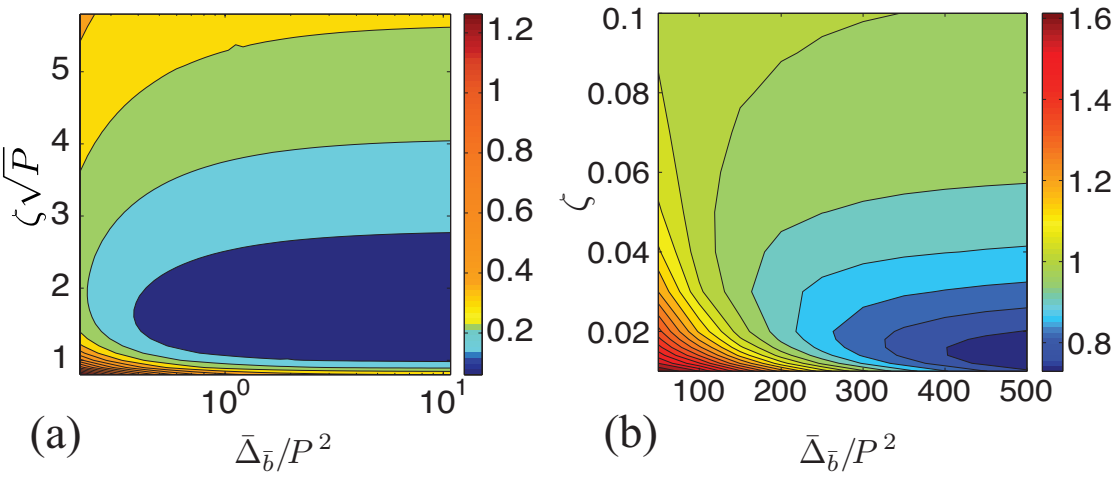

Figure 3.3: (color online). Contour plots of the minimum $g^{(2)}(0)$ in steady state versus the experimental control parameters $\bar{\Delta}_{\bar{b}} = \Delta_{\bar{b}}/\kappa$ and ζ. (a) $P = 100$, $\omega_m/\kappa = P$; (b) $g_0/\kappa = 0.1$, $\omega_m/\kappa = 500$, $P = 5$ and $\alpha_e = 2\sqrt{\zeta}$.

To achieve single photon blockade using the scheme illustrated in Fig. 3.2(b), we also need to satisfy the inequalities given in Eq. (3.8), which requires optimization of the system parameters. After rescaling by κ and taking the resonance condition $\Delta_{\bar{b}} = \Delta_a + \omega_m\zeta$, there are four independent parameters: $(P, \omega_m/\kappa, \Delta_{\bar{b}}/\kappa, \zeta)$. P and ω_m/κ are device-dependent parameters we cannot tune, while $\Delta_{\bar{b}}/\kappa$ and ζ can be controlled by tuning the frequency and amplitude of the strong pumping laser. A simple theoretical analysis can be done for $\beta_{\bar{b}} \ll \kappa$ by neglecting quantum jumps in the master equation (see Appendix C for details). This gives the scaling in the quasi-steady state regime $g^2(0) \sim \kappa^2/g_{\rm nl}^2 + g_{\rm nl}^2/\omega_m^2\zeta^2$, which is optimized when $\zeta \sim 1/\sqrt{P}$

and $g^{(2)}(0) \sim 1/\sqrt{P}$. Numerical simulations of the master equation, however, show that the optimal antibunching scales as $1/P$, as seen in Fig. 2(a) and in the full contour plots of $g^{(2)}(0)$ versus $\Delta_{\bar{b}}$ and ζ shown in Fig. 3. This anomalous scaling is caused by pumping into the dark states $|0, 0, n\rangle$. The region of the parameter space for optimal performance is roughly given by $\Delta_{\bar{b}}/\kappa > P^2$ and $1/\sqrt{P} < \zeta < 1$. These results demonstrate that near the instability, the figure of merit for observing the photon blockade is $P \gg 1$ and not simply $g_0/\kappa \gg 1$.

3.5 Experimental considerations and case study

There is an additional constraint that, in order to use the resonant $\bar{b}^\dagger ad$ interaction term, the photon tunneling rate J must be much smaller than the mechanical frequency ω_m. For the membrane in the middle setup, these conditions may be challenging to achieve due to the high reflectivity required for the membrane. This could be circumvented by instead utilizing the $a^\dagger dd$ nonlinearity, which has no such requirement. One can also consider using differential modes in 'zipper' optomechanical crystals [108], where the photon tunneling rate can be tuned over a wide range by controlling the separation between the two cavities.

Finally, successfully working near the instability requires the classical power fluctuations in the pump laser to be small enough to prevent the system from crossing the instability. More precisely, the amplitude fluctuations in the pump must be less than the instability parameter ζ (defined below Eq. (3.3)), which has an optimum value greater than $1/\sqrt{P}$; thus, for P less than 10^3, this requires stabilizing the

pump power below the 5 % level, which is readily achievable.

Case study – Experimentally these effects could be observed for systems with strong sideband resolution $\omega_m \gg \kappa$ and relatively large single photon optomechanical coupling $g_0 \sim \kappa$. Hybrid photonic-phononic crystals are a promising route to realize both these constraints [27], as are mechanical membranes placed in the middle of a high-finesse optical cavity as illustrated in Fig. 3.1(a) [101]. State of the art photonic-phononic crystals have achieved optomechanical coupling $g_0/2\pi$ above 1 MHz [109, 110] and mechanical frequency $\omega_m/2\pi \sim 10$ GHz [111]. Optical quality factors as high as nine million have also been reported in silicon photonic crystal cavities, which gives cavity decay rate of $\kappa/2\pi \sim 20$ MHz [112]. In such a case with $g_0/\kappa = 0.1$ and $\omega_m/\kappa = 500$, P can be as large as 5 in current devices. Fig. 3.3(b) shows the full range of antibunching obtainable for this P, in the optimal case we find that it can be as small as 0.8, more than an order of magnitude improvement compared to what would be expected away from the instability ~ 0.99 [35]. To satisfy the condition $\gamma_\uparrow \ll \kappa$, we need $\omega_m/4\zeta\Delta_b \ll 1$ and $\gamma_m \bar{n}_{\rm th}/2\zeta \ll \kappa$, which imply $\Delta_b \gg \omega_m/4\zeta$ and $\bar{n}_{\rm th} \ll 2\zeta\kappa/\gamma_m$. This gives an minimum requirement on the Q $\cdot$ frequency product: $Q_m \cdot \omega_m/2\pi > \omega_m/2\zeta\kappa \cdot k_B T/h$, which requires cryogenic temperatures. In principle, room temperature operation is possible for mechanical oscillators at frequencies above 10 GHz and quality factors above 10^6.

3.6 Conclusion

We have presented a scheme to realize few-photon interactions in strongly driven, two-mode optomechanical systems. Our approach suggests a new figure of merit for realizing strong optomechanical coupling and demonstrates that current devices, previously thought to have weak coupling, may be able to be pushed into the regime of strong single-photon nonlinearity. This would allow one to achieve deterministic entanglement of light in optomechanical systems, which has far-ranging applications in quantum information science.

Chapter 4: Cooling a harmonic oscillator by optomechanical modification of its bath

4.1 Introduction

Recent years have seen dramatic experimental and theoretical progress in optomechanics [21,24], ranging from ground state cooling [27] and squeezing [113,114] to quantum nonlinear optomechanics [31–36]. These advances rely upon improvements in optomechanical coupling, particularly the single phonon-single photon coupling rate, and upon increasing mechanical quality factor, which enables lower heat loads and corresponds to higher sensitivity and longer quantum coherence times. However, the longer-term target of single photon nonlinear optics with optomechanical systems remains out of reach. Furthermore, for many sensing applications, the thermal noise remains a fundamental limit for relevant resonator designs, regardless of progress in the use of quantum correlations [107,113,114], as typically the signal to be sensed is transduced to a force on the mechanical system which is in competition with the quantum Brownian motion-induced Langevin force from the thermal bath.

In the present work, we shall focus on thermal noise reduction for mechan-

ical resonators, utilizing the standard tool box provided by optomechanics. This is crucial for improving the signal-to-noise ratio of mechanical devices, operating either in the classical regime or in the quantum regime. We are motivated by recent advances in phononic-band gap engineering as a principle for improved quality factor [110, 111, 115] – but here, we engineer a dissipative band-gap dynamically via the optomechanical interaction, rather than a constant bandgap during fabrication. Specifically, we introduce a generic coupled-oscillator model to describe mechanical systems whose damping is primarily via elastic wave radiation through the boundary, i.e., clamping loss. We then consider how optomechanical coupling to the clamping region enables dynamical control over the coupled mechanical resonator. This leads to the counterintuitive outcome: increasing optical power simultaneously reduces the temperature and linewidth of the mechanical mode, in contrast to direct optomechanical cooling. After introducing this model, we describe a specific resonator design that enables testing of these concepts using current techniques, and analyze the regime in which clamping losses are likely to dominate, finding that a low temperature and high mechanical frequencies our approach may find wide application.

4.2 Toy model

We consider a toy model of two coupled quantum harmonic oscillators with annihilation operators a and b, resonant frequencies ω_a and ω_b, and a coupling strength between them λ. Each harmonic oscillator is also coupled to its own heat bath at temperature T_a and T_b with rates γ_a and γ_b. In addition, optomechanical

cooling is introduced to oscillator b via coupling to a red detuned optical mode c with frequency ω_c and damping κ, as shown in Fig. 4.1.

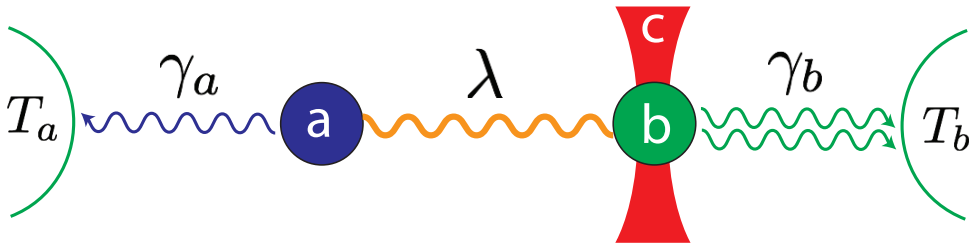

Figure 4.1: Schematic of the coupled harmonic oscillator system, with optomechanical cooling on oscillator b. We are interested in the regime where a couples weakly to its heat bath, which means $\gamma_a \ll \lambda, \gamma_b$.

The effective Hamiltonian of the three mode system when pumped with a laser follows immediately (with $\hbar = 1$, and neglecting the weak nonlinear correction):

$$\begin{aligned} H_{\text{eff}} &= -\Delta c^\dagger c + \omega_a a^\dagger a + \omega_b b^\dagger b + \lambda(a + a^\dagger)(b + b^\dagger) \\ &\quad -\alpha g_0 (b + b^\dagger)(c + c^\dagger). \end{aligned} \tag{4.1}$$

where $\alpha = E/(i\Delta - \kappa/2)$ is the pump-induced coherent state in the optical cavity and assumed to be real without loss of generality (by choosing an appropriate phase for the pump strength E), g_0 is the quantum optomechanical coupling, and $\Delta = \omega_p - \omega_c$ is the detuning of the pump laser. We consider $\omega_a \sim \omega_b \sim -\Delta$, and include mechanical damping of a and b with rates γ_a, γ_b, and optical loss with rate κ [24]. Under the rotating wave approximation, the Heisenberg-Langevin equations in the input-output formalism are as follows:

$$\dot{c} = i\Delta c - \frac{\kappa}{2} c + i\alpha g_0 b + \sqrt{\kappa} c_{\text{in}}, \tag{4.2a}$$

$$\dot{a} = -i\omega_a a - \frac{\gamma_a}{2}a - i\lambda b + \sqrt{\gamma_a}a_{\rm in}, \tag{4.2b}$$

$$\dot{b} = -i\omega_b b - \frac{\gamma_b}{2}b - i\lambda a + i\alpha g_0 c + \sqrt{\gamma_b}b_{\rm in}. \tag{4.2c}$$

This set of linear equations can be solved by moving to the frequency domain. We successively solve for $c(\omega)$, then b, then a. For example, $c(\omega) = \frac{i\alpha g_0 b + \sqrt{\kappa}c_{\rm in}}{-i(\omega+\Delta)+\kappa/2}$. We immediately set $c \approx \frac{1}{\alpha g_0}(i\frac{\Gamma}{2}b + \sqrt{\Gamma}c_{\rm in})$ in the sideband-resolved limit with $|\Delta+\omega| \ll \kappa/2$ where $\Gamma = 4|\alpha g_0|^2/\kappa$ is the optically-induced damping of mode b. Continuing, we find

$$\chi_b^{-1} b(\omega) = -i\lambda a + \sqrt{\gamma_b}b_{\rm in} + i\sqrt{\Gamma}c_{\rm in} \tag{4.3a}$$

$$\text{where } \chi_b = [-i(\omega-\omega_b) + (\gamma_b+\Gamma)/2]^{-1} \tag{4.3b}$$

is the susceptibility of mode b for $\lambda = 0$.

Finally, we find for mode a

$$\chi_a^{-1} a = \sqrt{\gamma_a}a_{\rm in} - i\chi_b\lambda\left(\sqrt{\gamma_b}b_{\rm in} + i\sqrt{\Gamma}c_{\rm in}\right) \tag{4.4a}$$

$$\text{with } \chi_a = \left[-i(\omega-\omega_a) + \gamma_a/2 + \chi_b\lambda^2\right]^{-1} \tag{4.4b}$$

Examining these equations, we see that mode a's resonant response, as described by the susceptibility χ_a, have a frequency and damping that depend, via $\lambda^2\chi_b$, upon the properties of the optomechanically damped mode b. Specifically, examining the real and imaginary components, we have

$$\omega_a' = \omega_a + \frac{\lambda^2(\omega-\omega_b)}{(\omega-\omega_b)^2 + (\gamma_b+\Gamma)^2/4}, \tag{4.5a}$$

$$\gamma_a' = \gamma_a + \frac{\lambda^2(\gamma_b+\Gamma)}{(\omega-\omega_b)^2 + (\gamma_b+\Gamma)^2/4}, \tag{4.5b}$$

Let us examine the particular scenario when the cooperativity between a and b satisfies $\mathcal{C}_{ab} \equiv \frac{4\lambda^2}{\gamma_a\gamma_b} \gg 1$ and $\frac{\gamma_b+\Gamma}{\gamma_a} \gg \mathcal{C}_{ab}$. This corresponds to the intrinsic

damping of mode a being dominated by its coupling through b to b's bath, while simultaneously being able to examine b's response as broader than a's. We will further focus on $|\omega_b - \omega_a| \ll \gamma_b + \Gamma$, as provides the maximum modification of damping. This allows us to expand $\omega_a' \approx \omega_a$ and $\gamma_a' \approx \gamma_a + \Gamma_a$ with $\Gamma_a \equiv \frac{4\lambda^2}{\gamma_b+\Gamma}$. When the optomechanical damping of mode b increases, the linewidth of mode a becomes narrower, and eventually reaches its intrinsic damping γ_a. We finally get

$$a \approx \frac{\sqrt{\gamma_a}a_{\rm in} + i\sqrt{\Gamma_a\left(\frac{\gamma_b}{\gamma_b+\Gamma}\right)}b_{\rm in} + \sqrt{\Gamma_a\left(\frac{\Gamma}{\gamma_b+\Gamma}\right)}c_{\rm in}}{-i(\omega-\omega_a) + (\gamma_a+\Gamma_a)/2} \tag{4.6}$$

This regime (damping of a primarily via mode b, which in turn is damped optically by a sideband-resolved coupling to mode c) lets us examine the effective temperature. Specifically, using the input noise correlations of $b_{\rm in}$ in the frequency domain,

$$\left\langle b_{\rm in}^\dagger(\omega) b_{\rm in}(\omega')\right\rangle = \bar{n}\delta(\omega+\omega') \tag{4.7a}$$

$$\left\langle b_{\rm in}(\omega) b_{\rm in}^\dagger(\omega')\right\rangle = (\bar{n}+1)\delta(\omega+\omega') \tag{4.7b}$$

where $\bar{n} = 1/(e^{\hbar\omega/k_BT}-1)$ is the average phonon occupation number of a harmonic oscillator of frequency ω when it is in thermal equilibrium with a heat bath at temperature T. We have the same for $a_{\rm in}$ and $c_{\rm in}$, and we assume $T_a = T_b = T_c = T$. The optical frequency is many orders of magnitude higher than mechanical frequency, so at the same temperature, the photon occupation number of the optical environment is completely negligible. Now we find the average position fluctuation $n_{\rm eff} + 1/2 \equiv \left\langle (a+a^\dagger)^2\right\rangle/2$ (since $\langle n|\,(a+a^\dagger)^2\,|n\rangle = 2n+1$) to be

$$n_{\rm eff} = \frac{\gamma_a\bar{n} + \Gamma_a\left(\frac{\gamma_b}{\Gamma+\gamma_b}\bar{n}\right)}{\gamma_a+\Gamma_a} \tag{4.8}$$

where $\bar{n}$ is evaluated at ω_a. This expression is also consistent with the result from detailed balance relation [11]. We can minimize this occupation by a setting the optomechanical cooperativity $\mathcal{C}_{\rm OM} \equiv \Gamma/\gamma_b$ of b to

$$\mathcal{C}_{\rm OM} \to \mathcal{C}^*_{\rm OM} \equiv \sqrt{1+\mathcal{C}_{ab}}\ ,$$

which gives

$$\frac{n^*_{\rm eff}}{\bar{n}} = \frac{2}{1+\sqrt{1+\mathcal{C}_{ab}}}.$$

Thus in principle even ground state cooling is achievable, if the mechanical oscillator cooperativity $\mathcal{C}_{ab} \gtrsim 16\bar{n}^2$. Curiously, this cooling arises with *reduction* of the linewidth of mode a, with the limiting linewidth $\gamma_a + \Gamma^*_a = \gamma_a\sqrt{1+\mathcal{C}_{ab}}$.

Finally, to confirm these approximations, we numerically examine the same regime, but without making the rotating wave approximation or any narrowband approximations – this enables us to include counterrotating terms and their associated heating. We plot the rescaled position fluctuation spectrum $S_{xx}(\omega) = \int_{-\infty}^{+\infty} {\rm d}t e^{i\omega t}\langle x(t)x(0)\rangle$ and rescaled effective temperature $T_{\rm eff}/T$ below in Fig. 4.2. We find that when $g_0\alpha, \lambda \ll \omega_a, \omega_b$ our approximate theory and the exact results are in agreement.

4.3 Example implementation

To design an optomechanical system that captures the main features of the toy model, we need three basic components: i) two coupled mechanical resonators; ii) one resonator is limited by thermoelastic damping, and the other is limited by clamping loss; iii) optomechanical cooling primarily on the second resonator. With

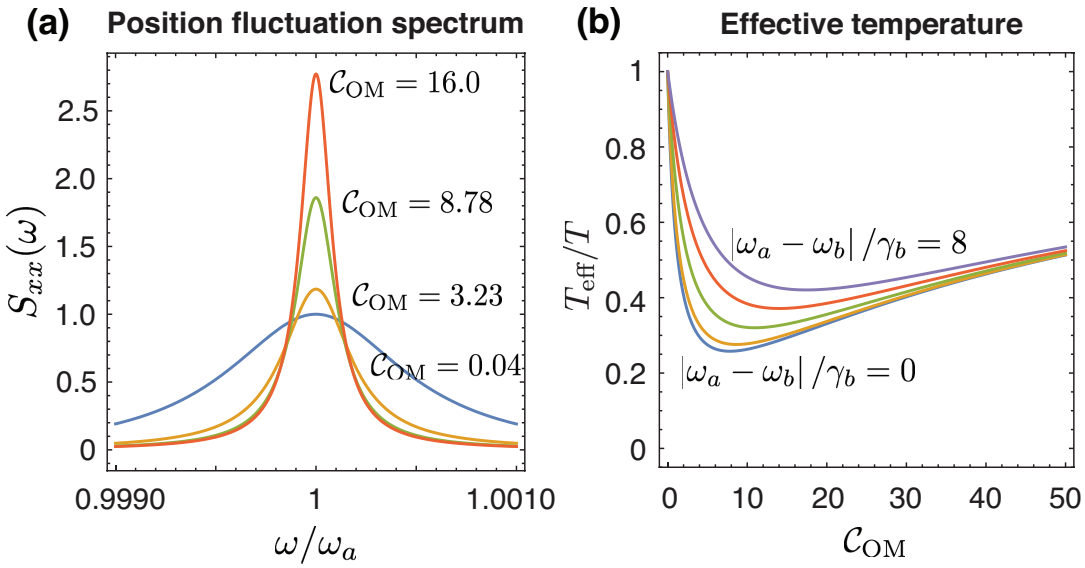

Figure 4.2: (a) Rescaled position fluctuation spectrum for different values of optomechanical cooperativity $\mathcal{C}_{\rm OM}$, with the mechanical oscillator cooperativity chosen as $\mathcal{C}_{\rm ab} = 8$; (b) Rescaled effective temperature as a function of $\mathcal{C}_{\rm OM}$ for $\mathcal{C}_{\rm ab} = 50$ and different values of $|(\omega_a - \omega_b)|/\gamma_b$.

these goals in mind, we can design a system that is shown in Fig. 4.3. In this design, there are two nearly identical quarter-wave mechanical resonators on the left arm and right arm of a large beam resonator, denoted as a_L and a_R. The lengths of the two arms may not be exactly the same (or the left-right symmetry may be broken by defects). This asymmetry leads to different resonant frequencies for the two resonators, with $\omega_L = \omega_0(1+\epsilon)$ and $\omega_R = \omega_0(1-\epsilon)$, as shown in Fig. 4.3.

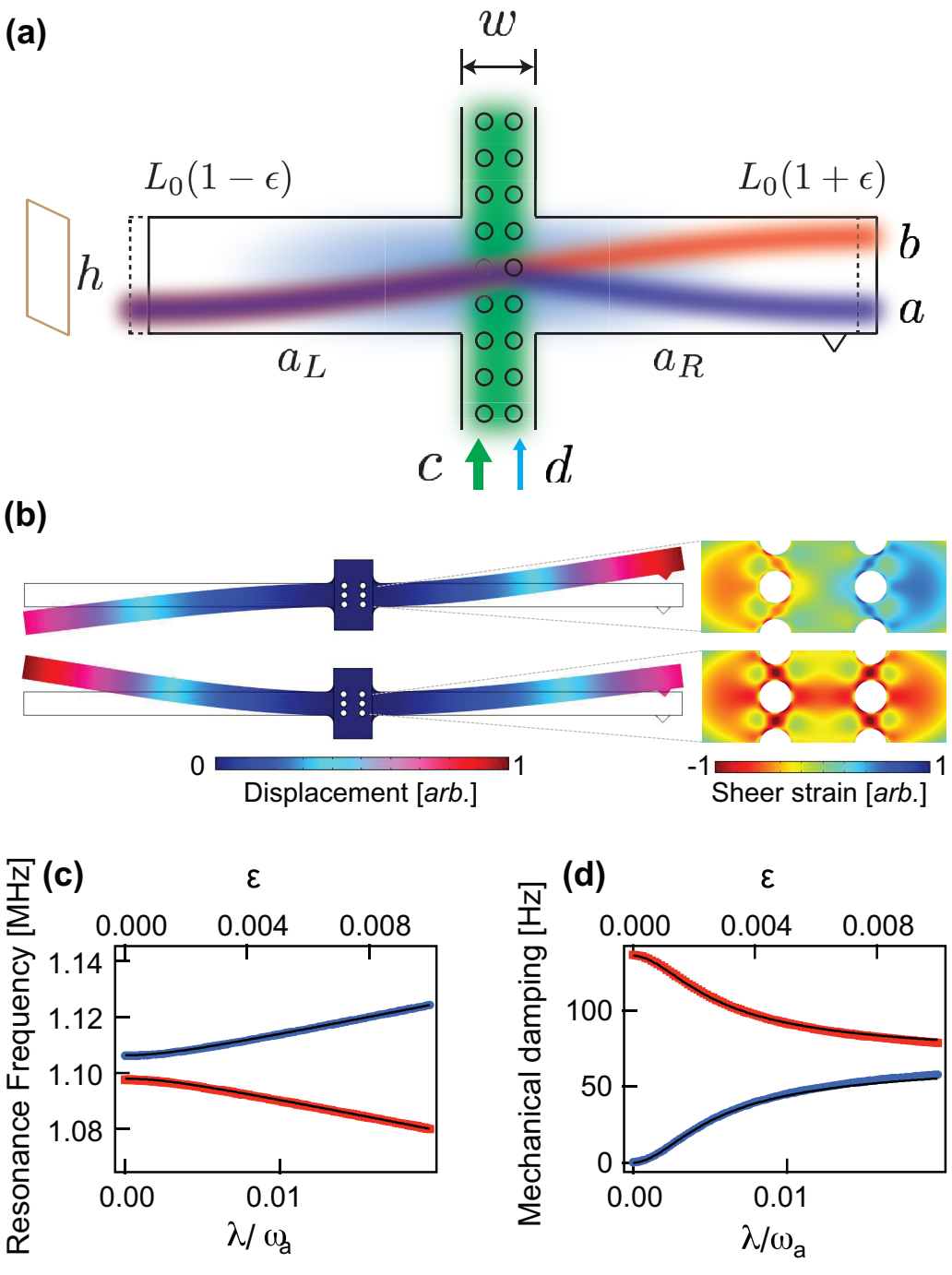
(a)
w
$L_0(1-\epsilon)$
$L_0(1+\epsilon)$
h
b
a
a_L
a_R
c
d
(b)
0
1
Displacement [arb.]
-1
1
Sheer strain [arb.]
(c)
ε
0.000
0.004
0.008
Resonance Frequency [MHz]
1.14
1.12
1.10
1.08
0.00
0.01
λ/ ωa
(d)
ε
0.000
0.004
0.008
Mechanical damping [Hz]
100
50
0
0.00
0.01
λ/ωa

Figure 4.3: (a) Optomechanical design consisting of two similar quarter-wave beam resonators, nominal length L_0, coupled through a center support region, width w, containing a photonic crystal optical structure. (b) Simulated symmetric (top) and antisymmetric (bottom) eigenmodes, $\epsilon = 0$. Insets show the strain deformation of a single photonic defect (envisioned as part of a "zipper" photonic crystal resonator) that would lead to a strong strain-induced optomechanical coupling only between optical and mechanical modes of the same parity. (c,d) As the asymmetry, ϵ, is increased, the antisymmetric and symmetric modes are increasingly coupled, shifting the simulated eigenfrequencies and clamping losses (red squares, blue circles), consistent with fits to the theoretical model of Eq. (4.1) (black). Simulation parameters are L_0=20 μm, h=0.3 μm, and $w = 0.5$ μm, corresponding to $\omega_0 = 2\pi \times 1.102$ MHz and $\gamma_b/2 = 2\pi \times 70$ Hz clamping loss for an individual arm fabricated from silicon nitride.

For the purpose of force sensing, which we are going to discuss later in the paper, we also include a small atomic force microscope (AFM) tip on the right arm of the beam structure in our simulation. It has a left and right optical mode that should hybridize into symmetric and antisymmetric modes that couple to the corresponding mechanical modes.

To examine the mode structure, we consider coupling between the left and right sides through the support structure with a strength J. We see that symmetrical coupling of a_L and a_R through the support leads to normal modes $a = 1/\sqrt{2}(a_L + a_R)$

and $b = 1/\sqrt{2}(a_L - a_R)$, with the former having no clamping loss for $\epsilon = 0$ and the latter a clamping loss $\gamma_b \approx J^2\rho$ (by Fermi's golden rule). Physically, the symmetric mode has destructive interference which prevents excitation of support structure and the associated clamping loss, analogous to the reduction in damping observed in tuning-fork resonators, which can be seen in Fig. 4.3(d).

Meanwhile, the asymmetry couples a and b together with a rate $\lambda = \epsilon\omega_0$. In addition, there can be some intrinsic damping of mode a via, e.g., thermoelastic loss with a rate γ_a, while we account for most of the damping of b via clamping loss to the quasi-mode with rate γ_b. Under the rotating wave approximation, the mechanical parts of the Hamiltonian are the same as those in Eq. (4.1).

We notice that the coupling rate λ is proportional to the dimensionless asymmetry $\epsilon = |L_L - L_R| / (L_L + L_R)$ in the length of the two arms of the beam resonator. In principal, λ could be engineered in a wide range by fabricating resonators of different geometries or by temperature tuning of the length and speed of sound in the material.

In our proposed structure, the optical modes c and d are the anti-bond and bond fundamental modes in a "zipper" photonic crystal cavity [116] in the center of the beam (the support structure), with odd and even parity respectively. As shown in the simulation in Fig. 4.3(b), the anti-bond optical mode c couples mostly to the anti-symmetric mechanical mode b, while the bond optical mode d couples mostly to the symmetric mechanical mode a. Experimentally, mode c can be driven strongly to achieve the desired optomechanical cooling, and mode d serves as a weak probe mode in order to make measurements on mode a.

As the toy model suggests, the damping of oscillator a is assumed very weak ($\gamma_a \ll \gamma_b, \lambda$), so that the optomechanical cooling of oscillator b could be effectively "exported" to a through phonon tunneling. This naturally leads us to the question: what kind of oscillator design has this property? There are two main sources of mechanical damping in micro- and nano-mechanical resonators [117]: i) Boundary damping, or clamping loss, e.g elastic wave radiation from the material to its base through the boundary, and ii) material damping, which includes thermoelastic damping (TED), phonon-phonon interactions. The clamping loss represents the coupling from a resonator to its base, since phonons are exchanged through the boundary, while thermoelastic damping is the major contribution to the internal damping rate of a resonator.

Clamping loss has been studied extensively in the literature [118–121]. For a beam resonator where the thickness of the beam resonator is much smaller than the wavelength of the elastic wave propagating in its support, the flexural vibration can be described using the ideal beam theory. The support of clamping-free (C-F) beam resonators is usually modeled as semi-infinite and infinite thin-plate, respectively, with the same thickness as the beam resonator; all the vibration energy of a beam resonator entering the support structure is considered to be lost. It is the vibrating shear force that induces this energy loss. In [119], they studied the clamping loss using elastic wave radiation theory and found the quality factor of clamping-free (C-F) beam resonators to be:

$$Q_{\mathrm{C-F}} \propto (L/h)^2 \tag{4.9}$$

where L is the length of the beam and h is its width.

Secondly, we look at the thermoelastic damping [122, 123]. Phonons traveling through a large elastic material will experience damping due to their nonlinear interaction with a surrounding bath of phonons. In the diffusive regime where the mean free path of these thermal phonons is much smaller than the wavelength of the acoustic mode, the interaction between the phonon mode and the thermal bath is captured by the material's thermal expansion coefficient (TEC), defined as $\alpha \equiv \frac{1}{L}\frac{\partial L}{\partial T}$, which is temperature dependent. According to [124], the quality factor corresponding to this damping mechanism is given by

$$Q_{\mathrm{TED}}^{-1} = \frac{E\alpha^2 T}{C_p} f(h/h_0), \tag{4.10}$$

where E is the material's Young's modulus, T is the temperature, C_p is the heat capacity at constant pressure, and $f(h/h_0)$ is a beam geometry function parametrized by a critical beam width h_0.

A detailed numerical estimate of these losses for a specific mechanical resonator such as SiN is possible, but here we remark that for short beams, the clamping loss, which grows as h^2/L^2, will always tend to dominate over the thermoelastic damping. For example, for a resonator with frequency $\Omega/2\pi = 1$ MHz, we have $h_0 = 6.546\, mm$. When $h \ll h_0$, we find $f(h/h_0) \to 5h^2/h_0^2$, which gives us a very high Q_{TED} (well beyond the usual material limits). In Appendix C, we show the numerical result for quality factor of the two types of damping mechanisms for different parameters.

4.4 Analysis of force sensing

The proposed scheme for reducing the thermal load of the mechanical oscillator is useful for force sensing, where thermal noise is a main obstacle towards building ultra-sensitive force detection devices. In our proposed structure Fig. 4.3(b), the mechanical mode of interest a couples to anti-bonded weak probe mode d, which has different parity from the bonded strong pump mode c and also higher frequency. Measuring the optical output signal $S(\omega)$ from d allows the sensing of force $f(\omega)$ experienced by mechanical mode a, as shown in [107]:

$$S(\omega) = \chi_X X_{d,\mathrm{in}}(\omega) + \chi_Y Y_{d,\mathrm{in}}(\omega) + \chi_F[F_{\mathrm{in}}(\omega) + f(\omega)], \tag{4.11}$$

with X, Y the quadratures of optical field and χ the susceptibilities for optical and force inputs.

We find that there exist a simple relation between the ultimate sensitivity (in units of $N/\sqrt{\mathrm{Hz}}$) for a mechanics based device and its thermal noise level, which can be calculated as the power spectral density of thermal fluctuating forces:

$$\eta(\omega) \equiv \sqrt{S_{FF}(\omega)} = \sqrt{\int_{-\infty}^{+\infty} \mathrm{d}t e^{i\omega t} \left\langle F_{\mathrm{in}}(t) F_{\mathrm{in}}(0) \right\rangle} \tag{4.12}$$

In the case of our coupled harmonic oscillator system, if oscillator a is used for force sensing, then we get better sensitivity because of the reduction in its thermal load. The force on a harmonic oscillator is defined as

$$F = \dot{p} = -i\sqrt{\frac{\hbar m \omega_a}{2}}(\dot{a} - \dot{a}^\dagger), \tag{4.13}$$

so the corresponding fluctuating force in frequency domain can be found from

Eq. (4.6)

$$F_{\rm in}(\omega) \;=\; -i\sqrt{\frac{\hbar m\omega_a}{2}}\left[\sqrt{\gamma_a}a_{\rm in}+i\sqrt{\Gamma_a\left(\frac{\gamma_b}{\gamma_b+\Gamma}\right)}b_{\rm in}-\text{h.c.}\right] \tag{4.14}$$

Using the noise correlation functions Eq. (4.7), we can calculate its spectral density in the narrow band limit as

$$\begin{aligned} S_{FF}(\omega) &= \int \mathrm{d}\omega' \left\langle |F_{\rm in}(\omega)F_{\rm in}(\omega')| \right\rangle \\ &= \frac{\hbar m\omega_a}{2}\left[\gamma_a+\Gamma_a\left(\frac{\gamma_b}{\gamma_b+\Gamma}\right)\right](2\bar{n}+1) \\ &\approx m\left[\gamma_a+\frac{4\lambda^2\gamma_b}{(\gamma_b+\Gamma)^2}\right]k_{\rm B}T \\ &= \left[1+\frac{\mathcal{C}_{ab}}{(1+\mathcal{C}_{\rm OM})^2}\right]m\gamma_a k_{\rm B}T \end{aligned} \tag{4.15}$$

where we recall $\mathcal{C}_{\rm OM} = \Gamma/\gamma_b$ is the optomechanical cooperativity and $\mathcal{C}_{ab} = \frac{4\lambda^2}{\gamma_a\gamma_b}$ is the cooperativity between a and b. When the optically induced damping rate Γ is large compared to γ_b, we have substantial noise reduction and thus improved sensitivity for the device compared to conventional optomechanical cooling. In the latter case, we could have the noise floor of Eq. (4.15) but with $\mathcal{C}_{\rm OM} = 0$.

4.5 Conclusion

Here we proposed an efficient scheme for cooling a harmonic oscillator by decreasing dissipation via optomechanical cooling. We studied the practical conditions to realize this cooling scheme, and also identified a realistic optomechanical design that has the potential to realize it. Potential applications include mechanics

based force sensing, and other related areas where reducing the thermal load via non-conventional techniques is need.

Chapter 5: Chiral phonon theory in 1-d optomechanical systems

5.1 Introduction

The examination of quantum optomechanics, which studies the radiation pressure-mediated interaction between light and mechanical motion in the quantum regime [4–7], has become accessible via crucial experimental advances [21, 22, 24], as evidenced by recent results such as the ground state cooling of mechanical resonator [25–27], the generation of squeezed states of light [28–30], and studies of single-photon nonlinear optics [31–36] in various optomechanics platforms. An example optomechanical interaction occurs in Brillouin scattering (BS), where acoustic vibrations are induced by acoustic-optic coupling [125–127], and optomechanical cooling via Brillouin scattering (BS) has already been demonstrated [128].

In a recent experiment [Appendix D], the chiral behavior of phonons in silica microsphere resonator were observed. Kim *et.al.* showed that the linewidth of phonon propagating in one direction that is optomechanically cooled via forward Brillouin scattering has been broadened, while the linewidth of phonon propagating in the opposite direction is narrower. This signature of chiral phonons – broken symmetry of the scattering properties of forward/backward propagating phonons – becomes more evident when the input optical power of the control beam is increasing.

As an analogy to emerging studies of chiral photonics interacting with emitters [129–131], the observed chiral phonon broken symmetry in microsphere resonator could be a candidate platform for the study of chiral networks of phononic modes.

Here we introduce a model of loss by considering the high angle elastic scattering between a particular high quality factor (Q) mechanical mode of interest and a continuum of lossy bulk mechanical modes. We suggest that when the optical coupling cools the co-propagating high-Q and bulk mechanical modes, the optical modification of scattering between these bulk modes and the counter-propagating high-Q mode simultaneously improves the quality factor and reduces the thermal load of this high-Q mode, leading to the dynamical creation of a cold 'phononic shield' [132].

We detail our theoretical model in Section II. We then calculate the linewidth and effective temperature of phonons using linear response theory in Section III to explain the key findings of the experiment [Appendix D]. Finally, we fit the linewidth data of the experimental and estimate some of the key parameters in Section IV.

5.2 Model

5.2.1 Photon-phonon interaction

We consider a model of acousto-optic interaction in a multi-mode whispering gallery-type resonator that supports co-propagating photon and phonon modes. Photons from an adjacent waveguide are interfaced with the resonator optical modes through evanescent coupling. Phonons that occupy a surface acoustic wave resonator

mode, are annihilated via forward Brillouin scattering process along with the creation of anti-Stokes scattered photons as shown in Fig. 5.1.

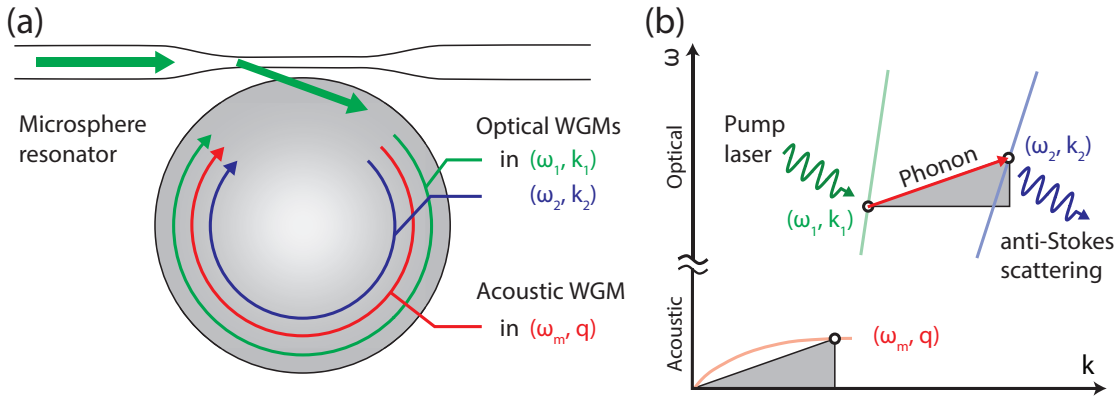

Figure 5.1: (a) The generation of anti-Stokes photon (blue) and absorption of phonon (red) from a pump photon (green) via forward Brillouin scattering process. Due to symmetry, the resonator supports both degenerate pairs of clock-wise and counter clock-wise photons and phonons. (b) Dispersion relation for phonon and photons and coherent acousto-optical interaction.

We can use the rotational symmetry of the system to write the displacement field ϕ and electromagnetic field ψ as the following forms:

$$\phi = \sum_{q,,m} f_{q,m}(\vec{r}) \left[b_{q,m} e^{iqr} + b_{-q,m} e^{-iqr} + \text{H.C.} \right] \tag{5.1}$$

$$\psi = \sum_{k,m} g_{k,m}(\vec{r}) \left[c_{k,m} e^{ikr} + c_{-k,m} e^{-ikr} + \text{H.C.} \right] \tag{5.2}$$

where f is a mode profile function, b and c are the annihilation operator for phonon and photons respectively, and q, m are the quantum numbers representing different momentum and angular momentum eigenstates. The interaction between ϕ and ψ comes from acoustic-optical effect: a change in the susceptibility ϵ of the material

because of the strain from the displacement, so it can be calculated as

$$V \approx \int d^3r \frac{1}{2}\frac{\partial\epsilon}{\partial s} s \left|\psi\right|^2, \tag{5.3}$$

where the strain field is related to the displacement field by $s = \partial_r \phi$, where r is the radius of the ring, and we take $\partial\epsilon/\partial s$ to be a constant determined by material properties. In explicit form, the interaction is

$$\begin{aligned} V &= \frac{1}{2}\frac{\partial\epsilon}{\partial s}\int d^3r \sum_{q,m} f_{q,m}(\vec{r}) iq \left(b_{q,m}e^{iqr} - b_{-q,m}e^{iqr}\right) \\ &\times \sum_{k,k',m,m'} g_{k,m}(\vec{r}) g_{k',m'}(\vec{r}) \frac{\hbar\sqrt{\omega_k\omega_{k'}}}{2\epsilon(\mathrm{Vol})} \left[c_{k,m}c_{k',m'}e^{i(k+k')r} + c_{k,m}c^\dagger_{k',m'}e^{i(k-k')r} + \mathrm{H.C.}\right], \end{aligned} \tag{5.4}$$

where Vol is the effective mode volume. The integral over the exponential factors gives us a mode-matching condition for different photon-phonon interaction processes, e.g. $b_{q,m}c_{k,m}c^\dagger_{k',m'}$ for creating a new photon from annihilating a phonon and a photon pair.

5.2.2 Quasi-mode picture

We consider two nearby (in frequency) optical modes of the resonator that couple to the vibrational excitations of the underlying medium, through Brillouin acousto-optic scattering. Labelling these modes c_P (for pump) and c (for the higher frequency anti-Stokes probe mode), we write the optomechanical interaction

$$V = \sum_k (b_k + b^\dagger_{-k})(\lambda^*_k c^\dagger_P c + \lambda_k c^\dagger c_P) + \ldots c^\dagger_P c_P + \ldots c^\dagger c. \tag{5.5}$$

where λ_k describes coupling between these modes, which will naturally account for quasi-phase matching and other constraints. The terms with elipses in front we

neglect due to a lack of phase-matching.

Upon strong optical pumping of the c_P mode, we can look at the fluctuation away from the classical steady state with amplitude α, $c_P \to \alpha + c_P$, and similarly for b_k. Thus, at order $\alpha \gg 1$, we find (with a trivial gauge transform of c) [21, 24]

$$V_\alpha = \sum_k \alpha\lambda_k(b_k + b_{-k}^\dagger)(c + c^\dagger) \tag{5.6}$$

where now $\lambda_k \in \mathbb{R}$. We define the pump-enhanced coupling $\Lambda_k = |\alpha\lambda_k|$.

Let us single out two high Q mechanical modes representing a time-reversed pair of interest, which has an intrinsic degeneracy for clockwise (CW) and counter-clockwise (CCW) propagation, relabeling them a_+ and a_-. These are also coupled to the b_k modes in a quasi-mode theory of mechanical damping. We have c coupled to a_+ but not to a_-, again due to phase matching (momentum conservation). The scattering of phonons off disorder within the material can mix phonons with different momenta [133], but we neglect the same-same scattering $b_k \leftrightarrow a_+$ since it does not break chiral symmetry, and so should be included in the definition of the achiral modes. The only relevant term is the $b_k \leftrightarrow a_-$ scattering. We now want to understand the mediated interaction between a_- and c through the coupling the bulk modes b_k.

Moving to the Fourier domain, and adding a weak thermalization of b_k modes with rate η, we have the equations of motion in the rotating wave approximation ($\Delta < 0, |\Delta| \gg \kappa$) [39, 46, 134]:

$$-i\nu c = i\Delta c - \kappa/2 c + \sqrt{\kappa} c_{in} - i\sum_k \Lambda_k b_k \tag{5.7a}$$

$$-i\nu a_- = -i\omega_m a_- - i\sum_k \mu_k b_k \tag{5.7b}$$

$$-i\nu b_k = -i\omega_k b_k - \eta/2 b_k + \sqrt{\eta} b_{k,in} - i\Lambda_k c - i\mu_k a_- \tag{5.7c}$$

with ν the Fourier frequency, ω_m the mechanical frequency, κ the optical damping, μ_k the coupling between a_- and b_k.

We can solve the b_k equation, getting

$$\begin{aligned} -i\sum_k \Lambda_k b_k \quad &= -i\sum_k \Lambda_k \frac{\sqrt{\eta} b_{k,in} - i\Lambda_k c - i\mu_k a_-}{i(\omega_k - \nu) + \eta/2} \\ &= -\alpha^2 \sum_k \frac{\lambda_k^2}{i(\omega_k - \nu) + \eta/2} c \\ &\quad - \alpha \sum_k \frac{\lambda_k \mu_k}{i(\omega_k - \nu) + \eta/2} a_- + \sqrt{\Gamma} b_{in} \end{aligned} \tag{5.8}$$

where we define a new input field

$$\sqrt{\Gamma} b_{in} \equiv -i\alpha \sum_k \lambda_k \frac{\sqrt{\eta}}{i(\omega_k - \nu) + \eta/2} b_{k,in} \tag{5.9}$$

We see that the c equation Eq. (5.7a) has a new damping term due to the real part of the sum over k. Converting the sum to an integral over bath frequencies $\sum_k = \int \rho(\omega) d\omega$, we can perform the integral within the rotating wave approximation (allowing us to take the lower bound of frequencies to minus infinity) and recover

$$\begin{aligned} \sum_k \frac{\lambda_k^2}{i(\omega_k - \nu) + \eta/2} &= \int \rho(\omega) \lambda(\omega)^2 \frac{1}{i(\omega - \nu) + \eta/2} d\omega \\ &= \pi \rho(\nu) \lambda(\nu)^2 + \mathcal{P}(\ldots) \end{aligned} \tag{5.10}$$

where we have the principal value part of the integral leading to a frequency shift, while the other component leads to decay of the c mode. This defines $\Lambda = 2\pi\alpha^2 \rho(\nu)\lambda(\nu)^2$. We also get a damping of a_-, $\gamma_{a_-} = 2\pi\rho(\nu)\mu(\nu)^2$, which leads to the backscatter-

induced loss of phonons. However, there is a cross term in the damping,

$$\alpha\chi \equiv \alpha 2\pi\lambda(\nu)\mu(\nu)\rho(\nu) \tag{5.11}$$

suggesting interference between two decay pathways. We can understand that the effective c and a_- equations of motion are generated by an effective Hamiltonian with two imaginary terms for damping:

$$-i\kappa/2c^\dagger c - i\left(\sqrt{\Lambda}c + \sqrt{\gamma_{a_-}}a_-\right)^\dagger\left(\sqrt{\Lambda}c + \sqrt{\gamma_{a_-}}a_-\right)/2 \tag{5.12}$$

That is, damping occurs for a superposition of the c and a_- mode.

5.2.3 Simpler version of the model

This relatively complicated model above can be reduced in the rotating-wave approximation (RWA), narrowband limit to a much simpler model. Specifically, let us define a new self-consistent quasi-mode b. We then have for its equation of motion

$$-i\nu b = -i\nu b - \Gamma/2b + \sqrt{\Gamma}b_{in} - i(\alpha\tilde{\lambda}c + \tilde{g}a_-) \tag{5.13}$$

where we see that the frequency dependence drops out – due to the continuum nature of the actual b_k modes. We get the same physics as the above model if we take $\gamma_b = \frac{\pi}{\rho}$. The continuum model of the quasi-mode also suggests that its damping rate is large compared to the intrinsic damping rate for phonons: $\Gamma \gg \gamma_b$.

We can arrive at a simper description of the system by defining the quasi-mode b from the continuum model and by using the rotating-wave approximation(RWA) in the narrowband limit. The system supports both degenerate clock-wise (CW)

and counter clock-wise (CCW) phonons because of rotational symmetry, so we have the high-Q mechanical modes $a_\pm$ and the lossy quasi-modes $b_\pm$, with + stands for CW mode and − stands for CCW mode. We make the following assumptions based on the continuum model:

1. phonon backscattering occurs between high-Q mode and the quasi-mode ($a_+ \longleftrightarrow b_-$, $a_- \longleftrightarrow b_+$) with strength V_0, and between modes of the same type ($a_+ \longleftrightarrow a_-$, $b_+ \longleftrightarrow b_-$) with strength V_1.

2. the forward (reverse) optical mode $c_{+(-)}$ couples to the high-Q mode $a_{+(-)}$ and the quasi-mode $b_{+(-)}$ with different weights. The forward optical mode c_+ couples to a_+ via direct optomechanical interaction with strength $G = \alpha\lambda$ and couples to the quasi-mode with strength αg_0, and the backward optical mode c_- couples to a_- with strength $\beta\lambda$ and couples to the quasi-mode with strength βg_0.

3. the mechanical modes $a_{+(-)}$ and $b_{+(-)}$ have different damping rates γ and Γ with $\gamma \ll \Gamma$, but the damping is symmetric between the $\pm$ modes. We also assume that Γ is in the same order as the optical loss rate κ, both of which are much larger than γ.

A model with these assumptions is shown below in Fig. 5.2(a), and its effective hamiltonian of the system is given by

$$\begin{aligned} H_{\text{eff}} &= -\Delta(c_+^\dagger c_+ + c_-^\dagger c_-) + \omega_m(a_+^\dagger a_+ + a_-^\dagger a_-) + \omega_b(b_+^\dagger b_+ + b_-^\dagger b_-) + \alpha c_+^\dagger(\lambda a_+ + g_0 b_+) + \text{h.c.} \\ &\quad +\beta c_-^\dagger(\lambda a_- + g_0 b_-) + \text{h.c.} + V_0(a_+^\dagger b_- + a_-^\dagger b_+ + \text{h.c.}) + V_1(a_+^\dagger a_- + b_+^\dagger b_- + \text{h.c.}) \end{aligned}$$

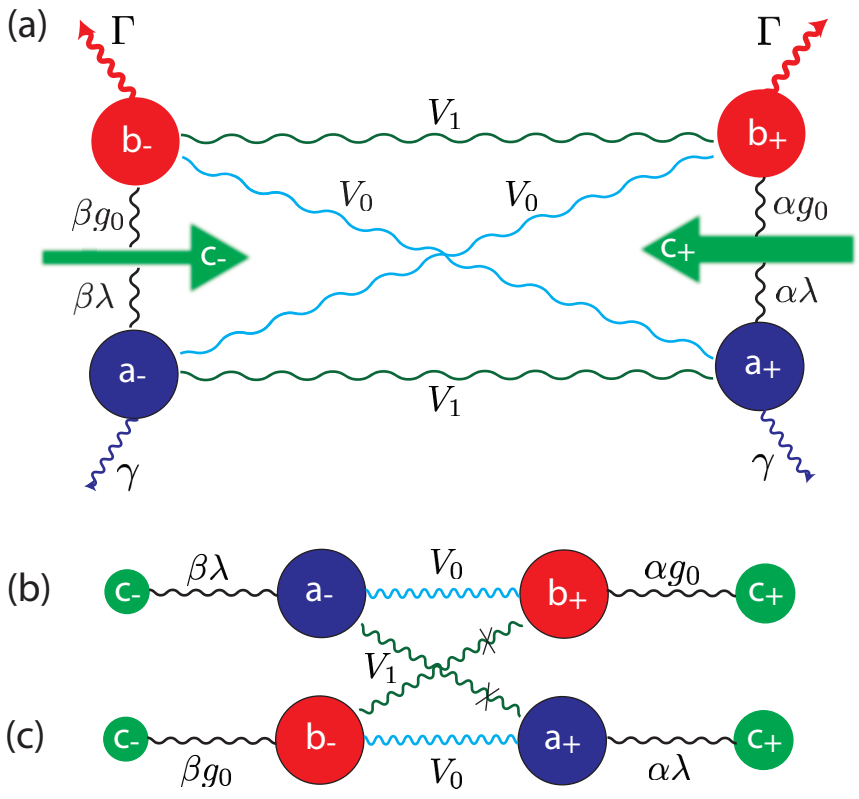

Figure 5.2: Simplified multi-mode theory of optomechanical interaction and phonon scattering. (a) For each propagating direction, a quasi-mode b and a particular mode a are coupled to the driving field c with different rates. Phonon back-scattering happens between the two directions. (b-c): We neglect the phonon scattering between the same species (the V_1 lines) and also assume that the optical driving fields couple to the quasi-mode and particular mode separately, since the driving field is very strong. With these assumptions, we can break the loop in a into two sub diagrams.

$$-i\frac{\kappa}{2}(c_+^\dagger c_+ + c_-^\dagger c_-) - i\frac{\gamma}{2}(a_+^\dagger a_+ + a_-^\dagger a_-) - i\frac{\Gamma}{2}(b_+^\dagger b_+ + b_-^\dagger b_-), \tag{5.14}$$

where the optical and mechanical loss are modeled by anti-Hermitian hamiltonian. Here we used a nominal frequency ω_b for the quasi-modes $b_\pm$, but when we go to the

Fourier domain, its frequency dependence will drop out, in the sense that $\omega_b \to \nu$.

While the dynamics of the system can, in principle, be solved numerically, the loop structure in this coupled six-mode system will make the result quite complicated and it is hard for us to interpret the main physics in the system. We assume the g_0 parameter is larger than λ, such that the optical field couples more strongly to the bulk modes $b_\pm$. We can then break the loop into two pieces by cutting the wavy lines representing V_1 interactions, both of which consists of two mechanical modes and two optical modes, as shown in Fig. 5.2(b-c).

5.3 System dynamics

5.3.1 Linear response

We now focus on Fig. 5.2(b) and Fig. 5.2(c) to calculate the linewidth for forward phonon a_+ and backward phonon a_-. In the experiment [Appendix D], the reverse pump power is about 10 times smaller than that of forward pump, so we neglect the effect of reverse optical mode c_- first. For Fig. 5.2(b), as shown in our toy model, we have

$$\begin{aligned} H_{\text{toy}} &= -\Delta(c_+^\dagger c_+ + c_-^\dagger c_-) + \omega_m a_-^\dagger a_- + \omega_b b_+^\dagger b_+ \\ &\quad + \alpha g_0(c_+^\dagger b_+ + b_+^\dagger c_+) + \beta\lambda(a_- c_-^\dagger + c_-^\dagger a_-) \\ &\quad + V_0(a_-^\dagger b_+ + b_+^\dagger a_-) - i\frac{\kappa}{2}(c_+^\dagger c_+ + c_-^\dagger c_-) \\ &\quad - i\frac{\gamma}{2}a_-^\dagger a_- - i\frac{\Gamma}{2}b_+^\dagger b_+. \end{aligned} \tag{5.15}$$

We write down the Heisenberg-Langevin equations for each mode and transform to frequency domain to solve the equations.

$$-i\nu c_+ = i\Delta c_+ - \frac{\kappa}{2}c_+ + \sqrt{\kappa}c_+^{\text{in}} - i\alpha g_0 b_+, \tag{5.16a}$$

$$-i\nu c_- = i\Delta c_- - \frac{\kappa}{2}c_- + \sqrt{\kappa}c_-^{\text{in}} - i\beta\lambda a_-, \tag{5.16b}$$

$$-i\nu a_- = -i\omega_m a_- - \frac{\gamma}{2}a_- + \sqrt{\gamma}a_-^{\text{in}} - i\beta\lambda c_- - iV_0 b_+, \tag{5.16c}$$

$$-i\nu b_+ = -i\nu b_+ - \frac{\Gamma}{2}b_+ + \sqrt{\Gamma}b_+^{\text{in}} - i\alpha g_0 c_+ - iV_0 a_-. \tag{5.16d}$$

As shown before, the frequency dependence of the quasi-mode $b_\pm$ drops out in the Fourier domain. We now proceed to eliminate c_+, c_- and b_+ to understand the behavior of a_-. From the equation for b_+ Eq. (5.16d) we have

$$b_+ = \frac{\sqrt{\Gamma}b_+^{\text{in}} - i\alpha g_0 c_+ - iV_0 a_-}{\Gamma/2} \tag{5.17}$$

plug this into the equation for c_+, we have an equation which only relates c_+ and a_-:

$$\left[-i(\nu+\Delta)+\kappa/2\right]c_+ = \sqrt{\kappa}c_+^{\text{in}} - i\alpha g_0 \frac{\sqrt{\Gamma}b_+^{\text{in}} - i\alpha g_0 c_+ - iV_0 a_-}{\Gamma/2} \tag{5.18}$$

This simplifies to

$$\left[-i(\nu+\Delta)+\kappa/2+\frac{\alpha^2 g_0^2}{\Gamma/2}\right]c_+ = \sqrt{\kappa}c_+^{\text{in}} - i\frac{\alpha g_0}{\sqrt{\Gamma}/2}b_+^{\text{in}} - \frac{\alpha g_0 V_0}{\Gamma/2}a_- \tag{5.19}$$

From the left hand side of the equation, we see an optomechanical modification to the damping rate for c_+. Also, the c_+ mode is effectively coupled to the a_- mode via the interaction with b_+, which means the properties of a_- could possibly be

modified by a driving field in the opposite direction. We are going to analyze this in more details in following section. We further define the susceptibility of c_+ as $\tilde{\kappa} \equiv -i(\nu+\Delta)+\kappa/2+2\alpha^2 g_0^2/\Gamma$, then

$$c_+ = \frac{\sqrt{\kappa}c_+^{\rm in} - i\frac{\alpha g_0}{\sqrt{\Gamma}/2}b_+^{\rm in} - \frac{\alpha g_0 V_0}{\Gamma/2}a_-}{\tilde{\kappa}}. \tag{5.20}$$

We now put this optical field back into the b_+ equation, we get

$$\begin{aligned} b_+ &= \frac{\sqrt{\Gamma}b_+^{\rm in} - i\alpha g_0 \frac{\sqrt{\kappa}c_+^{\rm in} - i\frac{\alpha g_0}{\sqrt{\Gamma}/2}b_+^{\rm in} - \frac{\alpha g_0 V_0}{\Gamma/2}a_-}{\tilde{\kappa}} - iV_0 a_-}{\Gamma/2} \\ &= \frac{1}{\sqrt{\Gamma}/2}\left(1-\frac{\alpha^2 g_0^2}{\Gamma\tilde{\kappa}/2}\right)b_+^{\rm in} - \frac{i\alpha g_0\sqrt{\kappa}}{\Gamma\tilde{\kappa}/2}c_+^{\rm in} \\ &\quad -\frac{iV_0}{\Gamma/2}\left(1-\frac{\alpha^2 g_0^2}{\Gamma\tilde{\kappa}/2}\right)a_-. \end{aligned} \tag{5.21}$$

The equation for c_-

$$c_- = \frac{\sqrt{\kappa}c_-^{\rm in} - i\beta\lambda a_-}{-i(\nu+\Delta)+\kappa/2}, \tag{5.22}$$

which indicates that c_- is only modified by the coupling to a_-. We can put b_+ and c_- back into the equation for a_-, and get

$$\begin{aligned} \chi_-^{-1}a_- &= \sqrt{\gamma}a_-^{\rm in} - \frac{i\beta\lambda\sqrt{\kappa}}{-i(\nu+\Delta)+\kappa/2}c_-^{\rm in} - \frac{V_0\alpha g_0\sqrt{\kappa}}{\Gamma\tilde{\kappa}/2}c_+^{\rm in} \\ &\quad -\frac{iV_0}{\sqrt{\Gamma}/2}\left(1-\frac{\alpha^2 g_0^2}{\Gamma\tilde{\kappa}/2}\right)b_+^{\rm in} \end{aligned} \tag{5.23}$$

where

$$\begin{aligned} \chi_-^{-1} &= -i(\nu-\omega_m)+\gamma/2+\frac{\beta^2\lambda^2}{-i(\nu+\Delta)+\kappa/2} \\ &\quad +\frac{V_0^2}{\Gamma/2}\left(1-\frac{\alpha^2 g_0^2}{\Gamma\tilde{\kappa}/2}\right) \end{aligned} \tag{5.24}$$

is the susceptibility of a_- to input fiels.

Similarly, for the forward phonon mode a_+, we can find its equation of motion by interchanging α with β, a_+ with a_-, and c_+ with c_-:

$$\begin{aligned}\chi_+^{-1}a_+ &= \sqrt{\gamma}a_+^{\rm in} - \frac{i\alpha\lambda\sqrt{\kappa}}{-i(\nu+\Delta)+\kappa/2}c_+^{\rm in} - \frac{V_0\beta g_0\sqrt{\kappa}}{\Gamma\tilde{\kappa}'/2}c_-^{\rm in} \\ &\quad -\frac{iV_0}{\sqrt{\Gamma}/2}\left(1-\frac{\beta^2 g_0^2}{\Gamma\tilde{\kappa}'/2}\right)b_-^{\rm in}\end{aligned} \tag{5.25}$$

with $\tilde{\kappa}' \equiv -i(\nu+\Delta)+\kappa/2+2\beta^2 g_0^2/\Gamma$ and

$$\begin{aligned}\chi_+^{-1} &= -i(\nu-\omega_m)+\gamma/2+\frac{\alpha^2\lambda^2}{-i(\nu+\Delta)+\kappa/2} \\ &\quad +\frac{V_0^2}{\Gamma/2}\left(1-\frac{\beta^2 g_0^2}{\Gamma\tilde{\kappa}'/2}\right)\end{aligned} \tag{5.26}$$

5.3.2 Phonon linewidth

We can define the cooperativities as $\mathcal{C}_\alpha = 4\alpha^2 g_0^2/\Gamma\kappa$ and $\mathcal{C}_\beta = 4\beta^2 g_0^2/\Gamma\kappa$, which are both dimensionless parameters describing the strength of optomechanical coupling of the quasi-modes relative to cavity decay rate and mechanical damping rate.

The modified linewidth of the $a_\pm$ phonons, as a result of optomechanical cooling/heat, is given by the real part of its susceptibility, so we have

$$\begin{aligned}\gamma_{a_+}(\nu) &= 2{\rm Re}(\chi_{a_+}^{-1}(\nu)) \\ &= \gamma+\frac{\alpha^2\lambda^2\kappa}{(\nu+\Delta)^2+\kappa^2/4} \\ &\quad +\frac{4V_0^2}{\Gamma}\left[1-\frac{2\beta^2 g_0^2}{\Gamma}\frac{(1+\mathcal{C}_\beta)\kappa/2}{(\nu+\Delta)^2+(1+\mathcal{C}_\beta)^2\kappa^2/4}\right],\end{aligned} \tag{5.27}$$

and

$$\gamma_{a_-}(\nu) = 2{\rm Re}(\chi_{a_-}^{-1}(\nu))$$

$$= \gamma + \frac{\beta^2\lambda^2\kappa}{(\nu+\Delta)^2+\kappa^2/4} + \frac{4V_0^2}{\Gamma}\left[1 - \frac{2\alpha^2 g_0^2}{\Gamma}\frac{(1+\mathcal{C}_\alpha)\kappa/2}{(\nu+\Delta)^2+(1+\mathcal{C}_\alpha)^2\kappa^2/4}\right], \tag{5.28}$$

For the special case of $\nu = -\Delta$, we have

$$\gamma_{a_+} = \gamma + \frac{4\alpha^2\lambda^2}{\kappa} + \frac{4V_0^2}{\Gamma}\frac{\kappa}{\kappa + 4\beta^2 g_0^2/\Gamma} \tag{5.29a}$$

$$= \gamma + \frac{4\alpha^2\lambda^2}{\kappa} + \frac{4V_0^2}{\Gamma}\frac{1}{1+\mathcal{C}_\beta}, \tag{5.29b}$$

$$\gamma_{a_-} = \gamma + \frac{4\beta^2\lambda^2}{\kappa} + \frac{4V_0^2}{\Gamma}\frac{\kappa}{\kappa + 4\alpha^2 g_0^2/\Gamma} \tag{5.29c}$$

$$= \gamma + \frac{4\beta^2\lambda^2}{\kappa} + \frac{4V_0^2}{\Gamma}\frac{1}{1+\mathcal{C}_\alpha}. \tag{5.29d}$$

This shows that the phonon linewidth has a strong dependence on the optomechanical cooperativities and thus on the optical driving strength α and β.

5.3.3 Frequency shift

The modification of mechanical linewidth (cooling or heating) can come with a change in the effective phonon resonant frequency, since a complex term is added to the phonon susceptibility due to the optomechanical coupling. The change in phonon frequency is related to the imaginary part of the susceptibility, and is calculated as

$$\delta\omega_{a_+}(\nu) = \frac{\alpha^2\lambda^2(\nu+\Delta)}{(\nu+\Delta)^2+\kappa^2/4} + \frac{2V_0^2}{\Gamma}\frac{2\beta^2 g_0^2}{\Gamma} \times \frac{\nu+\Delta}{(\nu+\Delta)^2+(1+\mathcal{C}_\beta)^2\kappa^2/4}, \tag{5.30}$$

$$\delta\omega_{a_-}(\nu) = \frac{\beta^2\lambda^2(\nu+\Delta)}{(\nu+\Delta)^2+\kappa^2/4} + \frac{2V_0^2}{\Gamma}\frac{2\alpha^2 g_0^2}{\Gamma} \times \frac{\nu+\Delta}{(\nu+\Delta)^2+(1+\mathcal{C}_\alpha)^2\kappa^2/4}. \tag{5.31}$$

The maximum frequency shift occurs when $\nu = -\Delta + \kappa/2$,

$$\delta\omega_{a_+}(-\Delta+\kappa/2) = \frac{\alpha^2\lambda^2}{\kappa} + \frac{2V_0^2}{\Gamma}\frac{\mathcal{C}_\beta}{1+(1+\mathcal{C}_\beta)^2}, \tag{5.32}$$

$$\delta\omega_{a_-}(-\Delta+\kappa/2) = \frac{\beta^2\lambda^2}{\kappa} + \frac{2V_0^2}{\Gamma}\frac{\mathcal{C}_\alpha}{1+(1+\mathcal{C}_\alpha)^2}. \tag{5.33}$$

The second term of the frequency shift is of second order, so the main contribution comes from the first term, which is 1/4 of the optically induced damping rate $4\alpha^2\lambda^2/\kappa$. In [Appendix D], the observed largest optomechanical damping rate is about $40 \sim 50$ kHz , so the frequency shift is at most 12.5 kHz. The cavity linewidth is 5.2 MHz and the detuning of the anti-Stoke line ranges from 0.2 MHz to 0.7 MHz at high power, which makes the frequency shift almost negligible.

If the phase matching condition is satisfied, then we expect $\Delta \approx -\omega_m$. In this case, when we look at the frequency shift near original mechanical frequency $\nu \approx \omega_m$, we get $\nu + \Delta \approx 0$ and the frequency shift becomes completely negligible.

5.3.4 Effective temperature

Another important feature is the reduction in the effective temperature of the a_- mode, because of coherent damping. We look at the right hand side of equation (number) and assume that the optical noise is negligible compared to the thermal noise. We have the effective noise on a_- as

$$\sqrt{\gamma}a_-^{\text{in}} - \frac{iV_0}{\sqrt{\Gamma}/2}\left(1 - \frac{\alpha^2 g_0^2}{\Gamma\tilde{\kappa}/2}\right) b_+^{\text{in}} \tag{5.34}$$

The effective temperature of mode a_- is thus

$$T_{a_-}^{\text{eff}} = \frac{1}{\gamma_{a_-}}\left[\gamma T_{a_-} + \frac{V_0^2}{\Gamma/4}\left|1 - \frac{\alpha^2 g_0^2}{\Gamma\tilde{\kappa}/2}\right|^2 T_{b_+}\right]$$

$$= \frac{1}{\gamma_{a_-}}\left[\gamma T_{a_-} + \frac{4V_0^2}{\Gamma}\frac{(\nu+\Delta)^2+\kappa^2/4}{(\nu+\Delta)^2+(\kappa/2+2\alpha^2 g_0^2/\Gamma)^2}T_{b_+}\right] \tag{5.35}$$

When $\nu = -\Delta$, we have

$$\begin{aligned} T_{a_-}^{\text{eff}} &= \frac{1}{\gamma_{a_-}}\left[\gamma T_{a_-} + \frac{4V_0^2}{\Gamma}\frac{\kappa^2/4}{(\kappa/2+2\alpha^2 g_0^2/\Gamma)^2}T_{b_+}\right] \\ &= \frac{1}{\gamma_{a_-}}\left[\gamma T_{a_-} + \frac{4V_0^2}{\Gamma}\frac{1}{(1+\mathcal{C}_\alpha)^2}T_{b_+}\right] \end{aligned} \tag{5.36}$$

We also get similar expressions for the a_+ mode,

$$T_{a_+}^{\text{eff}} = \frac{1}{\gamma_{a_+}}\left[\gamma T_{a_+} + \frac{4V_0^2}{\Gamma}\frac{1}{(1+\mathcal{C}_\beta)^2}T_{b_-}\right]. \tag{5.37}$$

When the reverse pump β is much smaller compared to the forward pump α, this effect is not so significant for the a_+ mode. In general, we get a correction term to the effective temperature, which roughly scales as $1/(1+\mathcal{C}_{\alpha(\beta)})^2$. We plot the cooperativity dependence of the linewidth and temperatures below in Fig. 5.3.

5.3.5 Direct back-scattering corrections

We now consider the direct back scattering between $a_\pm$, with strength V_1, which couples the two systems in Fig. 5.2(b) that we have so far assumed to be independent. We have the hamiltonian as

$$\begin{aligned} H &= \omega_{a_+}a_+^\dagger a_+ + \omega_{a_-}a_-^\dagger a_- + V_1(a_+^\dagger a_- + a_-^\dagger a_+) \\ &\quad -i\frac{\gamma_{a_+}}{2}a_+^\dagger a_+ - i\frac{\gamma_{a_-}}{2}a_-^\dagger a_- \end{aligned} \tag{5.38}$$

Because of this coupling, there is an additional correction to the damping rates,

$$-i\nu a_+ = -i\omega_{a_+}a_+ - \frac{\gamma_{a_+}}{2}a_+ - iV_1 a_- + \sqrt{\gamma_{a_+}}a_+^{\text{in}}$$

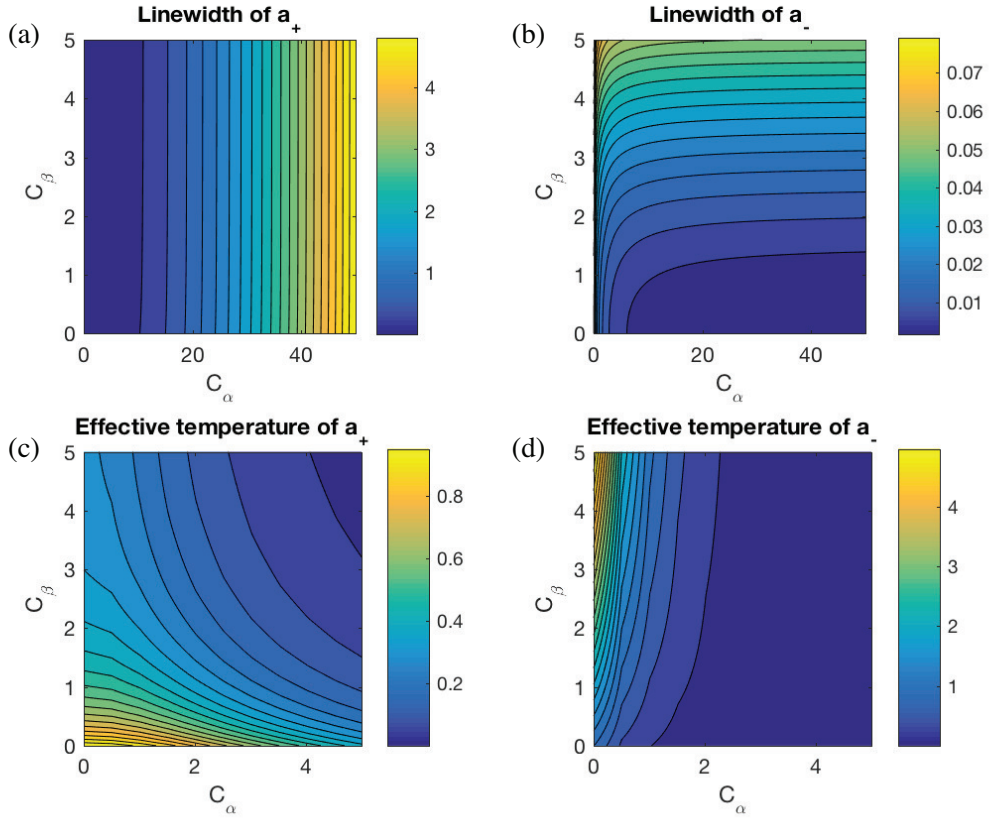

Figure 5.3: Choosing a set of rescaled parameters of $\omega_m = 1$, $\gamma = 0.001$, $\kappa = 0.1$, $\lambda = 0.001$, $g_0 = 0.005$, $\Gamma = 0.05$, $V_0 = 0.02$ and assuming that the initial thermal bath temperature T is the same for all four modes, we plot γ_{a_+}/γ, γ_{a_-}/γ, $T^{\text{eff}}_{a_+}/T$ and $T^{\text{eff}}_{a_-}/T$ in (a)-(d) respectively.

$$-i\nu a_- \;=\; -i\omega_{a_-}a_- - \frac{\gamma_{a_-}}{2}a_- - iV_1 a_+ + \sqrt{\gamma_{a_-}}a^{\text{in}}_-$$

this directly gives the new V_1 interaction corrected linewidth

$$\tilde{\gamma}_{a_+} \;=\; \gamma_{a_+} + \frac{V_1^2\gamma_{a_-}}{(\nu-\omega_{a_-})^2 + \gamma_{a_-}^2/4} \tag{5.40a}$$

$$\tilde{\gamma}_{a_-} \;=\; \gamma_{a_-} + \frac{V_1^2\gamma_{a_+}}{(\nu-\omega_{a_+})^2 + \gamma_{a_+}^2/4} \tag{5.40b}$$

Since the the frequency shift for the mechanical resonators depends on the pump strength, the linewidth of the a_- mode gets smaller when forward pump power increases. However, there is an exception when $\nu = -\Delta$. At this point, the frequency shifts are zero, and ω_{a_+}, ω_{a_-} stay the same, so there is no change to the phonon linewidth when varying the pump power from the direct backscattering.

5.4 Experimental results and data fitting

5.4.1 Description of the chiral phonon experiment

A recent experimental test of this theory [Appendix D], considers a whispering gallery-type resonator with an intrinsic degeneracy for clockwise (CW) and counterclockwise (CCW) propagation for both phonons $a_\pm$ and photons $c_\pm$. Photons occupying the modes in the CW (CCW) direction can be coupled through Brillouin acousto-optic forward scattering from the CW (CCW) phonons. When pumping the lower-energy optical mode, anti-Stokes scattering to the higher mode annihilates phonons in the corresponding direction and leads to unidirectional optomechanical damping [128]. In the experiment, two optical sources are tuned to the lower frequency optical mode in both the CW and CCW directions, with different pump power.While one source is used as a strong pump to induce Brillouin cooling, the function of the second counter-propagating weak source is to merely measure the modification of the high-Q phonon behavior, and the possibility of chiral behavior.

In the experiment, a striking direction-dependence of the damping rates of the CW and CCW phonons was observed, as a result of the momentum conservation

rules described above that underly the Brillouin scattering interaction. The experimental data points are shown in Fig. 5.4 below. Since the relative power of the CW pump and CCW probe lasers in the experiment is $\sim 9:1$, there is some cooling of the a_- phonons as well.

In the following, we try to explain the experimental results obtained in [Appendix D] by fitting the data using the theoretical model of this paper.

5.4.2 Data fitting

First of all, we recall the relation between the amplitudes and pump power is given by

$$\begin{aligned}
\alpha^2 = \frac{P_+\kappa/2\hbar\omega}{\delta^2+\kappa^2/4} &= \frac{2}{\hbar\omega\kappa}\frac{P_+(\kappa/2)^2}{\delta^2+\kappa^2/4} = \frac{2}{\hbar\omega\kappa}\tilde{P}_+ = \eta\tilde{P}_+ \\
\beta^2 = \frac{P_-\kappa/2\hbar\omega}{\delta^2+\kappa^2/4} &= \frac{2}{\hbar\omega\kappa}\frac{P_-(\kappa/2)^2}{\delta^2+\kappa^2/4} = \frac{2}{\hbar\omega\kappa}\tilde{P}_- = \eta\tilde{P}_-
\end{aligned}$$

where $+$ is for CCW direction, $-$ is for CW direction and the coeffecient $\eta = 2/\hbar\omega\kappa$. Also, we consider the case when the reverse pump is much weaker than the forward pump with a ratio $P_+/P_- = \alpha^2/\beta^2 = 9.15$, then we can simplify the expression for the forward linewidth Eq. (5.27) and get

$$\begin{aligned}
\gamma_{a_+} &= \gamma + \frac{4\alpha^2\lambda^2}{\kappa} + \frac{4V_0^2}{\Gamma}\frac{\kappa}{\kappa + 4\beta^2 g_0^2/\Gamma} && (5.41) \\
&\approx \left(\gamma + \frac{4V_0^2}{\Gamma}\right) + \frac{4\alpha^2\lambda^2}{\kappa} \\
&= \gamma_{\text{eff}} + \frac{4\eta\lambda^2}{\kappa}\tilde{P}_+ && (5.42)
\end{aligned}$$

We fit the experimental data for forward phonon linewidth with a linear model of the following form:

$$y_+ = p_0 + p_1 \cdot x, \tag{5.43}$$

where x represents the detuning corrected pump power $\tilde{P}_+$ in units of μW and y represents the linewidth γ_{a_+} in units of kHz. Least square fitting results are shown in Fig. 5.4, and fit values are shown in Table 5.1.

The asymmetry between the strength of the forward and backward pump leads to a qualitatively different result for the backward phonon a_-, with its linewidth given by

$$\gamma_{a_-} \quad = \quad \gamma + \frac{4\beta^2\lambda^2}{\kappa} + \frac{4V_0^2}{\Gamma}\frac{\kappa}{\kappa + 4\alpha^2 g_0^2/\Gamma}. \tag{5.44}$$

The α^2 term can be large, and it is this term that leads to a substantial linewidth reduction for the backward phonon as we increase the forward pump power.

For the low power data, the ratio $r = \alpha^2/\beta^2$ is fixed at 9.15, but for the high power data, β itself is fixed at certain value β_0. For data taken under different conditions, we may have a discontinuous change in the reverse pump power. So we can use a piecewise function to describe the relation between the two pumps as:

$$\beta^2 = (\alpha \leq \alpha_0)\ \alpha^2/r + (\alpha > \alpha_0)\ s\alpha_0^2. \tag{5.45}$$

We can use a corresponding piecewise function to describe the data for the broadened linewidth at low power:

$$y_- = q_0 + q_1 \cdot x, \quad \text{for } (x < P_0). \tag{5.46}$$

This separate fitting for low power data and high power data is shown below in Fig. 5.4.

The fitting parameters are given below in the Table 5.1. For the forward propagating direction, the parameter $\vec{p} = (p_0, p_1)$ is quite consistent between low power and high power data. For the backward propagating direction, the situation is more complicated. From the lower power data, we can only get enough information about q_1 and q_2. At high power, the fitting would nominally take a form (based upon Eq. (5.44))

$$y_+ = q_2 + \frac{q_3}{q_4 + x} \tag{5.47}$$

However, fitting q_3, q_4 as well as β_0, leads to substantial correlation and likely overfitting. Instead, we focus on a simpler model at high power to capture the reduction of linewidth. Specifically, we fix $q_2 = q_0 + \alpha_0 q_1$ from the low power data, and set $q_4 = 0$.

5.5 Conclusion

In this article, we present a model for optomechanically induced chiral phonon behavior. We show that in Brillouin cooling experiments on traveling phonon populations, the linewidth of CW phonons is increased by the optomechanical interaction with optical driving fields, while the linewidth of CCW phonons is decreased at the same time. We also predict the effective temperature of CCW phonon will decrease by increasing the driving fields, which is in contrast to conventional optomechanical cooling where phonon linewidth and effective temperature move in different direc-

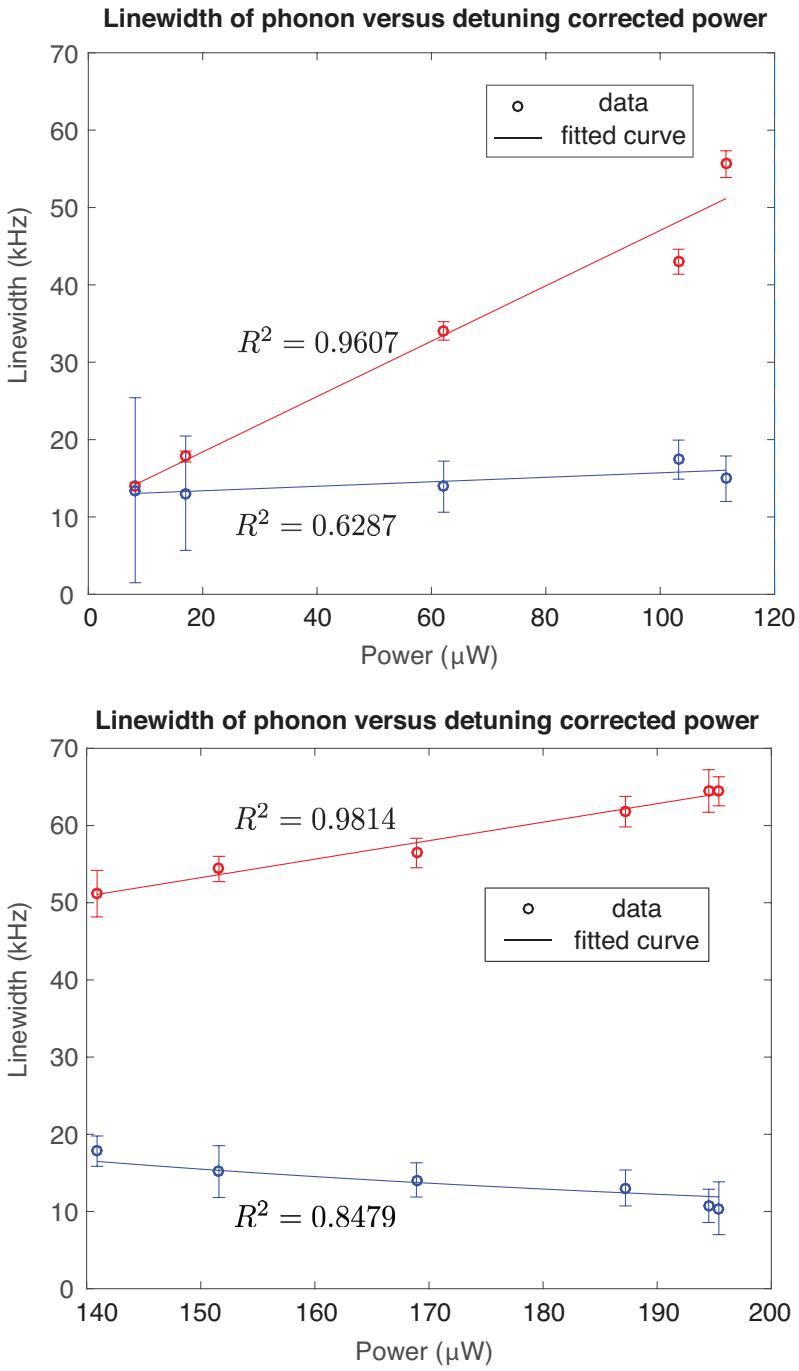

Figure 5.4: Red is for CCW phonon and blue is for CW phonon. Upper figure is for low power data and lower figure is for high power data. Experimental data points (in circles) are taken from [Appendix D].

Table 5.1: Fitting parameters

parameter (units)	value (low)	error (low)	value (high)	error (high)
$p_0 = \gamma_{\text{eff}}$ (kHz)	11.25	(1.42, 21.08)	17.31	(9.33, 25.29)
$p_1 = 4\eta\lambda^2/\kappa$ (kHz/μW)	0.36	(0.23, 0.49)	0.24	(0.19, 0.29)
$q_0 = \gamma$ (kHz)	12.8	(9.78, 15.83)	NA	NA
$q_1 = 4\eta\lambda^2/\kappa r$ (kHz/μW)	0.029	$(-0.012, 0.070)$	NA	NA
$q_3 = \kappa V_0^2/\eta g_0^2$ (kHz $\cdot$ μW)	NA	NA	2324	$(2130, 2517)$

tions. This model is able to explain the chiral behavior of phonon transport observed in a recent experiment [Appendix D].

Chapter 6: Multi-mode theory of chiral phonons

6.1 Introduction

Optomechanics, in the form of directional light-matter coupling via Brillouin scattering as a result of momentum conservation, leads to the symmetry breaking of light propagation [135–139]. These studies suggest new ways of building on-chip optical isolation device, which is important for applications in optical quantum computation [140, 141] and quantum simulations [142]. Similarly, we can imagine that the directional optomechanical interaction can also leads to the nonreciprocal transport of phonons. In the presence of phonon-phonon scattering via disorder/impurity, however, the transport properties of phonons traveling in both directions can be modified by the optics simultaneously. In a recent paper [Appendix D], actually, chiral transport of phonons has been observed in a whispering-gallery type microsphere resonator, due to acoustic-optic coupling and phonon scattering via impurities. Their experiment shows that the linewidth of clockwise and counter-clockwise phonons is modified in opposite ways at the same time.

A minimal theory for explaining the chiral phonons effect observed in [Appendix D] is possible with just a few assumptions. We assume that there are two optical modes (control and probe) and two phonon modes (forward and backward

propagating) in the system, so Brillouin scattering can be stimulated in the system [143, 144] and phonons can backscatter into each other via impurity/disorder induced scattering. A directional coupling to the optical fields optomechanically cools phonons in one direction [9, 11], while phonons in the other direction do not experience this optical modification directly because of phase unmatching. When considering a series of random phonon scattering processes which cause phonon diffusion [133], the asymmetry in the free phonon propagation due to optomechanical coupling eventually leads to the chiral behavior for phonon transport.

We propose a general multi-mode photon-phonon coupling and phono-phonon scattering model to show why this chiral transport is possible. In Sec II, we consider a model where multiple phonon modes are coupled to the optical mode at the same time, with different weights, due to phase matching. We also consider phonon-phonon scattering via impurity, with the introduction of a random scattering potential. Subsequently, in Sec III, we use an effective hamiltonian to find the linear response of phonons. In particular, we consider the case where only a few phonons are strongly coupled to the optical mode, and we use numerical simulation of the scattering potential to find the linear response function. The result is in agreement with a toy model of only two phonons and one photon, where the linewidth for the optically cooled mode is broadening, while the linewidth for the other mode is narrowing, with the increase of optical power. Finally, in Sec IV, we use perturbation expansion to calculate the phonon linear response of a multi-mode coupled system to find the phonon linewidth, and make some connections to the phonon diffusion.

6.2 Multi-mode theory of optomechanical interaction and phonon-phonon scattering

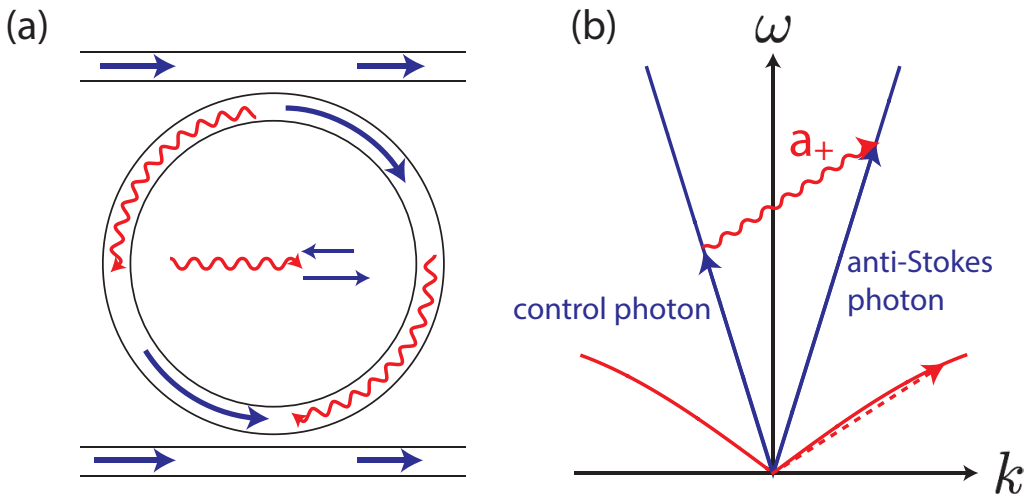

Figure 6.1: (a) Schematic of the ring waveguide resonator that supports two counter-propagating optical modes a_{L}, a_{R} and continuum of phonon modes $b_{\mathbf{q}}, b_{-\mathbf{q}}$. (b) The dispersion relation curves for photon (blue line) and acoustic phonon (red curves). An pump photon is scattered by an incoming phonon and produce a backward propagating photon at a higher energy. Both momentum and energy are conserved in this anti-Stokes Brillouin scattering process.

We consider a continuum theory for a quasi one dimensional waveguide resonator that supports photons and phonons at the same time. The phonons are subject to periodic boundary conditions (PBC) and the photons are send into the waveguide through evanescent coupling to a tapered optical fiber. The probe field is blue detuned from the control field with $\Delta = \omega_c - \omega_p$. Brillouin scattering is

possible by absorbing a phonon and a control photon and subsequently creating an anti-Stokes probe photon, as shown in Fig. 6.1.

The phonon modes in the waveguide could be understood as the second quantized form of the displacement field of the material. In the quasi-1D limit when the dimension of the cross section of the waveguide is small compared to the radius of the ring r_0, the displacement field in the longitudinal direction is described by $\boldsymbol{u} = u(x,t) = u(\theta,t)$. The Lagrangian of the system reads:

$$L = \int_0^{2\pi r_0} \mathcal{L} \mathrm{d}x = \int_0^{2\pi} \mathcal{L}_\theta \mathrm{d}\theta, \tag{6.1}$$

where the Lagrangian density is

$$\mathcal{L}_\theta = \frac{1}{2}\left[\rho_\theta (\partial_t u)^2 - \frac{Y}{r_0}(\partial_\theta u)^2\right], \tag{6.2}$$

ρ_θ is the density per unit angle and Y is the Young's modulus. The conjugate momentum is defined as

$$\pi = \frac{\partial \mathcal{L}_\theta}{\partial(\partial_t u)} = \rho_\theta \partial_t u, \tag{6.3}$$

so the Hamiltonian density is

$$\mathcal{H} = \pi \partial_t u - \mathcal{L}_\theta = \frac{1}{2}\left[\frac{\pi^2}{\rho_\theta} + \frac{Y}{r_0}(\partial_\theta u)^2\right]. \tag{6.4}$$

We now go to momentum space and expand u, π as:

$$u(\theta,t) = \sum_q u_q e^{iqr_0\theta}, \tag{6.5a}$$

$$\pi(\theta,t) = \sum_q \pi_q e^{iqr_0\theta}. \tag{6.5b}$$

The Hamiltonian is then integrated as

$$H = \int_0^{2\pi} \mathcal{H} \mathrm{d}\theta = 2\pi \sum_q \left(\frac{\pi_q \pi_{-q}}{2\rho_\theta} + \frac{1}{2}\rho_\theta \Omega_q^2 u_q u_{-q}\right) \tag{6.6}$$

where $\Omega_q = qv_s = q\sqrt{Y/\rho} = q\sqrt{Yr_0/\rho_\theta}$. Since π and u are both hermitian operators, we have $\pi_q^\dagger = \pi_{-q}$ and $u_q^\dagger = u_{-q}$. We can then define the following annihilation operator

$$b_q = \sqrt{\frac{\rho_\theta \Omega_q}{2\hbar}} \left(u_q + i \frac{1}{\rho_\theta \Omega_q} \pi_q \right). \tag{6.7a}$$

The Hamiltonian can be described by a set of decoupled quantum harmonic oscillators, namely phonons modes

$$H_{\text{phonon}} = 2\pi \sum_q \Omega_q b_q^\dagger b_q. \qquad (\hbar = 1) \tag{6.8}$$

We note that the phonon group velocity v_s is assumed constant, because we only consider the long wavelength phonons in the accoustic branch, as show in Fig. (6.1).

$$H_{\text{phonon}} = \sum_q \Omega_q b_q^\dagger b_q \tag{6.9}$$

The electric field of the optical mode in the resonator could be also be expanded as [39]

$$E(t, \theta) = \sum_k \sqrt{\frac{\hbar \omega_k}{2\epsilon V}} a_k e^{ikr_0\theta} + \text{h.c.}, \tag{6.10}$$

where ϵ is the susceptibility of the medium, $V = 2\pi r_0 A$ is the volume of the waveguide, a_k is the annihilation operator for mode k in the Heisenberg picture, and $\omega_k/2\pi$ is its frequency. The Hamiltonian of the optical field in second quantized form is

$$H_{\text{photon}} = \sum_k \omega_k a_k^\dagger a_k, \tag{6.11}$$

which represents a sum of independent quantum harmonic oscillators. Using periodic boundary conditions, we find that $\omega_k = n_k c/r_0$.

The interaction between mechanical motion and electromagnetic field comes from acoustic-optical effect: a change in the susceptibility of the material because of the strain from the displacement, so it could be calculated as

$$H_{\text{int}} \approx \int \frac{1}{2}\frac{\partial \epsilon}{\partial s} s \left|\mathcal{E}\right|^2 r_0 A \mathrm{d}\theta. \tag{6.12}$$

The strain field is related to the displacement field by $s = \partial_x u = \partial_\theta u / r_0$ and we take $\partial\epsilon/\partial s$ to be a constant determined by material properties. In explicit form, the interaction is

$$\begin{aligned} H_{\text{int}} &= \frac{1}{2} A \frac{\partial \epsilon}{\partial s} \int \sum_q i q r_0 u_q e^{i q r_0 \theta} \sum_{k,k'} \frac{\hbar\sqrt{\omega_k \omega_{k'}}}{2\epsilon V} \left[a_k a_{k'} e^{i(k+k')r_0\theta} + a_k a_{k'}^\dagger e^{i(k-k')r_0\theta} + \text{h.c.} \right] \mathrm{d}\theta \\ &= \frac{i\hbar}{8\pi\epsilon}\frac{\partial \epsilon}{\partial s} \int \sum_{q,k,k'} q\sqrt{\omega_k \omega_{k'}} \sqrt{\frac{\hbar}{2\rho_\theta \Omega_q}} \left(b_q + b_{-q}^\dagger \right) e^{i q r_0 \theta} \left[a_k a_{k'} e^{i(k+k')r_0\theta} + a_k a_{k'}^\dagger e^{i(k-k')r_0\theta} + \text{h.c.} \right] \\ &\quad \times \mathrm{d}\theta \\ &\approx i\frac{\hbar\omega_k}{8\pi} x_{\text{zpf}}^q \frac{\partial \epsilon}{\epsilon_0 \partial s} \sum_{qkk'} q (b_q a_k a_{k'}^\dagger + b_q^\dagger a_k^\dagger a_{k'}) f(q). \end{aligned} \tag{6.13}$$

In the last line, the function $f(q)$ represents the momentum and energy conservation conditions for forward Brillouin scattering (FBS), corresponding to integrating out θ and assumption of our effective 1D system. In the above calculation, however, we ignored the imaginary part of the wave vectors, misalignment of the optical and acoustic transverse modes, both of which give $f(q)$ a finite width in space. Looking only at the damping term, we have $\gamma = Bq^2$, where B is the phonon diffusion constant. There is also an imaginary term in the photon wavevector, which is related to the optical loss κ. Converting to momentum, we have $\tilde{q} = q - i\frac{\gamma}{2v}$ and $\tilde{k} = k - i\frac{\kappa}{2c}$. The integration over the spatial coordinate θ is not a δ-function anymore, but should

be replaced by the following function that has a finite width:

$$f(q) = \int_0^{2\pi} e^{i(\tilde{k}-\tilde{k}'+\tilde{q})r_0\theta}\mathrm{d}\theta = \frac{\gamma/2v + \kappa/c}{(\gamma/2v + \kappa/c) + i(\delta q)}, \tag{6.14}$$

where $\delta q = q - \Delta k = q - (k' - k)$.

Consider the following scenario: we drive the control mode a_k strongly and probe the anti-Stokes mode $a_{k'}$ with a weak field. We then linearize the hamiltonian by replacing a_k with its steady state amplitude $\alpha = \mathcal{E}/(-i\Delta + \kappa/2)$ where the input field amplitude is related to the input power by $\mathcal{E} = \sqrt{P_{\mathrm{in}}\kappa/\hbar\omega_k}$. The hamiltonian for the interacting system is

$$H = -\Delta a^\dagger a + \sum_q \Omega_q b_q^\dagger b_q + \sum_q ic_{\mathrm{cl}} q \left[f(q)a^\dagger b_q - f^*(q) b_q^\dagger a\right], \tag{6.15}$$

where a stands for the higher frequency anti-Stokes mode $a_{k'}$ and the linearized coupling speed

$$c_{\mathrm{cl}} = \frac{\hbar\omega_k}{8\pi} x_{\mathrm{zpf}}^q \frac{\partial\epsilon}{\epsilon_0 \partial s}\sqrt{\frac{P_{\mathrm{in}}\kappa/\hbar\omega_k}{\Delta^2 + \kappa^2/4}}. \tag{6.16}$$

We consider the case when the effective detuning of the anti-Stokes mode is close to the frequency of the phonon band: $\Delta = \omega_k - \omega_{k'} \approx -\Omega_q$.

What we have neglected is the presence of disorder/defects in the material, which causes phonon scatterings and thus mix phonons with different momenta. We model the defects as random fluctuations of the density of the material $\delta\rho$, and this gives an extra term in the hamiltonian of the system:

$$\begin{aligned} H_{\mathrm{defect}} &= \frac{1}{4\rho_0}\sum_{qq'}\sqrt{\Omega_q\Omega_{q'}}(b_q - b_{-q}^\dagger)(b_{q'} - b_{-q'}^\dagger)\int_0^{2\pi}\delta\rho(\theta)e^{i(q+q')r_0\theta}\mathrm{d}\theta \\ &= -\frac{1}{2\rho_0}\sum_{qq'}\sqrt{\Omega_q\Omega_{q'}} b_q b_{q'}^\dagger \delta\rho_{q-q'} \end{aligned}$$

$$= -\sum_{qq'} g_{qq'} b_q b_{q'}^\dagger \tag{6.17}$$

The scattering strength $g_{qq'}$ between phonon modes can be calculated numerically by modeling the density fluctuations $\delta\rho(\theta)$ as a random gaussian function. From the expression of g, we immediately realize that $g_{qq} = 0$ for $q \neq 0$, which means that the scattering potential always mixs phonons with different wavevector.

6.3 Linear response theory and random scattering potential simulation

Taking into account optomechanical interaction, phonon-phonon scattering and dissipation, the total effective hamiltonian of the system thus becomes:

$$\begin{aligned} H_{\text{eff}} &= -\Delta a^\dagger a + \sum_q \Omega_q b_q^\dagger b_q + \sum_q i c_{cl} q \left[f(q) a^\dagger b_q - f^*(q) b_q^\dagger a \right] \\ &\quad - \sum_{qq'} g_{qq'} b_q b_{q'}^\dagger - i\frac{\kappa}{2} a^\dagger a - i \sum_q \frac{\gamma_q}{2} b_q^\dagger b_q. \end{aligned} \tag{6.18}$$

The linear response of phonons can be found with the multi-mode effective hamiltonian using Heisenberg-Langevin equations:

$$\dot{a} = -i(-\Delta - i\kappa/2)a + \sqrt{\kappa} a_{\text{in}} + \sum_q c_{\text{cl}} q f(q) b_q, \tag{6.19a}$$

$$\dot{b}_q = -i(\Omega_q - i\gamma_q/2) b_q + \sqrt{\gamma_q} b_q^{\text{in}} - c_{\text{cl}} q f^*(q) a + i \sum_{q'} g_{q'q} b_{q'}. \tag{6.19b}$$

We can then move to frequency space and get a matrix equation for the mechanical modes after eliminating the optical mode by solution of Eq. (6.19a). We get

$$D\vec{b}(\omega) = -i\sqrt{\Gamma}\vec{b}_{\text{in}}(\omega) + M\vec{b}(\omega) + E\vec{b}(\omega). \tag{6.20}$$

We define $\vec{b} = [b_1, b_2, \cdots, b_q, \cdots]^T$ and the following matrices:

$$\Gamma_{qq'} = \gamma_q \delta_{qq'}, \tag{6.21a}$$

$$D_{qq'}(\omega) = (\Omega_q - \omega - i\gamma_q/2)\delta_{qq'}, \tag{6.21b}$$

$$M_{qq'}(\omega) = \frac{c_{\mathrm{cl}}^2 qq' f(q) f^*(q')}{(-\Delta - \omega) - i\kappa/2} = \lambda(\omega) \left|\phi\right\rangle \left\langle\phi\right|, \tag{6.21c}$$

$$E_{qq'} = g_{q'q}. \tag{6.21d}$$

The optical noise a_{in} is usually very small compared to the thermal noise b_{in}, so we find that

$$\vec{b}(\omega) = \chi(\omega)(-i\sqrt{\Gamma})\vec{b}_{\mathrm{in}}(\omega) = \frac{-i\sqrt{\Gamma}}{D - (M+E)}\vec{b}_{\mathrm{in}}(\omega). \tag{6.22}$$

Since the scattering rate $g_{qq'}$ is random, we can find a more realistic expression for the response matrix by taking the ensemble average of many density fluctuation configurations,

$$\bar{\chi}(\omega) \equiv \left\langle \frac{1}{D - (M+E)} \right\rangle. \tag{6.23}$$

The diagonal element of the response matrix $\bar{\chi}(\omega)$ gives the linear response of each mode:

$$b_q(\omega) = \bar{\chi}_{qq}(\omega) b_q^{\mathrm{in}}(\omega). \tag{6.24}$$

We first consider the case when the mode spacing of phonons is greater than phonon damping rate: $\Delta q > \gamma/v$. In this regime, only one particular phonon mode interacts resonantly with the optical mode, which means the main feature of the multi-mode theory is captured in a single-mode minimal theory, as described in Fig. 6.2(a). We can easily write down the Heisenberg-Langevin equations [39–41] for each mode and solve the equations in frequency domain. From its linear

response function, we can extract the approximate damping rates for each mode near resonance $\omega \approx \omega_m$,

$$\gamma_+ \approx \gamma_{\text{in}} + \gamma_{\text{opt}} + \frac{4g^2}{\gamma_{\text{in}}}, \tag{6.25a}$$

$$\gamma_- \approx \gamma_{\text{in}} + \frac{4g^2}{\gamma_{\text{in}} + \gamma_{\text{opt}}}. \tag{6.25b}$$

When $\Delta \approx -\omega_m$, the optomechanical damping rate is $\gamma_{\text{opt}} \approx 4\alpha^2/\kappa$ in the sideband resolved regime, where α is the pump enhanced optomechanical coupling rate. It is clear that when the pump strength α increases, the optomechanical damping rate γ_{opt} also increases, and this leads to broader linewidth for forward propagating phonon and narrower linewidth for backward propagating phonon at the same time.

We choose a few phonon modes and run a numerical simulation to directly calculate the linear response function by taking ensemble average of the random scattering potential. The numerical result is shown in Fig. 6.2(b), which is in good agreement with the analytical result for linewidth.

6.4 Perturbation expansion

On the other hand, when the phonon mode spacing is smaller than phonon damping rate $\Delta q < \gamma/v$, multiple phonons contribute to the interaction process and the loss in the backward propagating direction is shared among the modes. We first need to find out the linewidth of different phonon modes and how they depend on the pump power. In the following section, we setup a formal calculation of linear response function using perturbation expansion. Our goal is still the valuation of

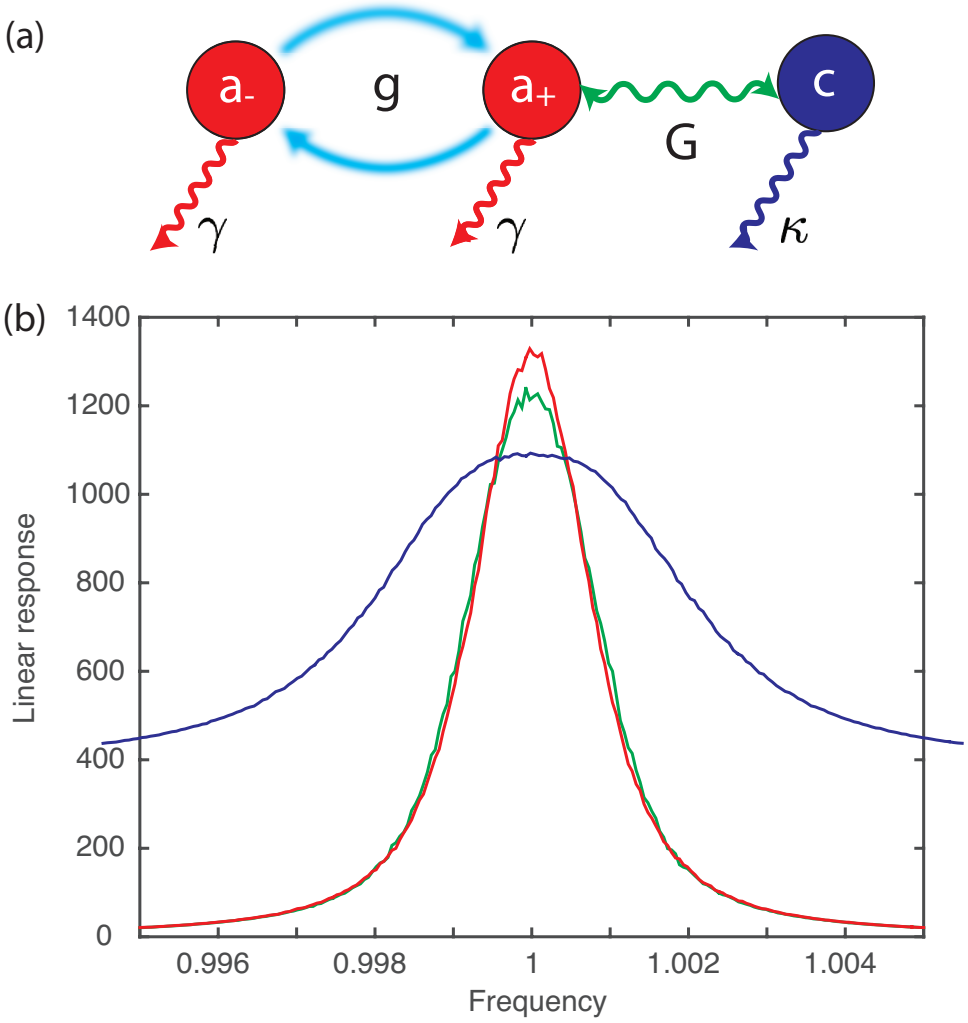

Figure 6.2: Linear response of different phonon modes as a function of rescaled frequency. Green curve represents the response of phonons without the optomechanical coupling, red (blue) curve represents the response of backward (forward) propagating phonon when the optomechanical coupling is turned on.

the following ensemble averaged propagator:

$$\left\langle \frac{1}{D-(M+E)} \right\rangle, \tag{6.26}$$

which would be able to tell us the frequency shift and modified linewidth of each phonon mode.

We now expand the denominator up to second order in E:

$$\begin{aligned}
(D-M-E)^{-1} &= (D-M)^{-1} + (D-M)^{-1}E(D-M)^{-1} \\
&\quad +(D-M)^{-1}E(D-M)^{-1}E(D-M)^{-1} + \cdots \\
&\approx D^{-1} + D^{-1}MD^{-1} + \left(D^{-1} + D^{-1}MD^{-1}\right) E \left(D^{-1} + D^{-1}MD^{-1}\right) \\
&\quad + \left(D^{-1} + D^{-1}MD^{-1}\right) E \left(D^{-1} + D^{-1}MD^{-1}\right) E \left(D^{-1} + D^{-1}MD^{-1}\right)
\end{aligned} \tag{6.27}$$

Because of the random property of the scattering potential, only terms with even number of E have a nonzero ensemble average [133]. We keep only first order terms in the operator M and second order in E, and get

$$\left\langle [D-M-E)]^{-1} \right\rangle = (D-\tilde{M})^{-1} \tag{6.28}$$

with

$$\tilde{M} \approx M + \left\langle ED^{-1}E \right\rangle + \left\langle ED^{-1}MD^{-1}E \right\rangle + \left\langle MD^{-1}ED^{-1}E \right\rangle + \left\langle ED^{-1}ED^{-1}M \right\rangle \tag{6.29}$$

The first term represents the optomechanical interaction, the second term comes from the random scattering between free phonons, and the last three terms come from the scattering of optomechanically damped phonons. We also find near resonance, the last two terms cancel each other, because of the destructive interference

of two scattering pathways. We also can take high order corrections into account, with a partial summation we write the result as the following:

$$\tilde{M} \approx M + \left\langle E \frac{1}{D - M} E \right\rangle \tag{6.30}$$

Its meaning becomes obvious. The modification to the free propagation of phonons has two contributions, the direct optomechanical interaction M and two successive scatterings E with a optomechanically modified phonon propagation $1/(D - M)$ in between, as shown in the diagram below in Fig. 6.3.

The random Gaussian noise like scattering potential satisfies

$$\langle E_{q_1 q_2} E_{q_3 q_4} \rangle = \bar{U}^2 \delta_{q_1+q_3, q_2+q_4} \tag{6.31}$$

As noted before, when $q = q'$, we have $E_{qq'} = 0$, since there is no scattering happening. Because of this reason, we want to avoid a pole when performing summation or integration. This eventually leads to the asymmetry for forward ($q > 0$) and backward ($q < 0$) phonons, because of the different poles we choose.

To find the linear response of the phonons, we want to calculate the diagonal element of the matrix $\tilde{M}$. We focus on the second term, which in more explicit form is

$$\left\langle E \frac{1}{D - M} E \right\rangle_{ii} = \sum_{j,k} \langle E_{ij} E_{ki} \rangle \left(\frac{1}{D - M} \right)_{jk} = \bar{U}^2 \sum_{j \neq i} \left(\frac{1}{D - M} \right)_{jj} . \tag{6.32}$$

The corresponding diagram for calculation is also shown in Fig. 6.3. With this result, it is now much easier to calculate the linear response of phonons, since we get rid of the ensemble average over the random scattering. In principle, it is possible to

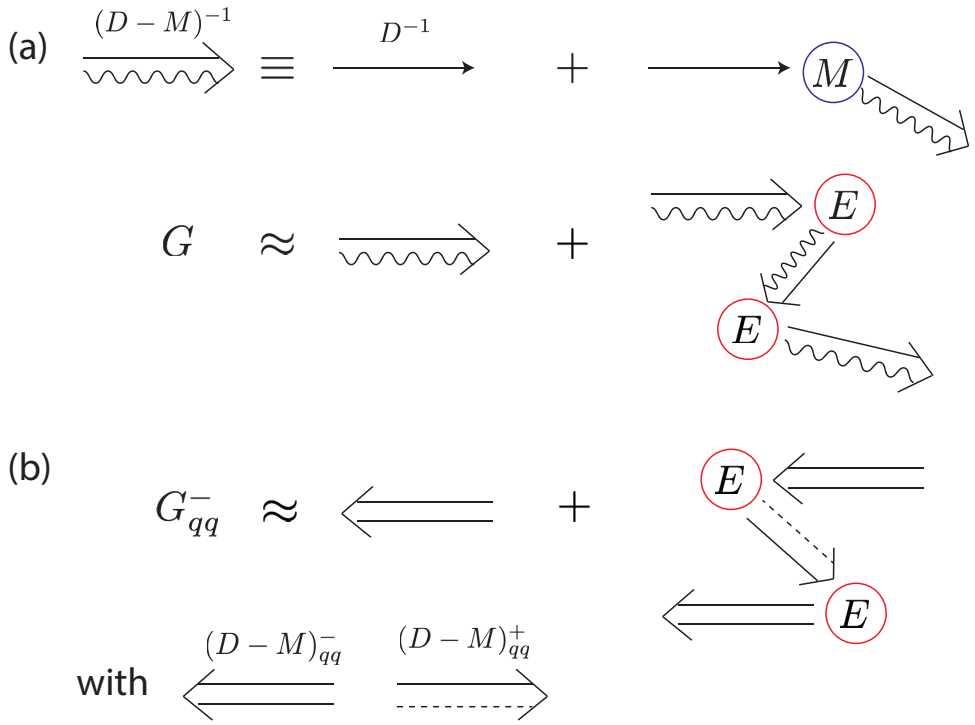

Figure 6.3: Propagator and perturbation expansion. (a) The phonon propagator $G = \langle D - M - E \rangle^{-1}$ is the sum of optomechanically modified propagator and two successive scatterings with a modified propagator in between. (b) The diagonal element of the propagator for backward propagating phonon is the sum of diagonal element of optomechanically modified back propagator and the diagonal element of two successive scatterings with en optomechanically modified forward propagator in between.

find a analytical form for the above expression, but for our purpose, we perform a numerical calculation and still get a meaningful result, as shown below in Fig. 6.4.

We see that as the pump power increases, the linewidth of the CCW phonon keeps narrowing but saturates eventually, while the linewidth of the CW phonon first narrows when the power is very small, but then keeps growing rapidly after some critical power. We note that the linewidth versus mode index curve shown below is not to be confused with the linear response curve plotted in Fig. 6.2(b). In the linewidth curve, the horizontal axis is the phonon mode index, which is approximately proportional to its resonance frequency, while in the linear response curve, the horizontal axis is the probing frequency in the spectrum. The decrease of the linewidth of back-propagating (CCW) phonon also suggests a decrease of the diffusion constant material, if we recall the relation between diffusion and phonon damping $\gamma = Bq^2$. The damping of back-propagating (CCW) phonon mainly comes from its scattering with disorder/impurity of the material, and it is also not directly modified by the optics, since the mode-matching function $f(q)$ is near zero, as shown below. The decrease in diffusion comes from a decrease in the second term of Fig. 6.3(b), where two scatterings happens with a modified forward phonon propagator in between.

We can also try to find the exact result for the $(D-M)^{-1}$ matrix. Specifically, we have $M = \lambda P$, with $P = |\phi\rangle\langle\phi|$ a rank-1 projector and $\lambda = \frac{N^2}{(\Delta-\omega)-i\kappa/2}$ with $N^2 = \sum_q \Omega_q^2 |f(q)|^2$. This gives the result:

$$PD^{-1}P = gP$$

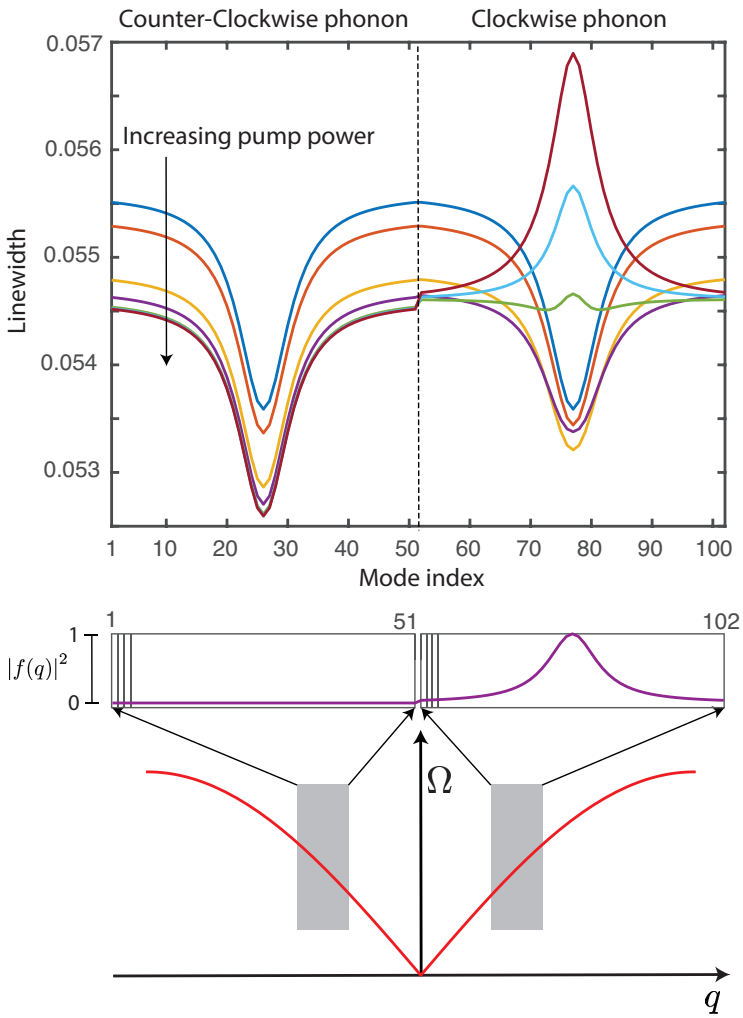

Figure 6.4: Chiral phonon effect. (Lower) We symmetrically choose 51 equally spaced phonon modes for both $q > 0$ and $q < 0$ in the long wavelength linear dispersion regime. (Upper) By setting the center frequency of phonon to be 1, phonon mode spacing $\Delta q = 0.0001$, cavity linewidth $\kappa = 0.01$, intrinsic mechanical damping $\gamma = 0.001$, detuning $\Delta = -1$, phonon-phonon scattering $\bar{U} = 0.001$, we plot the linewidth of different phonon modes for different values of optomechanical coupling $c_{\rm cl}q = 0, 0.1, 0.3, 0.5, 1.0, 1.25, 1.5$. We see the symmetry breaking for CW and CCW phonons. The overall feature size is set by the mode-matching function $f(q)$, which has a width of ~ 20 mode spacing.

with $g = \langle\phi| D^{-1} |\phi\rangle$. Thus the series

$$G_M \equiv \frac{1}{D - \lambda P} = D^{-1} + \lambda D^{-1} P D^{-1} + \lambda^2 D^{-1} P D^{-1} P D^{-1} + \dots \tag{6.33}$$

$$= D^{-1} + \lambda D^{-1} P D^{-1} + \lambda^2 g D^{-1} P D^{-1} + \lambda^3 g^2 D^{-1} P D^{-1} + \dots \tag{6.34}$$

$$= D^{-1} + \lambda \left(\sum_{n=0}^{\infty} (\lambda g)^n \right) D^{-1} P D^{-1} \tag{6.35}$$

$$= D^{-1} + \frac{1}{\lambda^{-1} - g} D^{-1} P D^{-1} \tag{6.36}$$

Let us take a moment to estimate g. We have, near the resonance in $f(q)$,

$$g(\omega) = \frac{\sum_q \Omega_q^2 |f(q)|^2 \frac{1}{\Omega_q - \omega - i\gamma_q/2}}{N^2} \approx \frac{\pi i \rho(\omega) \omega^2 |f(q_\omega)|^2}{N^2}$$

where the resonance value $\Omega_{q_\omega} = \omega$, and phonon density of states $\rho(\Omega)$. We have used the usual delta function description of $1/(x - i\epsilon) = \pi i \delta(x) + \mathcal{P}$ (the Sokhotski-Plemelj theorem). We only keep the contribution from q near the phase-matching condition, preventing a second pole for the non-coupled light from contributing. We remark that g is purely imaginary, and acts to effectively broaden the value κ by an amount $\tilde{\kappa} - \kappa = 2N^2 g = 2\pi i \rho(\omega) \omega^2 |f(q_\omega)|^2$.

Let us consider the prefactor $(1/\lambda - g)^{-1}$ in more detail. Writing it out, we have

$$\eta \equiv \frac{1}{1/\lambda - g} \approx \frac{N^2}{(\Delta - \omega) - i\tilde{\kappa}/2} \ .$$

When the optical power is small, $N^2 \to 0$, as expected. As the optical power becomes large, $\tilde{\kappa} \gg \kappa$, and there is an effective increase in the range over which these effects can occur. Note that $N^2/|f(q)|^2$ does not change with power, so $\eta \to i \frac{N^2}{\pi \rho(\omega) \omega^2 |f(q_\omega)|^2}$. In general, the prefactor η is in the positive imaginary part of the complex plane.

From this result, we can look again at

$$G = \frac{1}{D - \lambda P - E} = G_M + G_M E G \tag{6.37}$$

$$= G_M + G_M E (G_M + G_M E G) \tag{6.38}$$

Putting in the average over disorder, we have

$$\langle G \rangle = G_M + G_M \langle E G_M E G \rangle \tag{6.39}$$

$$\approx G_M + G_M \langle E G_M E \rangle \langle G \rangle \tag{6.40}$$

$$\Rightarrow \quad G_M^{-1} \langle G \rangle = \mathbb{I} + \langle E G_M E \rangle \langle G \rangle \tag{6.41}$$

$$\langle G \rangle = \frac{1}{G_M^{-1} - \langle E G_M E \rangle} \tag{6.42}$$

The factorization of the mean value is the key point here, and the only approximation.

Evaluating this, we have

$$\tilde{M} = \lambda P + \left\langle E D^{-1} E \right\rangle + \frac{1}{1/\lambda - g} \left\langle E D^{-1} P D^{-1} E \right\rangle \tag{6.43}$$

$$= M + \Sigma_D + \Sigma_P \tag{6.44}$$

where Σ_D is the self-energy term that leads to diffusion in the absence of the optical field, and Σ_P is the new term that will cancel some of this self-energy, leading to reduced diffusion.

We look first at the regular diffusion term. We have, using the averaging of $\langle E_{qq'} E_{kk'} \rangle = \bar{U}^2 \delta_{q+k,q'+k'}$,

$$\left\langle E D^{-1} E \right\rangle_{qk} = \bar{U}^2 \sum_{k'} (D^{-1})_{q-k+k',k'}$$

The diagonal nature of D in the plane-wave basis means that $q-k=0$ is the only contribution. Thus the effect is purely diagonal, and given by $\bar{U}^2 \sum_{k'} (D^{-1})_{k',k'} \approx \pi i \rho(\omega) \bar{U}^2$. This is the loss via diffusion that we expect from disorder.

Averaging over the disorder, we get

$$-W_{q-k} \equiv \left\langle E D^{-1} P D^{-1} E \right\rangle_{qk} = \bar{U}^2 \sum_{k'} (D^{-1} P D^{-1})_{q-k+k',k'}$$

Looking at the modes with q such that $f(q) \approx 0$, we can neglect the M term for the diagonal contributions. We can also approximate $D^{-1}PD^{-1}$ with terms that correspond only to those near q_0, the ones with $f(q_0)$ largest – everything else is suppressed. That is, we can take P to be a width w approximation to a delta function near $q = q_0$, which means only terms in the sum with $|k' - q_0| < w$ and $|q - k + k' - q_0| < w$ contribute. This leads to an effect for a narrow range of $|q-k| \lesssim w$. Working near resonance, D^{-1} is nearly purely imaginary; the product is thus real and negative. So we expect the overall term to be of order $-\bar{U}^2 W$ with $W \sim |g|^2$. Note that the minus sign, combined with the fact that η is the upper half plane, means that this effect strictly decreases the diffusion term near the resonance.

We can bound this by noting:

$$-W_{k-q=0} = \sum_{k'} (D^{-1} P D^{-1})_{k',k'} = \mathrm{Tr}[D^{-1} P D^{-1}] = \langle \phi | \, D^{-2} \, | \phi \rangle$$

We can evaluate this, in principle to g et a (frequency-dependent) contribution. For specificity, let us consider a simplified case where $|qf(q)|^2$ is a lorenztian of width Γ about $q_c = c_{cl}\omega_c$ and maximum of Aq_c^2, where A is a power-dependent unitless prefactor. We also take $\rho = \frac{L}{c_{cl}}$. Explicit integration gives

$$N^2 = A\omega_c^2 \rho \frac{\pi \Gamma}{2} \tag{6.45}$$

$$g = \frac{i}{\Gamma/2 - i(\omega - \omega_c)} \tag{6.46}$$

$$W = \left(\frac{1}{\Gamma/2 - i(\omega - \omega_c)}\right)^2 \tag{6.47}$$

Looking near resonance, for small ρ, we recover for $k \approx -q_c$, and $\Delta = \omega_c$,

$$\frac{\tilde{M}_{kk}}{Dk^2} \approx i\left[1 - \frac{A\Gamma\omega_c^2}{2}\frac{1}{(\kappa + A\pi\omega_c^2\rho)/2}\left(\frac{1}{\Gamma/2}\right)^2\right] = i\left[1 - \frac{4A\omega_c^2}{\tilde{\kappa}\Gamma}\right]$$

normalized with the laser-free diffusion constant $D = \pi\rho\bar{U}^2/k^2$. At high power (large A), this further simplifies to

$$D_A/D \approx 1 - \frac{4}{\pi\rho\Gamma}$$

That is, the diffusion is reduced, but the reduction is limited by the number of states that fit in the width of the phase matching, $\sim \rho\Gamma$. If only a few states phase match, the reduction in diffusion could become large.

As an additional note, if we define $T_{\delta k} = \sum_k |k + \delta k\rangle \langle k|$, then in general the noise-averaged $D^{-1}PD^{-1}$ term is given by $\langle\phi| D^{-1}T_{\delta k}D^{-1} |\phi\rangle$ with $\delta k = k - q$. For the lorentzian case considered above, defining $\delta = c_{cl}\delta k$, this gives

$$W_{\delta k} = \frac{\Gamma}{(\Gamma + i\delta)(i(\omega_c - \omega) - \Gamma/2)(i(\omega_c + \delta - \omega) - \Gamma/2)}$$

6.5 Conclusion

We provide a general continuum model of phonon propagation with the presence of directional optomechanical interaction and random phonon-phonon scattering via impurities. We perform both numerical simulation of random potential and perturbative calculation of phonon propagator to find the linear response of the

phonons. Our result shows an increase of the linewidth of phonons directly couple to optics and a decrease of the linewidth of phonons propagating in the opposite direction as optical pump power increases. Furthermore, we see a decrease of the diffusion constant of the material, due to back-scattering to optomechanically modified phonons.

Appendix A: Normal mode splitting in the high reflectivity limit

A.1 Normal mode splitting in the high reflectivity limit

The hamiltonian of the cavity fields in this three-mirror system is

$$H_{\rm opt} = \hbar(\omega_c + fx)a_L^\dagger a_L + \hbar(\omega_c - fx)a_R^\dagger a_R - \hbar g(a_L^\dagger a_R + a_R^\dagger a_L), \quad \text{(A.1)}$$

Diagonalizing this coupled left/right mode hamiltonian, we find two new eigenfrequencies:

$$\omega_{cav,\pm}(x) = \omega_c \pm \sqrt{f^2x^2 + g^2}, \quad \text{(A.2)}$$

which correspond to the normal mode frequencies of the three-mirror system, and the difference between these two eigenfrequencies is exactly the normal mode splitting in Eq. (A.2),

$$2\sqrt{f^2x^2 + g^2} = \frac{c}{L}\arccos(|r_d|\cos(2kx)). \quad \text{(A.3)}$$

Matching the left and right hand sides at a small displacement range, we find $g = \arccos(|r_d|)c/2L$ and $f = -\sqrt{|r_d|\arcsin(|t_d|)/|t_d|}\omega_c/L$. In the high reflectivity limit ($|r_d| \to 1$, $|t_d| \to 0$), $g = |t_d|c/2L$ and $f = -\omega_c/L$, which implies that the coupling constant is proportional to the transmission of the middle mirror and that the dispersion of the cavity resonant frequency is linear. We have to mention that the full expression for the resonant frequency shift f is valid at both high and

moderate reflectivity, as soon as the displacement x is small compared with the wavelength of the cavity field. But problem rises at moderate reflectivity, because the normal mode splitting Ω increases as reflectivity decreases, and it approaches the free spectrum range of the large cavity with length $2L$. To avoid the coupling between multiple cavity modes, we only consider the high reflectivity case, which has been realized experimentally [72,145]. As studied in [146], photon absorption of the middle mirror leads to both heating and feedback cooling (through photothermal forces) effect. Since the middle mirror could be made to be highly reflective (above 99.8%), it may be reasonable to neglect these heating and cooling effects.

To simplify the hamiltonian, we define two new modes $a = (a_L + a_R)/\sqrt{2}$ and $b = (a_L - a_R)/\sqrt{2}$. If we drive mode a strongly at frequency ω_L, we can move to the rotating frame with respect to the pump laser, then we have the hamiltonian of the whole system (vibrating mirror, cavity modes and pump):

$$\begin{aligned} H &= \frac{p^2}{2m} + \frac{1}{2}m\omega_m^2 x^2 + \hbar(\Delta_c - g)a^\dagger a + \hbar(\Delta_c + g)b^\dagger b \\ &\quad -\hbar\omega_c \frac{x}{L}(a^\dagger b + b^\dagger a) + i\hbar E(a^\dagger - a), \end{aligned} \tag{A.4}$$

where $\Delta_c = \omega_c - \omega_L$ is the cavity detuning, and E is the pump strength which is related to input laser power P_{in} and cavity damping κ by $|E| = \sqrt{P_{in}\kappa/\hbar\omega_L}$.

A.2 Solve the equations of motion

To solve the reduced Heisenberg-Langevin equations, we define the quadratures of mode b as $X = (b + b^\dagger)/\sqrt{2}$, $Y = (b - b^\dagger)/i\sqrt{2}$, and move to frequency

domain by Fourier transform, obtaining the following equations of motion:

$$
\begin{aligned}
-i\omega x(\omega) &= p(\omega)/m, && \text{(A.5a)}\\
-i\omega p(\omega) &= -m\omega_m^2 x(\omega) - \gamma p(\omega) + \frac{\sqrt{2}\hbar\omega_c\alpha}{L}X(\omega) + F_{in}(\omega), && \text{(A.5b)}\\
-i\omega X(\omega) &= -\kappa X(\omega) + \Delta Y(\omega) + \sqrt{2\kappa}X_{in}(\omega), && \text{(A.5c)}\\
-i\omega Y(\omega) &= -\kappa Y(\omega) - \Delta X(\omega) + \frac{\sqrt{2}\omega_c\alpha}{L}x(\omega) + \sqrt{2\kappa}Y_{in}(\omega). && \text{(A.5d)}
\end{aligned}
$$

From this set of coupled linear equations, we find,

$$
\begin{aligned}
X(\omega) &= \frac{1}{(\kappa - i\omega)^2 + \Delta^2}\left[\frac{\sqrt{2}\omega_c\alpha\Delta}{L}x(\omega) + \sqrt{2\kappa}(\kappa - i\omega)X_{in}(\omega) + \sqrt{2\kappa}\Delta Y_{in}(\omega)\right],\\
Y(\omega) &= \frac{1}{(\kappa - i\omega)^2 + \Delta^2}\left[\frac{\sqrt{2}\omega_c\alpha}{L}(\kappa - i\omega)x(\omega) + \sqrt{2\kappa}(\kappa - i\omega)Y_{in}(\omega) - \sqrt{2\kappa}\Delta X_{in}(\omega)\right].
\end{aligned}
$$

At zero detuning $\Delta = 0$, $X(\omega)$ is unchanged, while $Y(\omega)$ is modulated by oscillator displacement $x(\omega)$ [21]. Measuring $Y(\omega)$ will give us the information about oscillator displacement. At finite detuning, however, both quadratures are related to oscillator displacement. Putting the field quadratures back into the equation of motion for the oscillator, we have

$$
x(\omega) = \chi(\omega)F_{in}(\omega) + \chi(\omega)\frac{2\hbar G\sqrt{\kappa}}{(\kappa - i\omega)^2 + \Delta^2}\left[(\kappa - i\omega)X_{in}(\omega) + \Delta Y_{in}(\omega)\right], \tag{A.6}
$$

with $G = \omega_c\alpha/L$ and $\chi(\omega)$ is the susceptibility of the optomechanical system to force,

$$
\chi(\omega) = \left\{ m\left[\omega_m^2 - \omega^2 - i\gamma\omega - \frac{2\hbar G^2\Delta/m}{(\kappa - i\omega)^2 + \Delta^2}\right]\right\}^{-1}. \tag{A.7}
$$

A.3 Force detection sensitivity and optimization

The vacuum radiation input noise b_{in} is delta correlated and the thermal fluctuating force is approximated as white noise thus is also delta correlated, so we have the following correlation relations in frequency domain:

$$\langle X_{in}(\omega)X_{in}(\omega')\rangle = \langle Y_{in}(\omega)Y_{in}(\omega')\rangle = \frac{1}{2}\delta(\omega+\omega'), \tag{A.8a}$$

$$\langle X_{in}(\omega)Y_{in}(\omega')\rangle = -\langle Y_{in}(\omega)X_{in}(\omega')\rangle = \frac{i}{2}\delta(\omega+\omega'), \tag{A.8b}$$

$$\langle F_{th}(\omega)F_{th}(\omega')\rangle = 2m\gamma k_B T\delta(\omega+\omega'), \tag{A.8c}$$

from which we have

$$\begin{aligned}
S_{FF}(\omega) &= 2m\gamma k_B T + \frac{1}{2}\left|\frac{\chi_X(\omega)-i\chi_Y(\omega)}{\chi_F(\omega)}\right|^2 \\
&= 2m\gamma k_B T \\
&\quad +\frac{1}{2}\left|\frac{2\hbar\sqrt{\kappa}G}{\kappa-i\omega+i\Delta}+\frac{(\kappa-i\Delta)^2+\omega^2}{2\sqrt{\kappa}G}\frac{\sin\theta-i\cos\theta}{\Delta\sin\theta+(\kappa-i\omega)\cos\theta}\chi^{-1}(\omega)\right|^2 \\
&= 2m\gamma k_B T + \frac{2\hbar^2\kappa G^2}{|\kappa-i\omega+i\Delta|^2} \\
&\quad +\frac{|(\kappa-i\Delta)^2+\omega^2|^2}{8\kappa G^2}\frac{m^2|{\omega'_m}^2-\omega^2-i\gamma'\omega|^2}{|\Delta\sin\theta+(\kappa-i\omega)\cos\theta|^2} \\
&\quad +\frac{\hbar}{2}(\kappa+i\Delta+i\omega)\frac{\sin\theta+i\cos\theta}{\Delta\sin\theta+(\kappa+i\omega)\cos\theta}m({\omega'_m}^2-\omega^2+i\gamma'\omega)+\text{c.c.}.
\end{aligned} \tag{A.9}$$

The first term is the thermal white noise. The second term proportional to G^2 comes the random back action force. The third term proportional to $1/G^2$ is the phase noise related to position measurement imprecision.

In the vicinity of $\theta_0 = -\arctan(\kappa/\Delta)$, $\theta = \theta_0 + \delta\theta$, and the optimal pump is approximated as

$$\alpha_*^2 = \alpha_0^2(1 - \frac{2\kappa}{\Delta}\delta\theta), \tag{A.10}$$

which leads to an effective mechanical frequency

$$\omega_m'^{\,2} = \omega_m^2 - \frac{2\hbar\Delta\omega_c^2\alpha^2/mL^2}{\kappa^2+\Delta^2} = \omega_m^2\frac{2\kappa}{\Delta}\delta\theta. \tag{A.11}$$

The susceptibilities at DC reduce to

$$|\chi_F|^2 = \frac{1}{2\hbar m\omega_m^2}\frac{\Delta}{\kappa}(1 - \frac{2\kappa}{\Delta}\delta\theta), \tag{A.12a}$$

$$|\chi_X - i\chi_Y|^2 = \left|(\frac{2\kappa}{\Delta} + i)\delta\theta\right|^2. \tag{A.12b}$$

In the limit $\delta\theta \to 0$, the force susceptibility remains finite, while the optical susceptibilities go to zero. So the total sensitivity is given by

$$\eta(\omega = 0) \approx 2m\gamma k_B T + \hbar m\omega_m^2\left(\frac{\Delta}{4\kappa} + \frac{\kappa}{\Delta}\right)\xi^2. \tag{A.13}$$

A.4 Effective squeezing hamiltonian

In the absence of dissipation, the effective hamiltonian for the reduced single-mode dynamics Eq. (2.4) could be written as:

$$H_{\text{eff}} = \frac{p^2}{2m} + \frac{1}{2}m\omega_m^2x^2 + \hbar\Delta b^\dagger b - \hbar Gx(b + b^\dagger). \tag{A.14}$$

Define a unitary operator $U = \exp[-ip\eta_1(b + b^\dagger)]\exp[-x\eta_2(b - b^\dagger)] = U_1U_2$, which satisfies $U^\dagger U = U_2^\dagger U_1^\dagger U_1U_2 = 1$, then

$$\tilde{x} = U^\dagger xU = U_2^\dagger U_1^\dagger xU_1U_2 = (1 + 2\hbar\eta_1\eta_2)x + \hbar\eta_1(b + b^\dagger), \tag{A.15a}$$

$$\tilde{p} = U^\dagger p U = U_2^\dagger U_1^\dagger p U_1 U_2 = p + i\hbar\eta_2(b - b^\dagger), \tag{A.15b}$$

$$\tilde{b} = U^\dagger b U = U_2^\dagger U_1^\dagger b U_1 U_2 = b + (x\eta_2 - ip\eta_1) + \hbar\eta_1\eta_2(b - b^\dagger). \tag{A.15c}$$

This guarantees that the commutation relations $[\tilde{x}, \tilde{p}] = i\hbar$, $[\tilde{b}, \tilde{b}^\dagger] = 1$, $[\tilde{x}, \tilde{b}] = [\tilde{x}, \tilde{b}^\dagger] = [\tilde{p}, \tilde{b}] = [\tilde{p}, \tilde{b}^\dagger] = 0$ are satisfied. The effective hamiltonian after this unitary transformation is given by

$$\tilde{H}_{\text{eff}} = U^\dagger H_{\text{eff}} U = \frac{\tilde{p}^2}{2m} + \frac{1}{2}m\omega_m^2\tilde{x}^2 + \hbar\Delta\tilde{b}^\dagger\tilde{b} - \hbar G\tilde{x}(\tilde{b} + \tilde{b}^\dagger), \tag{A.16}$$

or explicitly

$$\begin{aligned}
\tilde{H}_{\text{eff}} = {} & \frac{p^2}{2m} - \frac{(\hbar\eta_2)^2}{2m}(b - b^\dagger)^2 + i\frac{\hbar\eta_2}{m}p(b - b^\dagger) + \frac{1}{2}m\omega_m^2(1 + 2\hbar\eta_1\eta_2)^2x^2 \\
& + \frac{1}{2}m\omega_m^2(\hbar\eta_1)^2(b + b^\dagger)^2 + m\omega_m^2(1 + 2\hbar\eta_1\eta_2)\hbar\eta_1 x(b + b^\dagger) \\
& + \hbar\Delta\left[b^\dagger - \hbar\eta_1\eta_2(b - b^\dagger)\right]\left[b + \hbar\eta_1\eta_2(b - b^\dagger)\right] + \hbar\Delta(x^2\eta_2^2 + p^2\eta_1^2) \\
& + \hbar\Delta\eta_2 x(b + b^\dagger) + i\hbar\Delta\eta_1(1 + 2\hbar\eta_1\eta_2)p(b - b^\dagger) - \hbar G\hbar\eta_1(b + b^\dagger)^2 \\
& - \hbar G 2\eta_2(1 + 2\hbar\eta_1\eta_2)x^2 - \hbar G(1 + 4\hbar\eta_1\eta_2)x(b + b^\dagger).
\end{aligned} \tag{A.17}$$

We then try to derive the effective squeezing hamiltonian for the system. To achieve this, we need to eliminate the linear coupling between mechanical mode and optical mode, which requires the coefficients of $p(b - b^\dagger)$ and $x(b + b^\dagger)$ to be zero:

$$i\frac{\hbar\eta_2}{m} + i\hbar\Delta\eta_1(1 + 2\hbar\eta_1\eta_2) = 0, \tag{A.18a}$$

$$m\omega_m^2(1 + 2\hbar\eta_1\eta_2)\hbar\eta_1 + \hbar\Delta\eta_2 - \hbar G(1 + 4\hbar\eta_1\eta_2) = 0. \tag{A.18b}$$

The unitary transformation U is thus uniquely determined by solving these two equations. To simplify these equations, we define $x_0 = \hbar\eta_1$, $p_0 = \hbar\eta_2$, $x_\Delta =$

$\sqrt{\hbar/2m\Delta}$. After some simple algebra, we find that the above equations reduce to

$$p_0 = -\frac{\hbar x_0}{x_\Delta^2 + x_0^2}, \tag{A.19a}$$

$$x_0^2 + \frac{\omega_m^2 - \Delta^2}{2\Delta G} x_0 - x_\Delta^2 = 0, \tag{A.19b}$$

The squeezing of the optical mode in the hamiltonian is

$$\tilde{H}_{\rm osq} = \left[-\frac{p_0^2}{2m} + \frac{1}{2} m\omega_m^2 x_0^2 - \Delta x_0 p_0 (1 + \frac{x_0 p_0}{\hbar}) - \hbar G x_0 \right] (b^2 + b^{\dagger 2}). \tag{A.20}$$

When the pump is strong (thus $G = \omega_c \alpha / L$ is large) or $|\omega_m^2 - \Delta^2|$ is small ($\omega_m \approx \Delta$), we assume $|x_0| \gg |\frac{\omega_m^2 - \Delta^2}{2\Delta G}|$, then $x_0 \approx \pm x_\Delta$, and $p_0 \approx \mp\sqrt{m\hbar\Delta/2} = \mp p_\Delta$. The squeezing hamiltonian is

$$\tilde{H}_{\rm osq} \approx \left[\mp\hbar G \sqrt{\hbar/2m\Delta} + \frac{1}{4}\hbar\omega_m^2/\Delta \right] (b^2 + b^{\dagger 2}). \tag{A.21}$$

When the pump is weak (G small) or $|\omega_m^2 - \Delta^2|$ is large, we assume $|x_0| \ll |\frac{\omega_m^2 - \Delta^2}{2\Delta G}|$, then $x_0 = \frac{2\Delta G}{\omega_m^2 - \Delta^2} x_\Delta^2 = \frac{\hbar G}{m(\omega_m^2 - \Delta^2)}$, so $p_0 \approx -2m\Delta x_0$. In this case we can further choose $\omega_m \ll \Delta$ or $\omega_m \gg \Delta$. For $\omega_m \ll \Delta$, we have $x_0 \approx -\frac{\hbar G}{m\Delta^2}$, thus

$$\tilde{H}_{\rm osq} \approx -\hbar G x_0 (b^2 + b^{\dagger 2}) \approx -\frac{(\hbar G)^2}{m\Delta^2} (b^2 + b^{\dagger 2}), \tag{A.22}$$

for $\omega_m \gg \Delta$, we have $x_0 \approx \frac{\hbar G}{m\omega_m^2}$, thus

$$H_{\rm osq} \approx \left[\frac{1}{2} m\omega_m^2 x_0^2 - \hbar G x_0 \right] (b^2 + b^{\dagger 2}) \approx -\frac{(\hbar G)^2}{2m\omega_m^2} (b^2 + b^{\dagger 2}). \tag{A.23}$$

To conclude: for strong pump or $|\omega_m^2 - \Delta^2|$ small, squeezing depends linearly on G; for weak pump or $|\omega_m^2 - \Delta^2|$ large, squeezing depends on G^2. We note that $\Delta = \omega_m$ is equivalent to $2\kappa = 2g = \omega_m$ if the condition for optimal sensitivity and optimal pump $\Delta_c = g = \kappa$ is satisfied.

Appendix B: Nonlinear optomechanics

B.1 Diagonalization of the bilinear hamiltonian

The bilinear hamiltonian in the first line of Eq. (3.2) is

$$H_0 = \Delta_a a^\dagger a + \Delta_b b^\dagger b + \omega_m c^\dagger c - G_0(b + b^\dagger)(c^\dagger + c). \tag{B.1}$$

In this hamiltonian, mode a is already decoupled, so we only need to diagonalize the coupled harmonic oscillator subsystem $b - c$. Define the quadrature variables as

$$X_b = (b + b^\dagger)/\sqrt{2}, \quad Y_b = (b - b^\dagger)/i\sqrt{2}, \tag{B.2a}$$

$$X_c = (c + c^\dagger)/\sqrt{2}, \quad Y_c = (c - c^\dagger)/i\sqrt{2}. \tag{B.2b}$$

They satisfy the commutation relations $[X_b, Y_b] = [X_c, Y_c] = i$, $[X_b, X_c] = [X_b, Y_c] = [Y_b, X_c] = [Y_b, Y_c] = 0$. We can then rewrite the hamiltonian of the $b - c$ subsystem as

$$H_{bc} = \frac{1}{2}\Delta_b(X_b^2 + Y_b^2) + \frac{1}{2}\omega_m(X_c^2 + Y_c^2) - 2G_0 X_b X_c. \tag{B.3}$$

We now rescale the operators X_c and Y_c according to

$$X_c = X_c'\sqrt{\omega_m/\Delta_b}, \quad Y_c = Y_c'\sqrt{\Delta_b/\omega_m}, \tag{B.4}$$

but keep X_b and Y_b the same

$$X_b = X_b', \quad Y_b = Y_b'. \tag{B.5}$$

In this transformed basis the hamiltonian becomes

$$H_{bc} = \frac{1}{2}\Delta_b(X_b'^2 + Y_b'^2) + \frac{1}{2}\Delta_b\left(\frac{\omega_m^2}{\Delta_b^2}X_c'^2 + Y_c'^2\right) - 2G_0\sqrt{\frac{\omega_m}{\Delta_b}}X_b'X_c'. \quad \text{(B.6)}$$

We then make an unitary transformation to get the normal mode coordinates that yields

$$\begin{pmatrix} X_b' \\ X_c' \end{pmatrix} = \begin{pmatrix} \alpha & \beta \\ -\beta & \alpha \end{pmatrix} \begin{pmatrix} X_+ \\ X_- \end{pmatrix}, \quad \text{(B.7a)}$$

$$\begin{pmatrix} Y_b' \\ Y_c' \end{pmatrix} = \begin{pmatrix} \alpha & \beta \\ -\beta & \alpha \end{pmatrix} \begin{pmatrix} Y_+ \\ Y_- \end{pmatrix}. \quad \text{(B.7b)}$$

The commutation relations are preserved if $\alpha^2 + \beta^2 = 1$ (α, β are real). So the hamiltonian of the $b-c$ subsystem is given by

$$\begin{aligned} H_{bc} = \; & \tfrac{1}{2}\Delta_b\left(\alpha^2 + \tfrac{\omega_m^2}{\Delta_b^2}\beta^2 + \tfrac{4G_0}{\Delta_b}\sqrt{\tfrac{\omega_m}{\Delta_b}}\alpha\beta\right)X_+^2 + \tfrac{1}{2}\Delta_b\left(\beta^2 + \tfrac{\omega_m^2}{\Delta_b^2}\alpha^2 - \tfrac{4G_0}{\Delta_b}\sqrt{\tfrac{\omega_m}{\Delta_b}}\alpha\beta\right)X_-^2 \\ & + \tfrac{1}{2}\Delta_b\left(Y_+^2 + Y_-^2\right) + \left[\tfrac{1}{2}\Delta_b 2\alpha\beta(1 - \tfrac{\omega_m^2}{\Delta_b^2}) - 2G_0\sqrt{\tfrac{\omega_m}{\Delta_b}}(\alpha^2 - \beta^2)\right]X_+X_-. \quad \text{(B.8)} \end{aligned}$$

It is diagonal if the cross term X_+X_- is zero:

$$\Delta_b\alpha\beta(1 - \frac{\omega_m^2}{\Delta_b^2}) - 2G_0\sqrt{\frac{\omega_m}{\Delta_b}}(\alpha^2 - \beta^2) = 0. \quad \text{(B.9)}$$

This condition along with $\alpha^2 + \beta^2 = 1$ determines α and β for the normal modes. The diagonalized hamiltonian thus becomes

$$H_{bc} = \tfrac{1}{2}\Delta_b(\xi_+^2 X_+^2 + Y_+^2) + \tfrac{1}{2}\Delta_b(\xi_-^2 X_-^2 + Y_-^2) \quad \text{(B.10)}$$

with

$$\xi_+^2 = \alpha^2 + \tfrac{\omega_m^2}{\Delta_b^2}\beta^2 + \tfrac{4G_0}{\Delta_b}\sqrt{\tfrac{\omega_m}{\Delta_b}}\alpha\beta, \quad \text{(B.11a)}$$

$$\xi_-^2 \quad = \beta^2 + \tfrac{\omega_m^2}{\Delta_b^2}\alpha^2 - \tfrac{4G_0}{\Delta_b}\sqrt{\tfrac{\omega_m}{\Delta_b}}\alpha\beta. \tag{B.11b}$$

In the limit described in the Chapter 3 with $\omega_m \ll \Delta_b$, $\xi_+ \approx 1$ and $\xi_- \approx \eta\zeta$.

The diagonalized hamiltonian describes two decoupled harmonic oscillators HO+ and HO− with effective masses $m_\pm = \Delta_b^{-1}$ and effective frequencies $\omega_\pm = \Delta_b\xi_\pm$, so it can be rewritten as

$$\begin{aligned} H_{bc} &= H_+ + H_- \\ &= \frac{Y_+^2}{2\Delta_b^{-1}} + \frac{1}{2}\Delta_b^{-1}(\Delta_b\xi_+)^2 X_+^2 + \frac{Y_-^2}{2\Delta_b^{-1}} + \frac{1}{2}\Delta_b^{-1}(\Delta_b\xi_-)^2 X_-^2. \end{aligned} \tag{B.12}$$

We can write the wavefunction of the nth eigenstate of HO− (for example) in position representation:

$$\psi_n(X_-) = \frac{1}{\sqrt{2^n n!}}\left(\frac{\xi_-}{\pi}\right)^{1/4} e^{-\frac{\xi_-}{2}X^2} H_n(\sqrt{\xi_-}X_-). \tag{B.13}$$

as illustrated in Fig. 3.1(b) for the ground state ($n = 0$) and the first excited state ($n = 1$) for two values of ξ_-.

B.2 Hamiltonian in the normal mode basis

We now focus on the nonlinear interaction term in the hamiltonian (second line of Eq. (3.2)). We define new squeezed operators

$$d_\pm = \sqrt{\frac{\xi_\pm}{2}}X_\pm + i\sqrt{\frac{1}{2\xi_\pm}}Y_\pm, \tag{B.14}$$

so $[d_\pm, d_\pm^\dagger] = 1$, $[d_\pm, d_\mp^\dagger] = 0$, and $\xi_\pm^2 X_\pm^2 + Y_\pm^2 = 2\xi_\pm(d_\pm^\dagger d_\pm + 1)$. The bilinear hamiltonian H_0 written in new operators is

$$H_0 = \Delta_a a^\dagger a + \omega_+ d_+^\dagger d_+ + \omega_- d_-^\dagger d_-. \tag{B.15}$$

The new operators written in original operators are:

$$
\begin{aligned}
d_+ &= \frac{\sqrt{\xi_+}}{2}\left[\alpha(b+b^\dagger)-\beta\sqrt{\tfrac{\Delta_b}{\omega_m}}(c+c^\dagger)\right]+\tfrac{1}{2\sqrt{\xi_+}}\left[\alpha(b-b^\dagger)-\beta\sqrt{\tfrac{\omega_m}{\Delta_b}}(c-c^\dagger)\right],\\
d_- &= \frac{\sqrt{\xi_-}}{2}\left[\beta(b+b^\dagger)+\alpha\sqrt{\tfrac{\Delta_b}{\omega_m}}(c+c^\dagger)\right]+\tfrac{1}{2\sqrt{\xi_-}}\left[\beta(b-b^\dagger)+\alpha\sqrt{\tfrac{\omega_m}{\Delta_b}}(c-c^\dagger)\right].
\end{aligned}
$$

and the inverse:

$$
\begin{aligned}
b &= \frac{\alpha}{2}\left[\frac{1}{\sqrt{\xi_+}}(d_+ + d_+^\dagger)+\sqrt{\xi_+}(d_+ - d_+^\dagger)\right]+\frac{\beta}{2}\left[\frac{1}{\sqrt{\xi_-}}(d_- + d_-^\dagger)+\sqrt{\xi_-}(d_- - d_-^\dagger)\right],\\
c &= -\frac{\beta}{2}\left[\sqrt{\frac{\omega_m}{\xi_+\Delta_b}}(d_+ + d_+^\dagger)+\sqrt{\frac{\xi_+\Delta_b}{\omega_m}}(d_+ - d_+^\dagger)\right]+\frac{\alpha}{2}\left[\sqrt{\frac{\omega_m}{\xi_-\Delta_b}}(d_- + d_-^\dagger)+\sqrt{\frac{\xi_-\Delta_b}{\omega_m}}(d_- - d_-^\dagger)\right]
\end{aligned}
$$

Now it is straightforward to write the nonlinear interaction in terms of the normal mode coordinates:

$$
\begin{aligned}
H_{\rm nl} &= -g_0 a^\dagger b(c+c^\dagger)+\text{h.c.}\\
&= -g_0\sqrt{\frac{\omega_m}{\Delta_b}}\left[-\frac{\alpha\beta}{2\xi_+}(a+a^\dagger)(d_+ + d_+^\dagger)^2+\frac{\alpha\beta}{2}(a-a^\dagger)(d_+^2 - d_+^{\dagger 2})\right.\\
&\quad +\frac{\alpha^2-\beta^2}{2\sqrt{\xi_+\xi_-}}(a+a^\dagger)(d_+ + d_+^\dagger)(d_- + d_-^\dagger)+\frac{\beta^2}{2}\sqrt{\frac{\xi_-}{\xi_+}}(a-a^\dagger)(d_+ + d_+^\dagger)(d_- - d_-^\dagger)\\
&\quad -\frac{\alpha^2}{2}\sqrt{\frac{\xi_+}{\xi_-}}(a-a^\dagger)(d_- + d_-^\dagger)(d_+ - d_+^\dagger)+\frac{\alpha\beta}{2\xi_-}(a+a^\dagger)(d_- + d_-^\dagger)^2\\
&\quad \left.-\frac{\alpha\beta}{2}(a-a^\dagger)(d_-^2 - d_-^{\dagger 2})\right].
\end{aligned}
\tag{B.16}
$$

We now look at the simplified expressions of the normal mode operators and the nonlinear interaction hamiltonian in the regimes of interest. Define $\tan\phi = \frac{\omega_m}{\Delta_b}$, $r = 2\frac{G_0}{\omega_m}\sqrt{\frac{\omega_m}{\Delta_b}}$ and $\alpha = \cos\theta$, $\beta = \sin\theta$, then the diagonalization condition reduces to

$$
\tan 2\theta = r\tan 2\phi, \tag{B.17}
$$

and the normal mode energies become

$$\xi_{\pm}^2 = \frac{1}{2}(1+\tan^2\phi)\left(1 \pm \sqrt{\cos^2 2\phi + r^2 \sin^2 2\phi}\right). \tag{B.18}$$

We now consider the regime where the mechanical frequency is small compared to the detuning of mode b and the driving is so strong that r is close to 1. This allows us to introduce two small parameters $\eta \equiv \omega_m/\Delta_b$ and $\zeta \equiv \sqrt{1-r^2}$. When $\eta \ll 1$, $\tan\phi \approx \sin\phi \ll 1$, and we have

$$\xi_+ \approx 1 + r^2\omega_m^2/2\Delta_b^2 = 1 + r^2\eta^2/2, \tag{B.19a}$$

$$\xi_- \approx \sqrt{1-r^2}\omega_m/\Delta_b = \zeta\eta. \tag{B.19b}$$

The diagonalized hamiltonian becomes:

$$H_0 = \Delta_a a^\dagger a + (\Delta_b + \delta)\bar{b}^\dagger\bar{b} + \omega_m\zeta d^\dagger d, \tag{B.20}$$

with $\delta = r^2\omega_m\eta/2$ and the new notations for the normal modes are defined as:

$$\bar{b} \equiv d_+ \approx b - \frac{r}{2}\sqrt{\eta}(c+c^\dagger), \tag{B.21a}$$

$$d \equiv d_- \approx \frac{1}{2\sqrt{\zeta}}(c-c^\dagger) + \frac{\sqrt{\zeta}}{2}(c+c^\dagger) + \frac{r}{2}\sqrt{\frac{\eta}{\zeta}}(b-b^\dagger). \tag{B.21b}$$

The full hamiltonian, including the nonlinear terms, is thus given by Eq. (3.6).

B.3 Derivation of $g^2(0)$ when quantum jumps are neglected

Here we show the standard procedure for calculating the two-photon correlation function $g^2(0)$ in the quasi-steady state regime using an effective hamiltonian. We consider the hamiltonian Eq. (3.1) with antihermitian terms describing the dissipation and weak coherent probe field on the $\bar{b}$ mode at frequency $\omega_p = \Delta_{\bar{b}} - g_{\rm nl}$:

$$H_{\rm eff} = (\Delta_a - i\kappa/2)a^\dagger a + (\Delta_{\bar{b}} - i\kappa/2)\bar{b}^\dagger\bar{b} + \omega_m\zeta d^\dagger d$$

$$-g_{\rm nl}(a^\dagger \bar{b} + \bar{b}^\dagger a)(d + d^\dagger) + i\beta_{\bar{b}}(\bar{b}^\dagger e^{-i\omega_p t} - \bar{b} e^{i\omega_p t}). \tag{B.22}$$

The term $(a + a^\dagger)(d^2 + d^{\dagger 2} + 2d^\dagger d)$ has been neglected since its strength is weak in the limit $\Delta_b \gg \omega_m$ and it is also far off resonant. Moving to a frame rotating at ω_p for the optical fields and using the resonance condition $\Delta_{\bar{b}} = \Delta_a + \omega_m \zeta$, we get

$$\begin{aligned} H_{\rm eff} &= (-\omega_m \zeta - i\kappa/2) a^\dagger a + (g_{\rm nl} - i\kappa/2)\bar{b}^\dagger \bar{b} + \omega_m \zeta d^\dagger d \\ &\quad -g_{\rm nl}(a^\dagger \bar{b} + \bar{b}^\dagger a)(d + d^\dagger) + i\beta_{\bar{b}}(\bar{b}^\dagger - \bar{b}). \end{aligned} \tag{B.23}$$

The system evolves according to the effective hamiltonian and we can expand its quasi-steady state in the following basis:

$$\begin{aligned} |\psi\rangle_{\rm ss} &= |0,0,0\rangle + c_1 |0,1,0\rangle + c_2 |1,0,1\rangle + c_3 |0,1,2\rangle \\ &\quad + c_4 |0,2,0\rangle + c_5 |1,1,1\rangle + c_6 |2,0,2\rangle + c_7 |0,2,2\rangle + c_8 |200\rangle . \end{aligned} \tag{B.24}$$

Considering the following coupling between basis states

$$\begin{aligned} |0,1,0\rangle &\xleftrightarrow{g_{\rm nl}} |1,0,1\rangle \xleftrightarrow{\sqrt{2}g_{\rm nl}} |0,1,2\rangle \\ |0,2,0\rangle &\xleftrightarrow{\sqrt{2}g_{\rm nl}} |1,1,1\rangle \xleftrightarrow{2g_{\rm nl}} |2,0,2\rangle \\ &\xleftrightarrow{2g_{\rm nl}} |0,2,2\rangle \\ &\xleftrightarrow{\sqrt{2}g_{\rm nl}} |2,0,0\rangle \end{aligned}$$

and the pumping processes

$$\begin{aligned} |0,0,0\rangle &\xleftrightarrow{\pm i\beta_{\bar{b}}} |0,1,0\rangle \xleftrightarrow{\pm i\beta} |0,2,0\rangle \\ |1,0,1\rangle &\xleftrightarrow{\pm i\beta_{\bar{b}}} |1,1,1\rangle \\ |0,1,2\rangle &\xleftrightarrow{\pm i\beta_{\bar{b}}} |0,2,2\rangle , \end{aligned}$$

we can then construct the matrix representation of the effective hamiltonian.

The steady state is found using the Schrödinger equation:

$$0 = i\frac{\partial}{\partial t}\left|\psi\right\rangle_{\rm ss} = H_{\rm eff}\left|\psi\right\rangle_{\rm ss}. \tag{B.25}$$

Solving this set of algebra equations gives us the steady state $\left|\psi\right\rangle_{\rm ss}$. The $g^2(0)$ is calculated using Eq. (3.13) in the limit $\beta_{\bar{b}} \to 0$.

Appendix C: Damping mechanisms

In [119], they studied the clamping loss using elastic wave radiation theory. They found the quality factor of clamping-free (C-F) beam resonators:

$$Q_{\mathrm{C-F(n)}} = \left[\frac{0.24(1-v)}{(1+v)\Psi}\right] \frac{1}{(\beta_n \chi_n)^2} \left[\frac{L}{b}\right]^2 \tag{C.1}$$

where L is the length of the beam and b is its width. β_n is the mode constant for the n-th mode, and χ_n denotes the mode shape factor. v is the Poisson's ratio of the thin-plate which defined as the the negative ratio of transverse to axial strain, and Ψ is an integral parametrized by $z = c_L/c_T$, the ratio of the velocities of longitudinal and transverse waves. The general feature is that the quality factor $Q \propto (L/b)^2$, Taking $v = 0.28$, we get $\Psi = 0.336$. Choosing the lowest mode, gives $\beta = 0.597$, $\chi = -0.743$ and get $Q_{\mathrm{C-F}} = 2(L/b)^2$.

Secondly, we look at the thermoelastic damping [122, 123]. Phonons traveling through a large elastic material will experience damping due to their nonlinear interaction with a surrounding bath of phonons. If the mean free path of these thermal phonons is much smaller than the wavelength of the acoustic mode, then sufficient thermalization occurs to define a temperature locally, even when the system is not in a state of thermal equilibrium. In this diffusive regime, the interaction between the phonon mode and the thermal bath is captured by a single macroscopic parameter,

the material's thermal expansion coefficient (TEC), defined as $\alpha \equiv \frac{1}{L}\frac{\partial L}{\partial T}$, which is temperature dependent. According to [124], the quality factor corresponding to this damping mechanism is given by

$$Q_{\mathrm{TED}}^{-1} = \frac{E\alpha^2 T}{C_p}\left(\frac{6}{\xi^2} - \frac{6}{\xi^3}\frac{\sinh\xi + \sin\xi}{\cosh\xi + \cos\xi}\right), \tag{C.2}$$

where E is the material's Young's modulus, T is the temperature and C_p is the heat capacity at constant pressure. The parameter ξ is related to the geometry of the resonator and is defined as $\xi \equiv b\sqrt{\omega_0 C_p/2k\rho}$, where ω_0 is the frequency of the mode of interest, k is the thermal conductivity of the material, ρ is the material density and b is the width of the beam. We remark that for short beams, the clamping loss, which grows as b^2/L^2, will always tend to dominate over the thermoelastic damping, which only directly depends upon the beam width.

We now seek a numerical estimate of these losses for SiN resonators. As Q_{TED} has a quadratic dependence on α, thermal elastic damping might be very sensitive to changes in temperature. For example, the thermal expansion coefficient for silicon-nitride (Si_3N_4) at room temperature ($T \approx 300$ K) is $\alpha = 1.19 \times 10^{-6}$ K^{-1}, but at low temperatures, its value is quite different [**?**]. Under the Debye model of heat capacity, the thermal expansion coefficient can be approximated as

$$\alpha(T) = A\left(\frac{T}{\theta_D}\right)^3 \int_0^{\theta_D/T} \frac{x^4 \exp(x)}{[\exp(x)-1]^2}. \tag{C.3}$$

We can fit a set of experimental data points $\{\alpha_i, T_i\}$ from [**?**] to study the temperature dependence of thermal expansion coefficient. The result shows that $A = 1.18 \times 10^{-5}$ K^{-1} and $\theta_D = 1650$ K, which implies $\alpha = 5.06 \times 10^{-12}$ K^{-1} and $C_p = 3.02 \times 10^{-3}$ J/(mol $\cdot$ K) at 4.2 K. The Young's modulus of the material is

$E = 310$ GPa. Using these values, we find the ξ dependent term in Eq. (C.2) becomes $\xi^2/5$ when $\xi \to 0$ and becomes $6/\xi^2$ when $\xi \to +\infty$. We can also write the dimensionless parameter ξ as $\xi = b/b_0$ where $b_0 = \sqrt{2k\rho/\omega_0 C_p}$. Since thermal conductivity k scales as heat capacity C_p, b_0 is roughly temperature independent. Assuming $\omega_0/2\pi = 1$ MHz, we get $b_0 = 6546$ μm.

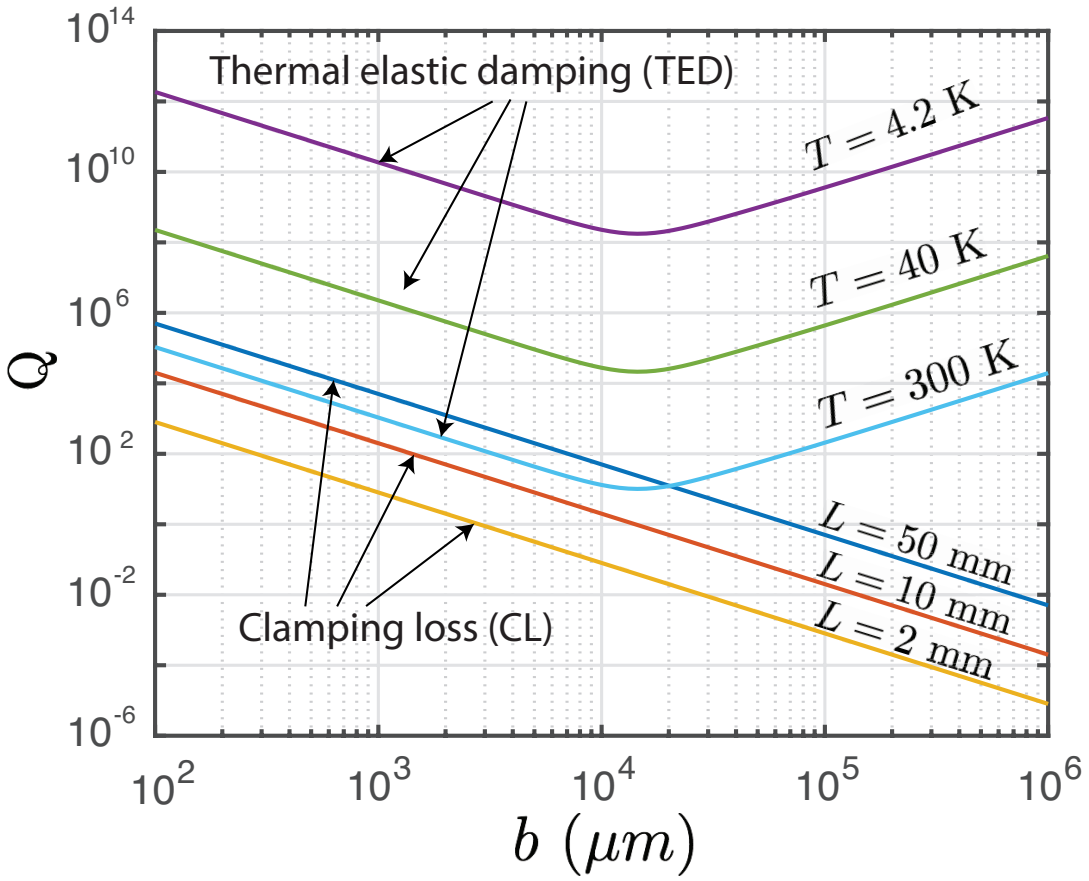

Figure C.1: Estimated contributions to quality factor for thermoelastic damping at different temperatures and quality factor for clamping loss at different resonator lengths as a function of the beam width b using parameters for SiN resonators described in the main text. Shorter beams have more pronounced clamping losses.

Fig. C.1 shows the quality factor for clamping loss and thermal elastic damping

as a function of the beam width b. We see that at sufficiently low temperature, it is always possible that $Q_{\mathrm{TED}} > Q_{\mathrm{CL}}$ (the upper half of the figure), which means the system is clamping loss limited. In this regime, the main damping mechanism is clamping loss. Since destructive interference happens in the symmetric mode a, its clamping loss rate is also very small, which satisfies the condition $\gamma_a \ll \gamma_b,\ \lambda$.

Appendix D: Narrowband optomechanical refrigeration of a chiral bath

Narrowband optomechanical refrigeration of a chiral bath

Seunghwi Kim[1], Xunnong Xu[2],
Jacob M. Taylor[2,3*], and Gaurav Bahl[1*]

[1] Mechanical Science and Engineering, University of Illinois at Urbana-Champaign
Urbana, Illinois 61801, USA
[2] Joint Quantum Institute, University of Maryland,
College Park, Maryland 20742, USA
[3] Joint Center for Quantum Information and Computer Science,
National Institute of Standards and Technology, Gaithersburg, Maryland 20899, USA
[*] To whom correspondence should be addressed; bahl@illinois.edu, jmtaylor@umd.edu

Abstract

The transport of sound and heat, in the form of phonons, is fundamentally limited by disorder-induced scattering. In electronic and optical settings, introduction of chiral transport provides robustness against such disorder by preventing elastic backscattering. Here we experimentally demonstrate a path for achieving robust phonon transport even in the presence of material disorder, by dynamically inducing chirality through optomechanical coupling. We demonstrate dramatic optically-induced chiral transport for clockwise and counterclockwise phonons in a symmetric resonator. The phenomenon leads to gain-free reduction of the intrinsic damping of the phonons, and is surprisingly also accompanied by a reduction in heat load of the mechanics. This technique has the potential to improve the thermal limits of resonant mechanical sensors, which cannot be attained through conventional optomechanical cooling.

Efforts to harness the optical and mechanical properties of achiral resonators are leading to new approaches for quantum noise limited sources [1–3], preparation of quantum states of matter [4–7], and ultra-high precision metrology [8–11]. Since all these efforts are aided by long coherence times for resonant excitations, they are fundamentally limited by structural disorder, even in systems with high symmetry, and by thermal noise in the

mechanics. While optomechanical cooling can lower the effective temperature of a mechanical oscillator it does not modify the heat load, and thus does not fundamentally modify the contribution of thermal noise [10, 11]. Surprisingly, chiral systems – that break parity symmetry – can provide improved transport properties, giving rise to unique physics ranging from nonreciprocal wave propagation to disorder-free transport via the edge states of quantum Hall systems [12–16]. Indeed, inducing nonreciprocal behavior by breaking time-reversal symmetry in nominally achiral devices forms the basis for circulators [17, 18] and recent proposals for optomechanical isolation [14, 16, 19, 20]. Here we consider an approach to dynamically impart chirality to achiral mechanical systems, which induces disorder-less transport while simultaneously improving the isolation of phonon modes from the ambient bath, lowering their heat load without added damping.

One particularly simple class of systems for examining chirality are passive devices having degenerate forward- and backward-propagating modes, such as ring cavities and whispering-gallery resonators (WGRs). We demonstrate a new technique for enabling improved coherence properties for phonons, by integrating induced time-reversal breaking [19] with opto-acoustic coupling in a WGR. Specifically, we show that optomechanical chiral cooling of phonon modes is possible. This phenomenon leads to induced chiral propagation in the clockwise (cw) and counterclockwise (ccw) phonon modes, resulting in the protection of the phonon pseudo-spins from disorder-induced scattering. Most notably, while the cw phonon mode experiences conventional optomechanical cooling [4–6, 21–23], the ccw mode is observed to cool without added dissipation, indicating a new form of optomechanical cooling that occurs through increased isolation from the thermal bath.

Let us consider a whispering gallery-type resonator with an intrinsic degeneracy for clockwise (cw) and counterclockwise (ccw) propagation for both phonons and photons. Our particular structure uses frequency-adjacent optical modes belonging to different mode families, that may be populated by cw or ccw photons (Fig. 1a), for a total of four optical modes for the experiment. These optical modes differ in (ω, k) space by the energy and momentum of a propagating high-Q phonon mode in the resonator. Photons occupying the modes in the cw (ccw) direction can thus only be coupled through Brillouin acousto-optic scattering from the cw (ccw) phonons, as illustrated. Verification of the Brillouin phase-matching between two optical modes and a phonon mode can be performed by means of forward Brillouin lasing [24] and induced transparency measurements [19]. In particular, when we pump the lower-energy optical mode, anti-Stokes scattering to the higher

mode annihilates phonons [23] in the corresponding direction and should lead to unidirectional optomechanical damping. As a result, this system should exhibit significant optically-induced chirality in the transport of phonons, which we may hope to observe by its modification of the high-Q mechanical mode that couples to the light (Fig. 1b). We note that there also exist other low-Q vibrational excitations of the resonator, i.e. the phonon bath, that also occupy (ω, k) space within the bandwidth of the optical modes. We collectively treat these as a phonon quasi-mode having large dissipation rate. This quasi-mode acts as a bath for the high-Q mode, while also directly coupling to the light.

Our experiments are performed with a silica WGR of diameter $\sim 150\,\mu$m at room temperature and atmospheric pressure, using a tapered fiber coupler for optical interface in the telecom band (Fig. 2). Direct coupling between optical modes in cw and ccw directions is negligible. To examine the potential for modification of the high-Q phonon behavior, and the possibility of chiral transport of sound, we set up the experiment with two optical sources tuned to the lower frequency optical mode in the clockwise (cw) and counter-clockwise (ccw) directions. The role of the cw "pump" is to induce cooling of the cw propagating phonons, while the role of the much smaller ccw "reverse probe" is to simply generate optical scattering from the counter-propagating phonons. The RF beat spectrum generated between the scattered light and the corresponding source in either direction provides a direct measure of the phonon mode spectrum (Supplement Sec. S5). In the experiment, the optical pump and probe sources are both derived from the same laser and are thus always at identical frequencies. Throughout the remainder of this work, no pump or probe field is delivered to the upper optical mode, in order to prevent coherent amplification of the phonons via Brillouin scattering.

Our first task is to measure the intrinsic damping of the high-Q phonon mode γ_m without any optical pumping. This is traditionally the minimum measurable phonon linewidth in any optomechanical cooling experiment. We perform this measurement by detuning the source laser from the optical resonance such that little to no optomechanical cooling is induced by either the pump or the probe. The zero-power phonon linewidth γ_m can be calculated by extrapolating measurements of cw and ccw phonon linewidths γ_{a+} and γ_{a-} using the theoretical model (Eqs. S10). A determining parameter for the optomechanical cooling rate is the detuning Δ_2 of the anti-Stokes scattered light from its optical mode, which we measure directly using the Brillouin Scattering Induced Transparency [19]. In Fig. 3a we plot linewidth

measurements of both cw and ccw phonon linewidth as a function of this detuning. We immediately see a striking direction-dependence of the damping rates of the cw and ccw phonons, that has never previously been reported. This dramatic chiral damping is a direct result of the momentum conservation rules that underly the Brillouin scattering interaction, and will not generally be available in traditional single-mode optomechanical systems. We note also that the relative power of the cw pump and ccw probe lasers is $\sim 9:1$, so there is some cooling of the a_- phonons as well.

As discussed below, the minimum measured linewidth γ_m in the above experiment will be larger than the intrinsic loss rate γ. This is because $\gamma_m = \gamma + 4V_0^2/\Gamma$ where the second term in Eqn. 2b (below), representing disorder-induced backscattering to the counter-propagating quasimode, is unavoidable. Here, we measure intrinsic damping γ_m to be about 12.5 ± 1.0 kHz. All uncertainties in this manuscript correspond to 95 % confidence bounds of the fitted value.

We now propose a model that illuminates how the optical coupling to the quasimodes allows us to change the role this disorder-induced backscattering plays in the damping and thermalization of the high-Q phonon modes. Specifically, we incorporate all the essential physics described above and illustrated in Fig. 1c as follows. We define the higher frequency optical modes c_σ, with $\sigma = +$ for cw photons and $\sigma = -$ for ccw photons. These couple to the high-Q phonon mode $a_\pm$ respectively, via direct optomechanical interaction with strength αh_0 (or βh_0), and also couple to the quasi-mode $b_\pm$ with strength αg_0 (or βg_0). In all cases these interactions preserve chirality σ. h_0 and g_0 are the bare (single photon/phonon) optomechanical coupling strengths, while α and β are the square root of the intracavity photon number in cw and ccw direction respectively.

We exclude a simpler model, of two degenerate mechanical modes and no additional quasi-modes, as it fails to produce two key features of the data. First, at low pump power, we would see some mode splitting, representing a breaking of circular symmetry from disorder-induced scattering. Second, at high pump powers, explored below, the lowest linewidth that the backward mode could achieve would be equivalent to its initial linewidth and its temperature would be equal to the bath temperature. Optical coupling to multiple mechanical modes is the next best alternative, and as we show below, describes these phenomena.

To see the role chirality plays, we now also include the existence of disorder-induced scattering between $a_\pm$ and $b_\mp$ modes having strength V_0 – a term that explicitly breaks the chiral symmetry. We can thus represent

this toy model system with the interaction Hamiltonian expression given by:

$$H_{\text{int}} = \alpha c_+^\dagger (h_0 a_+ + g_0 b_+) + \beta c_-^\dagger (h_0 a_- + g_0 b_-) + V_0 (a_-^\dagger b_+ + b_+^\dagger a_-) + \text{h.c.} \quad (1)$$

The full Hamiltonian model including the dissipation and detuning terms is provided in the Supplement. We can now derive the equations of motion for this system by means of the Heisenberg-Langevin equation (see Supplement Sec. S3) and extract the susceptibilities of the high-Q phonon modes $a_\pm$. The corresponding modal linewidths $\gamma_{a_\pm}$ can then be obtained as follows.

$$\gamma_{a_+} = \gamma + \frac{4\alpha^2 h_0^2}{\kappa} + \frac{4V_0^2}{\Gamma} \frac{1}{1+\mathcal{C}_\beta}, \quad (2a)$$

$$\gamma_{a_-} = \gamma + \frac{4\beta^2 h_0^2}{\kappa} + \frac{4V_0^2}{\Gamma} \frac{1}{1+\mathcal{C}_\alpha}. \quad (2b)$$

The last term in each expression is the disorder-induced modification. Here κ, γ, and Γ are the loss rates of the optical modes c_σ, the high-Q phonon modes a_σ, and the phonon quasi-modes b_σ respectively. The parameters $\mathcal{C}_\alpha$ and $\mathcal{C}_\beta$ are the quasi-mode optomechanical cooperativities defined as $4\alpha^2 g_0^2/\Gamma\kappa$ and $4\beta^2 g_0^2/\Gamma\kappa$, respectively.

With zero optical pumping, the model predicts $\gamma_{a+} = \gamma_{a-} = \gamma + 4V_0^2/\Gamma$ implying that the minimum measurable phonon mode linewidth in any conventional experiment is greater than the intrinsic loss rate γ, because disorder in the system causes loss via elastic backscattering into the $b_{\bar{\sigma}}$ quasi-mode. The model also predicts, irrespective of disorder-induced scattering, that asymmetric optical pump strengths α and β will induce chirality in the transport properties of phonons with $\gamma_{a+} \neq \gamma_{a-}$ as we saw previously. Most importantly, we note that the contribution of disorder-induced scattering can be minimized by increasing the cooperativities $\mathcal{C}_\alpha$ and $\mathcal{C}_\beta$. In the particular case where only the cw optical pump is provided ($\alpha \neq 0$, $\beta = 0$), γ_{a-} will approach the intrinsic loss rate γ, indicating a robustness against disorder-induced scattering. This effect has never previously been reported. In addition to phonon linewidth modification, this model also predicts a reduction in the effective temperature of the a_- phonon mode. Considering the effective thermal noise on a_- near resonance given by $\sqrt{\gamma} a_-^{\text{in}} - i2V_0/\sqrt{\Gamma}\,(1+\mathcal{C}_\alpha)\, b_+^{\text{in}}$, the effective temperature of mode a_- can be determined by the weighted sum of each bath's contribution divided by

the total damping:

$$T_{a_-}^{\text{eff}} = \frac{1}{\gamma_{a_-}} \left[\gamma T_{a_-} + \frac{4V_0^2}{\Gamma} \frac{1}{(1+\mathcal{C}_\alpha)^2} T_{b_+} \right] . \tag{3}$$

Notably, from Eqn. 2b and Eqn. 3 we predict that as the optical pump α increases, the thermal load on mode a_- will decrease more rapidly than the concurrent improvement in its linewidth.

We now return to the experimental results, to demonstrate the key predictions of this model: (i) dissipation associated with disorder-induced backscattering can be optically inhibited, (ii) the damping rate of ccw phonons can be brought below the intrinsic damping γ_m, and (iii) the process leads to a reduction in heat load. Here, we employ an erbium doped fiber amplifier (EDFA) to control the cw pump power while keeping the ccw probe power constant at 12.5 μW. The anti-Stokes Brillouin scattered light in the resonator is kept close to zero detuning from its optical mode to maximize cooling efficiency, i.e. $|\Delta_2/\kappa|$ is less than 10 %. Since the ccw probe adds some optical damping to the ccw phonons, the initial measurement of γ_{a-} is at 18 $\pm$1 kHz, which is greater than the measured zero-power linewidth γ_m.

When the cw pump power is increased, the added optical damping broadens the cw phonon linewidth γ_{a+} (Fig. 3b). The striking feature of this experiment is that the ccw phonon linewidth γ_{a-} simultaneously reduces, i.e. the ccw phonons become more coherent! We verify that the increased coherence of the ccw phonons is not associated with any gain (Fig. 3c). In fact, quite the opposite occurs, and the total integrated area under the phonon spectrum also reduces, indicating a reduction in heat load (i.e. cooling) of the a_- phonons. This heat load reduction occurs more rapidly than the linewidth improvement, as theoretically predicted.

Since the ccw optical probe was not modified in any way, the optically induced damping (about 4.5 kHz) from the probe remains constant. The reduction of the γ_{a-} linewidth thus indicates that a hidden contribution to dissipation is being eliminated when the cw pump power is increased. At the end of the experiment, the measured linewidth $\gamma_{a-} = 10.5 \pm 1.7$ kHz is well below the intrinsic damping $\gamma_m = 12.5 \pm 1$ kHz measured at the start of the experiment. Subtracting the optical damping from the probe gives an upper bound to the intrinsic thermalization rate for the mechanical mode $\gamma < 6$ kHz.

Our model indicates that the above measured reduction in the phonon linewidth γ_{a-} occurs in the disorder-induced scattering contribution to the intrinsic linewidth. In other words, the ccw propagating phonons achieve

significant robustness against disorder when the cw propagating phonons are cooled optically.

Our approach for inducing chiral behavior is, at present, confined to the narrowband response of a high-Q resonator system. However, such devices are already in use for metrological applications [8–11] including atomic force microscopes [25] and quantum-regime transducers [26, 27]. In all these cases, increasing the quality factor while reducing the heat load of the mechanical element would lead to a direct improvement in performance. Furthermore, the modification of phonon transport due to light may have substantial impact beyond current devices, as the ability to dynamically reconfigure the phononic behavior may change the realm of possibility as currently conceived. Still, robust demonstration of chiral asymmetry and non-reciprocal behavior remains close, but our work provides a foundation upon which to build such demonstrations.

References

[1] T. J. Kippenberg, R. Holzwarth, and S. A. Diddams, "Microresonator-based optical frequency combs," *Science*, vol. 332, no. 6029, pp. 555–559, 2011.

[2] J. Li, X. Yi, H. Lee, S. A. Diddams, and K. J. Vahala, "Electro-optical frequency division and stable microwave synthesis," *Science*, vol. 345, no. 6194, pp. 309–313, 2014.

[3] W. Loh, A. A. S. Green, F. N. Baynes, D. C. Cole, F. J. Quinlan, H. Lee, K. J. Vahala, S. B. Papp, and S. A. Diddams, "Dual-microcavity narrow-linewidth brillouin laser," *Optica*, vol. 2, pp. 225–232, Mar 2015.

[4] S. Gigan, H. Bohm, M. Paternostro, F. Blaser, G. Langer, J. Hertzberg, K. Schwab, D. Bauerle, M. Aspelmeyer, and A. Zeilinger, "Self-cooling of a micromirror by radiation pressure," *Nature*, vol. 444, pp. 67–70, Nov 2006.

[5] O. Arcizet, P.-F. Cohadon, T. Briant, M. Pinard, and A. Heidmann, "Radiation-pressure cooling and optomechanical instability of a micromirror," *Nature*, vol. 444, pp. 71–74, Nov 2006.

[6] J. Chan, T. M. Alegre, A. H. Safavi-Naeini, J. T. Hill, A. Krause, S. Gröblacher, M. Aspelmeyer, and O. Painter, "Laser cooling of a

nanomechanical oscillator into its quantum ground state," *Nature*, vol. 478, no. 7367, pp. 89–92, 2011.

[7] E. Verhagen, S. Deleglise, S. Weis, A. Schliesser, and T. J. Kippenberg, "Quantum-coherent coupling of a mechanical oscillator to an optical cavity mode," *Nature*, vol. 482, pp. 63–67, Feb. 2012.

[8] J. D. Teufel, T. Donner, M. A. Castellanos-Beltran, J. W. Harlow, and K. W. Lehnert, "Nanomechanical motion measured with an imprecision below that at the standard quantum limit," *Nat. Nanotech.*, vol. 4, pp. 820–823, Nov. 2009.

[9] G. Anetsberger, E. Gavartin, O. Arcizet, Q. P. Unterreithmeier, E. M. Weig, M. L. Gorodetsky, J. P. Kotthaus, and T. J. Kippenberg, "Measuring nanomechanical motion with an imprecision below the standard quantum limit," *Phys. Rev. A*, vol. 82, p. 061804, Dec 2010.

[10] A. G. Krause, M. Winger, T. D. Blasius, Q. Lin, and O. Painter, "A high-resolution microchip optomechanical accelerometer," *Nat. Photonics*, vol. 6, pp. 768–772, Oct. 2012.

[11] E. Gavartin, P. Verlot, and T. J. Kippenberg, "A hybrid on-chip optomechanical transducer for ultrasensitive force measurements," *Nat. Nanotech.*, vol. 7, pp. 509–514, June 2012.

[12] B. I. Halperin, "Quantized Hall Conductance, Current-Carrying Edge States, and the Existence of Extended States in a Two-Dimensional Disordered Potential," *Phys. Rev. B*, vol. 25, no. 4, pp. 2185–2190, 1982.

[13] Z. Wang, Y. Chong, J. D. Joannopoulos, and M. Soljacic, "Observation of unidirectional backscattering-immune topological electromagnetic states," *Nature*, vol. 461, pp. 772–775, Aug. 2009.

[14] M. Hafezi, S. Mittal, J. Fan, A. Migdall, and J. M. Taylor, "Imaging topological edge states in silicon photonics," *Nat. Photonics*, vol. 7, pp. 1001–1005, Oct. 2013.

[15] R. Süsstrunk and S. D. Huber, "Observation of phononic helical edge states in a mechanical topological insulator," *Science*, vol. 349, no. 6243, pp. 47–50, 2015.

[16] V. Peano, M. Houde, C. Brendel, F. Marquardt, and A. A. Clerk, "Topological phase transitions and chiral inelastic transport induced by the squeezing of light," *Nat. Commun.*, vol. 7, Mar. 2016.

[17] R. Fleury, D. L. Sounas, C. F. Sieck, M. R. Haberman, and A. Alu, "Sound Isolation and Giant Linear Nonreciprocity in a Compact Acoustic Circulator," *Science*, vol. 343, pp. 516–519, Jan. 2014.

[18] N. A. Estep, D. L. Sounas, J. Soric, and A. Alu, "Magnetic-free non-reciprocity and isolation based on parametrically modulated coupled-resonator loops," *Nat. Phys.*, vol. 10, pp. 923–927, Nov. 2014.

[19] J. Kim, M. C. Kuzyk, K. Han, H. Wang, and G. Bahl, "Non-reciprocal Brillouin scattering induced transparency," *Nat. Phys.*, vol. 11, pp. 275–280, Mar. 2015.

[20] C.-H. Dong, Z. Shen, C.-L. Zou, Y.-L. Zhang, W. Fu, and G.-C. Guo, "Brillouin-scattering-induced transparency and non-reciprocal light storage," *Nat. Commun.*, vol. 6, Feb. 2015.

[21] F. Marquardt, A. A. Clerk, and S. M. Girvin, "Quantum theory of optomechanical cooling," *J. Mod. Opt.*, vol. 55, no. 19-20, pp. 3329–3338, 2008.

[22] Y.-S. Park and H. Wang, "Resolved-sideband and cryogenic cooling of an optomechanical resonator," *Nat. Phys.*, vol. 5, no. 7, pp. 489–493, 2009.

[23] G. Bahl, M. Tomes, F. Marquardt, and T. Carmon, "Observation of spontaneous Brillouin cooling," *Nat. Phys.*, vol. 8, pp. 203–207, Mar. 2012.

[24] G. Bahl, J. Zehnpfennig, M. Tomes, and T. Carmon, "Stimulated optomechanical excitation of surface acoustic waves in a microdevice," *Nat. Commun.*, vol. 2, pp. 403–406, 2011.

[25] Y. Liu, H. Miao, V. Aksyuk, and K. Srinivasan, "Wide cantilever stiffness range cavity optomechanical sensors for atomic force microscopy," *Opt. Express*, vol. 20, pp. 18268–18280, Jul 2012.

[26] R. W. Andrews, A. P. Reed, K. Cicak, J. D. Teufel, and K. W. Lehnert, "Quantum-enabled temporal and spectral mode conversion of microwave signals," *Nat. Commun.*, vol. 6, 11 2015.

[27] J. Bochmann, A. Vainsencher, D. D. Awschalom, and A. N. Cleland, "Nanomechanical coupling between microwave and optical photons," *Nat. Phys.*, vol. 9, pp. 712–716, 11 2013.

Acknowledgements

Funding for this research was provided through the Air Force Office for Scientific Research (AFOSR) Young Investigator program and DARPA MTO.

Author contributions

SK, JMT and GB conceived and designed the experiments. SK developed the experimental setup and carried out the experiments. XX and JMT developed the theoretical analysis. All authors jointly analyzed the data and co-wrote the paper. JMT and GB supervised all aspects of this project.

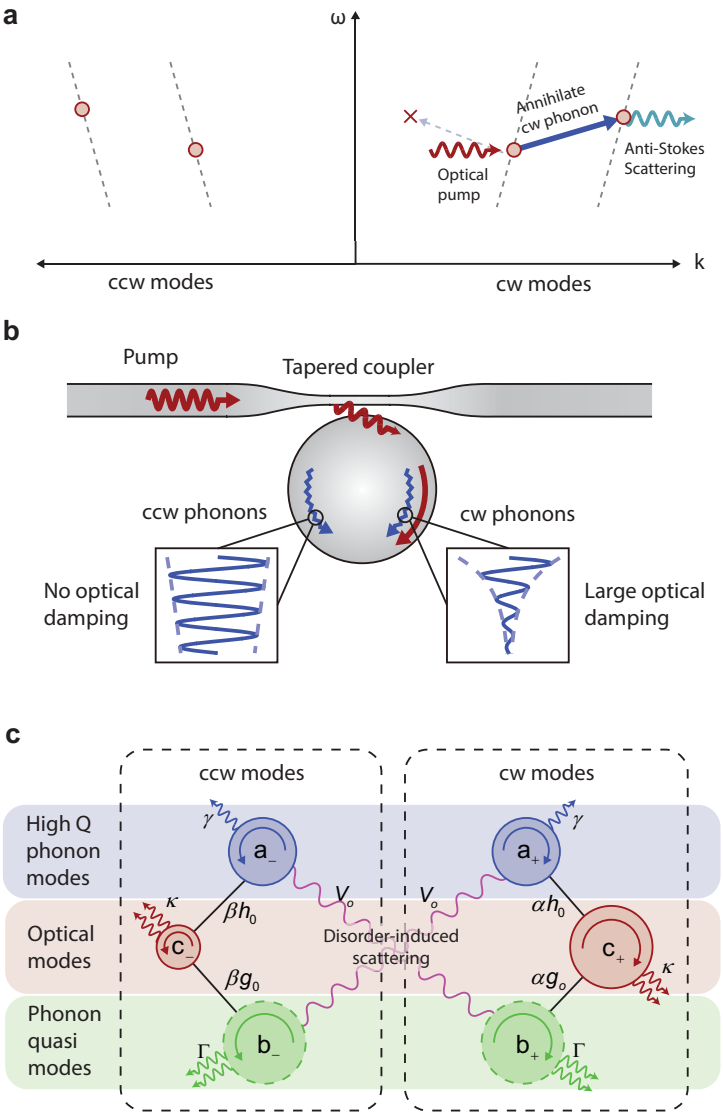

Figure 1: Chiral cooling and modal coupling relationships in a whispering gallery resonator. **(a)** Configuration of the two requisite optical modes (with cw and ccw degeneracy) is illustrated in (ω, k) space. Anti-Stokes Brillouin scattering from cw pumping of the lower mode annihilates only cw phonons due to the strict phase-matching requirement, while ccw phonons remain nominally unaffected. **(b)** Directional optical interface to the resonator modes is achieved via tapered optical fiber. Unidirectional optical pumping results in dramatic chiral damping of the phonons. **(c)** Model for coupling between the anti-Stokes (higher frequency) optical modes $c_\pm$, high-Q phonon modes $a_\pm$, and phonon quasi-modes $b_\pm$ in cw and ccw directions. Light couples to the $a_\pm$ and $b_\pm$ phonons with different optomechanical interaction strength, while disorder-induced scattering between phonons occurs with strength V_0. Details on individual parameters are provided in the text.

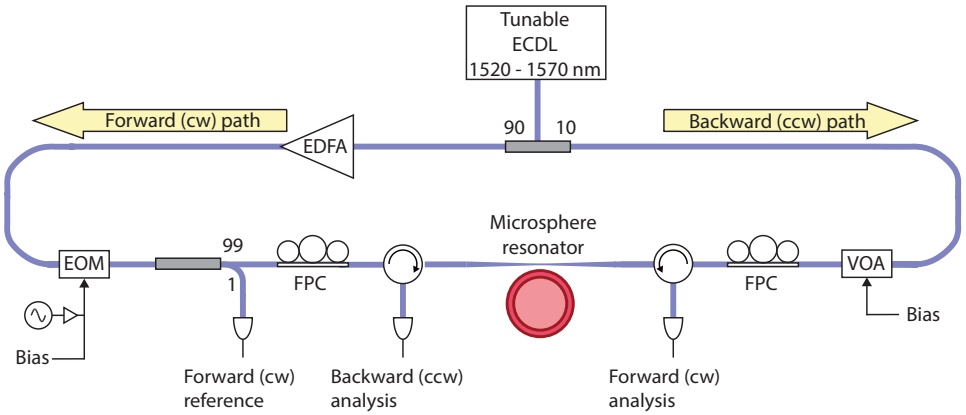

Figure 2: Experimental setup for optomechanical refrigeration of a chiral bath. We perform the experiment using a silica whispering-gallery microsphere resonator that is interfaced via tapered optical fiber. A 1520 nm to 1570 nm tunable external cavity diode laser (ECDL) generates the cw pump and ccw probe sources. An Erbium-doped fiber amplifier (EDFA) controls the cw pump power, for both optomechanical cooling [23] and for monitoring the cw phonon spectrum. An electro optic modulator (EOM) is employed when needed, for measuring the detuning of anti-Stokes scattered light from its optical mode through an induced transparency measurement [19]. A variable optical attenuator (VOA) is used to control the ccw probe, which monitors the ccw phonon spectrum. Fiber polarization controllers (FPC) are used to optimize coupling between the fiber and resonator in both directions.

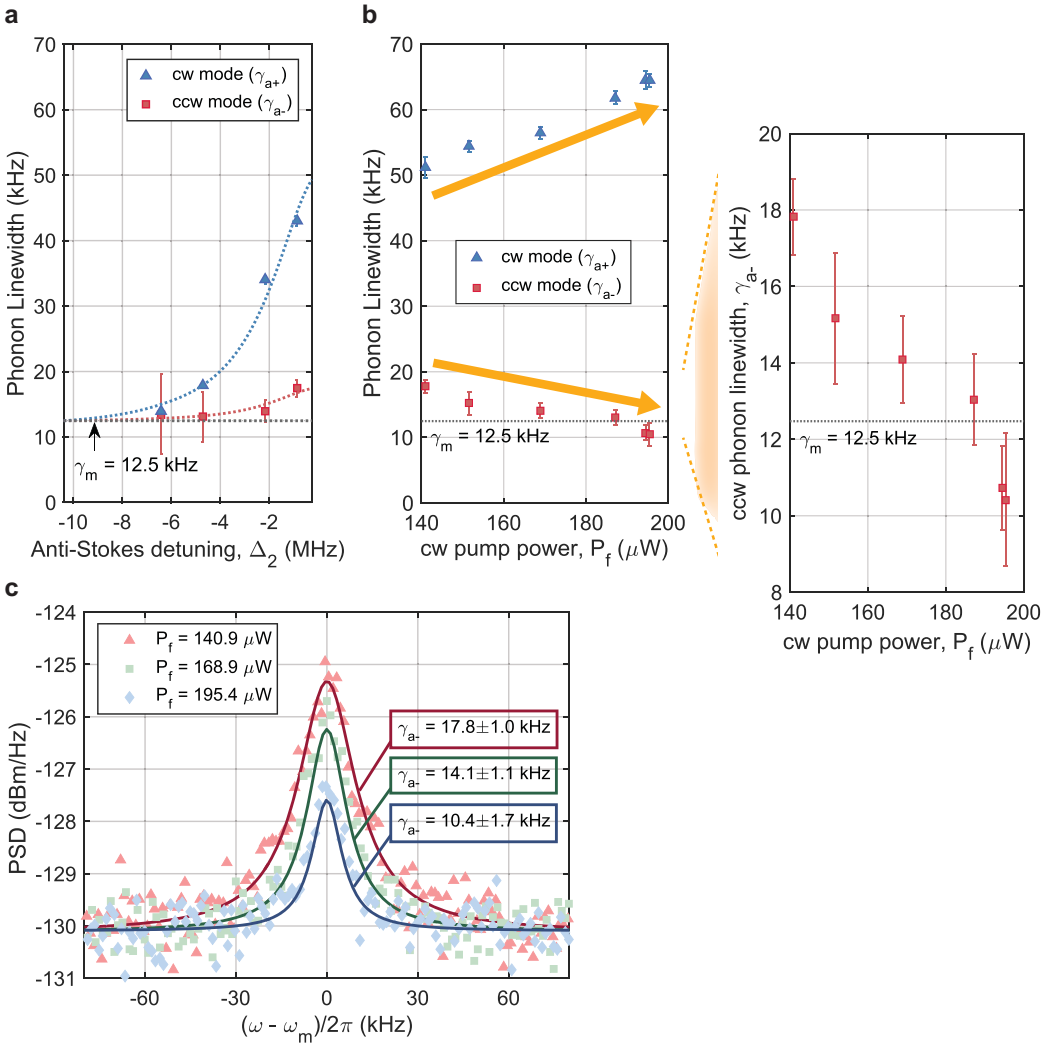

Figure 3: Optically inducing phonon chirality in a silica whispering gallery resonator. **(a)** Experimental estimation of intrinsic phonon linewidth γ_m and observation of chiral asymmetry in dissipation of phonons. **(b)** Observation of increasing coherence of ccw propagating phonons during optomechanical cooling of the cw propagating phonons. The phonon linewidth γ_{a-} is seen to drop below the previously known 'lower-limit' of γ_m, indicating a reduction in the disorder induced dissipation. **(c)** Verification of gain-free spectral narrowing (γ_{a-}) and cooling by reduction of heat load (reduction in spectrum area) of the ccw phonons when the cw pump power is increased in the experiment of subfigure (b). Error bars correspond to 95 % confidence interval.

Bibliography

[1] Johannes Kepler. *De Cometis Libelli Tres*. 1619.

[2] James Clerk Maxwell. *A treatise on electricity and magnetism Vol I, Vol II*. Oxford : Clarendon Press, 1873.

[3] Peter Lebedew. Untersuchungen ber die druckkrfte des lichtes. *Annalen der Physik*, 311(11):433–458, 1901.

[4] Carlton M. Caves, Kip S. Thorne, Ronald W. P. Drever, Vernon D. Sandberg, and Mark Zimmermann. On the measurement of a weak classical force coupled to a quantum-mechanical oscillator. i. issues of principle. *Rev. Mod. Phys.*, 52:341–392, Apr 1980.

[5] V.B. Braginsky, S.E. Strigin, and S.P. Vyatchanin. Parametric oscillatory instability in fabryperot interferometer. *Physics Letters A*, 287(56):331 – 338, 2001.

[6] V.B. Braginsky, S.E. Strigin, and S.P. Vyatchanin. Analysis of parametric oscillatory instability in power recycled {LIGO} interferometer. *Physics Letters A*, 305(34):111 – 124, 2002.

[7] T. J. Kippenberg, H. Rokhsari, T. Carmon, A. Scherer, and K. J. Vahala. Analysis of radiation-pressure induced mechanical oscillation of an optical microcavity. *Phys. Rev. Lett.*, 95:033901, Jul 2005.

[8] B P Abbott et al. Ligo: the laser interferometer gravitational-wave observatory. *Reports on Progress in Physics*, 72(7):076901, 2009.

[9] Stefano Mancini, David Vitali, and Paolo Tombesi. Optomechanical cooling of a macroscopic oscillator by homodyne feedback. *Phys. Rev. Lett.*, 80:688–691, Jan 1998.

[10] O. Arcizet, P.F Cohadon, T. Briant, M. Pinard, and A. Heidmann. Radiation-pressure cooling and optomechanical instability of a micromirror. *Nature*, 444:71, 2006.

[11] Florian Marquardt, Joe P. Chen, A. A. Clerk, and S. M. Girvin. Quantum theory of cavity-assisted sideband cooling of mechanical motion. *Phys. Rev. Lett.*, 99:093902, Aug 2007.

[12] T. A. Palomaki, J. D. Teufel, R. W. Simmonds, and K. W. Lehnert. Entangling mechanical motion with microwave fields. *Science*, 342(6159):710–713, 2013.

[13] A. D. O'Connell, M. Hofheinz, M. Ansmann, Radoslaw C. Bialczak, M. Lenander, Erik Lucero, M. Neeley, D. Sank, H. Wang, M. Weides, J. Wenner, John M. Martinis, and A. N. Cleland. Quantum ground state and single-phonon control of a mechanical resonator. *Nature*, 464(7289):697–703, 04 2010.

[14] T. A. Palomaki, J. W. Harlow, J. D. Teufel, R. W. Simmonds, and K. W. Lehnert. Coherent state transfer between itinerant microwave fields and a mechanical oscillator. *Nature*, 495(7440):210–214, 03 2013.

[15] William D. Phillips. Nobel lecture: Laser cooling and trapping of neutral atoms. *Rev. Mod. Phys.*, 70:721–741, Jul 1998.

[16] M. H. Anderson, J. R. Ensher, M. R. Matthews, C. E. Wieman, and E. A. Cornell. Observation of bose-einstein condensation in a dilute atomic vapor. *Science*, 269(5221):198–201, 1995.

[17] K. B. Davis, M. O. Mewes, M. R. Andrews, N. J. van Druten, D. S. Durfee, D. M. Kurn, and W. Ketterle. Bose-einstein condensation in a gas of sodium atoms. *Phys. Rev. Lett.*, 75:3969–3973, Nov 1995.

[18] D. Leibfried, R. Blatt, C. Monroe, and D. Wineland. Quantum dynamics of single trapped ions. *Rev. Mod. Phys.*, 75:281–324, Mar 2003.

[19] Herbert Walther, Benjamin T H Varcoe, Berthold-Georg Englert, and Thomas Becker. Cavity quantum electrodynamics. *Reports on Progress in Physics*, 69(5):1325, 2006.

[20] Alexandre Blais, Ren-Shou Huang, Andreas Wallraff, S. M. Girvin, and R. J. Schoelkopf. Cavity quantum electrodynamics for superconducting electrical circuits: An architecture for quantum computation. *Phys. Rev. A*, 69:062320, Jun 2004.

[21] T. J. Kippenberg and K. J. Vahala. *Science*, 321:1172, 2008.

[22] Florian Marquardt and Steve M. Girvin. *Physics*, 2:40, 2009.

[23] G. J. Milburn and M. J. Woolley. An Introduction to Quantum Optomechanics. *acta physica slovaca*, 61(5):483–601, 2011.

[24] Markus Aspelmeyer, Tobias J. Kippenberg, and Florian Marquardt. Cavity optomechanics. *Rev. Mod. Phys.*, 86:1391–1452, Dec 2014.

[25] I. Wilson-Rae, N. Nooshi, W. Zwerger, and T. J. Kippenberg. Theory of ground state cooling of a mechanical oscillator using dynamical backaction. *Phys. Rev. Lett.*, 99:093901, Aug 2007.

[26] J D Teufel, Dale Li, M S Allman, K Cicak, A J Sirois, J D Whittaker, and R W Simmonds. Circuit cavity electromechanics in the strong-coupling regime. *Nature*, 471(7337):204–8, March 2011.

[27] Jasper Chan, T P Mayer Alegre, Amir H Safavi-Naeini, Jeff T Hill, Alex Krause, Simon Gröblacher, Markus Aspelmeyer, and Oskar Painter. Laser cooling of a nanomechanical oscillator into its quantum ground state. *Nature*, 478(7367):89–92, October 2011.

[28] Daniel W. C. Brooks, Thierry Botter, Sydney Schreppler, Thomas P. Purdy, Nathan Brahms, and Dan M. Stamper-Kurn. Non-classical light generated by quantum-noise-driven cavity optomechanics. *Nature*, 488(7412):476–480, 08 2012.

[29] Amir H. Safavi-Naeini, Simon Groblacher, Jeff T. Hill, Jasper Chan, Markus Aspelmeyer, and Oskar Painter. Squeezed light from a silicon micromechanical resonator. *Nature*, 500(7461):185–189, 08 2013.

[30] T. P. Purdy, P.-L. Yu, R. W. Peterson, N. S. Kampel, and C. A. Regal. Strong optomechanical squeezing of light. *Phys. Rev. X*, 3:031012, Sep 2013.

[31] A. Nunnenkamp, K. Børkje, and S. M. Girvin. Single-photon optomechanics. *Phys. Rev. Lett.*, 107:063602, Aug 2011.

[32] P. Rabl. Photon blockade effect in optomechanical systems. *Phys. Rev. Lett.*, 107:063601, Aug 2011.

[33] Andreas Kronwald and Florian Marquardt. Optomechanically induced transparency in the nonlinear quantum regime. *Phys. Rev. Lett.*, 111:133601, Sep 2013.

[34] Marc-Antoine Lemonde, Nicolas Didier, and Aashish A. Clerk. Nonlinear interaction effects in a strongly driven optomechanical cavity. *Phys. Rev. Lett.*, 111:053602, Aug 2013.

[35] K. Børkje, A. Nunnenkamp, J. D. Teufel, and S. M. Girvin. Signatures of nonlinear cavity optomechanics in the weak coupling regime. *Phys. Rev. Lett.*, 111:053603, Aug 2013.

[36] Xunnong Xu, Michael Gullans, and Jacob M. Taylor. Quantum nonlinear optics near optomechanical instabilities. *Phys. Rev. A*, 91:013818, Jan 2015.

[37] A. Schliesser, P. Del'Haye, N. Nooshi, K. J. Vahala, and T. J. Kippenberg. Radiation pressure cooling of a micromechanical oscillator using dynamical backaction. *Phys. Rev. Lett.*, 97:243905, Dec 2006.

[38] T. P. Purdy, K. E. Grutter, K. Srinivasan, and J. M. Taylor. e-print arXiv:1605.05664, 2016.

[39] Marlan O. Scully and M. Suhail Zubairy. *Quantum Optics*. Cambridge University Press, 1997.

[40] C. W. Gardiner and P. Zoller. *Quantum Noise*. Springer, Berlin, third edition, 2004.

[41] D.F. Walls and Gerard J. Milburn. *Quantum Optics*. Springer, second edition, 2008.

[42] C. K. Law. Effective hamiltonian for the radiation in a cavity with a moving mirror and a time-varying dielectric medium. *Phys. Rev. A*, 49:433–437, Jan 1994.

[43] A. O. Caldeira and A. J. Leggett. Influence of dissipation on quantum tunneling in macroscopic systems. *Phys. Rev. Lett.*, 46:211–214, Jan 1981.

[44] Albert Einstein. *Investigations of the Theory of Brownian Movement*. Dover Publications, 1956.

[45] R. Kubo. *Rep. Prog. Phys.*, 29:255, 1966.

[46] V. F. Weisskopf and E. P. Wigner. *Z. Phys.*, 63:54, 1930.

[47] Benjamin S. Sheard, Malcolm B. Gray, Conor M. Mow-Lowry, David E. McClelland, and Stanley E. Whitcomb. Observation and characterization of an optical spring. *Phys. Rev. A*, 69:051801, May 2004.

[48] Thomas Corbitt, Yanbei Chen, Edith Innerhofer, Helge Müller-Ebhardt, David Ottaway, Henning Rehbein, Daniel Sigg, Stanley Whitcomb, Christopher Wipf, and Nergis Mavalvala. An all-optical trap for a gram-scale mirror. *Phys. Rev. Lett.*, 98:150802, Apr 2007.

[49] Valdimir B. Braginsky and Farid Ya. Khalili. *Quantum Measurement*. Cambridge University Press, 1992.

[50] Robert W. Boyd. Academic Press, Burlington, third edition edition, 2008.

[51] Markus Aspelmeyer, Pierre Meystre, and Keith Schwab. Quantum optomechanics. *Physics Today*, 65(7):29, 2012.

[52] G. Krishnan, C. U. Kshirsagar, G. K. Ananthasuresh, and N. Bhat. Reviews micromachined high-resolution accelerometers. *J. Indian Inst. Sci.*, 87:333, 2008.

[53] G. Binnig, C. F. Quate, and Ch. Gerber. Atomic force microscope. *Phys. Rev. Lett.*, 56:930–933, Mar 1986.

[54] A. A. Clerk, M. H. Devoret, S. M. Girvin, Florian Marquardt, and R. J. Schoelkopf. Introduction to quantum noise, measurement, and amplification. *Rev. Mod. Phys.*, 82:1155–1208, Apr 2010.

[55] A. Schliesser, R. Rivière, G. Anetsberger, O. Arcizet, and T. J. Kippenberg. Resolved-sideband cooling of a micromechanical oscillator. *Nature Physics*, 4:415, 2008.

[56] Mahmood Bagheri, Menno Poot, Mo Li, Wolfram P. H. Pernice, and Hong X. Tang. Dynamic manipulation of nanomechanical resonators in the high-amplitude regime and non-volatile mechanical memory operation. *Nat. Nano.*, 6:726, 2011.

[57] Min Xiao, Ling-An Wu, and H. J. Kimble. Precision measurement beyond the shot-noise limit. *Phys. Rev. Lett.*, 59:278–281, Jul 1987.

[58] Kip S. Thorne, Ronald W. P. Drever, Carlton M. Caves, Mark Zimmermann, and Vernon D. Sandberg. Quantum nondemolition measurements of harmonic oscillators. *Phys. Rev. Lett.*, 40:667–671, Mar 1978.

[59] a a Clerk, F Marquardt, and K Jacobs. Back-action evasion and squeezing of a mechanical resonator using a cavity detector. *New Journal of Physics*, 10(9):095010, September 2008.

[60] O. Arcizet, T. Briant, A. Heidmann, and M. Pinard. Beating quantum limits in an optomechanical sensor by cavity detuning. *Phys. Rev. A*, 73:033819, Mar 2006.

[61] J. D. Thompson, B. M. Zwickl, A. M. Jayich, Florian Marquardt, S. M. Girvin, and J. G. E. Harris. *Nature*, 452:72, 2008.

[62] A M Jayich, J C Sankey, B M Zwickl, C Yang, J D Thompson, S M Girvin, A A Clerk, F Marquardt, and J G E Harris. Dispersive optomechanics: a membrane inside a cavity. *New Journal of Physics*, 10(9):095008, 2008.

[63] Florian Marquardt. Quantum optomechanics. Les Houches Lecture Notes 2011, School on "Quantum Machines", 2011.

[64] G. S. Agarwal. *Phys. Rev. Lett.*, 53:1732, 1984.

[65] R. J. Thompson, G. Rempe, and H. J. Kimble. *Phys. Rev. Lett.*, 68:1132, 1992.

[66] M. Bhattacharya, H. Uys, and P. Meystre. *Phys. Rev. A*, 77:033819, 2008.

[67] Edmund X. DeJesus and Charles Kaufman. *Phys. Rev. A*, 35:5288, 1987.

[68] C. Genes, D. Vitali, P. Tombesi, S. Gigan, and M. Aspelmeyer. Ground-state cooling of a micromechanical oscillator: Comparing cold damping and cavity-assisted cooling schemes. *Phys. Rev. A*, 77:033804, Mar 2008.

[69] Alan Jeffrey and Daniel Zwillinger. *Table of Integrals, Series and Products*. Academic Press, sixth edition, 2000.

[70] K. Børkje and S. M. Girvin. Quantum optomechanics with a high-frequency dilational mode in thin dielectric membranes. *New Journal of Physics*, 14(8):085016, 2012.

[71] Rachele Fermani, Stefano Mancini, and Paolo Tombesi. Quantum limited force measurement in a cavityless optomechanical system. *Phys. Rev. A*, 70(4):045801, October 2004.

[72] Utku Kemiktarak, Mathieu Durand, Michael Metcalfe, and John Lawall. Cavity optomechanics with sub-wavelength grating mirrors. *New Journal of Physics*, 14(12):125010, 2012.

[73] M. J. Collett and C. W. Gardiner. Squeezing of intracavity and traveling-wave light fields produced in parametric amplification. *Phys. Rev. A*, 30(3):1386–1391, 1984.

[74] K. Stannigel, P. Rabl, A. S. Sørensen, M. D. Lukin, and P. Zoller. Optomechanical transducers for quantum-information processing. *Phys. Rev. A*, 84:042341, Oct 2011.

[75] G. J. Milburn. Quantum optical fredkin gate. *Phys. Rev. Lett.*, 62:2124–2127, May 1989.

[76] Q. A. Turchette, C. J. Hood, W. Lange, H. Mabuchi, and H. J. Kimble. Measurement of conditional phase shifts for quantum logic. *Phys. Rev. Lett.*, 75:4710–4713, Dec 1995.

[77] H. John Caulfield and Shlomi Dolev. Why future supercomputing requires optics. *Nature Photon.*, 4(5):261–263, May 2010.

[78] Jeremy L. O'Brien, Akira Furusawa, and Jelena Vučković. Photonic quantum technologies. *Nature Photon.*, 3(12):687–695, December 2009.

[79] K M Birnbaum, A Boca, R Miller, A D Boozer, T E Northup, and H J Kimble. Photon blockade in an optical cavity with one trapped atom. *Nature*, 436(7047):87–90, July 2005.

[80] David Press, Stephan Götzinger, Stephan Reitzenstein, Carolin Hofmann, Andreas Löffler, Martin Kamp, Alfred Forchel, and Yoshihisa Yamamoto. Photon antibunching from a single quantum-dot-microcavity system in the strong coupling regime. *Phys. Rev. Lett.*, 98:117402, Mar 2007.

[81] Lev S Bishop, J. M. Chow, Jens Koch, A. A. Houck, M. H. Devoret, E. Thuneberg, S. M. Girvin, and R. J. Schoelkopf. *Nature Phys.*, 5:105, 2009.

[82] Thomas Volz, Andreas Reinhard, Martin Winger, Antonio Badolato, Kevin J Hennessy, and Evelyn L Hu. Ultrafast all-optical switching by single photons. *Nature Photon.*, 6(September):605–609, 2012.

[83] Ranojoy Bose, Deepak Sridharan, Hyochul Kim, Glenn S. Solomon, and Edo Waks. Low-photon-number optical switching with a single quantum dot coupled to a photonic crystal cavity. *Phys. Rev. Lett.*, 108:227402, May 2012.

[84] Wenlan Chen, Kristin M Beck, Robert Bücker, Michael Gullans, Mikhail D Lukin, Haruka Tanji-Suzuki, and Vladan Vuletić. All-optical switch and transistor gated by one stored photon. *Science*, 341(6147):768–70, August 2013.

[85] Andreas Reiserer, Norbert Kalb, Gerhard Rempe, and Stephan Ritter. A quantum gate between a flying optical photon and a single trapped atom. *Nature*, 508(7495):237–240, April 2014.

[86] T G Tiecke, J D Thompson, N P de Leon, L R Liu, V Vuletic, and M D Lukin. Nanophotonic quantum phase switch with a single atom. *Nature*, 508(7495):241–244, April 2014.

[87] A. Imamoglu, H. Schmidt, G. Woods, and M. Deutsch. Strongly interacting photons in a nonlinear cavity. *Phys. Rev. Lett.*, 79:1467–1470, Aug 1997.

[88] M. D. Lukin and A. Imamoglu. Nonlinear optics and quantum entanglement of ultraslow single photons. *Phys. Rev. Lett.*, 84:1419–1422, Feb 2000.

[89] Chi-Ching Lin, Meng-Chang Wu, Bor-Wen Shiau, Yi-Hsin Chen, Ite A. Yu, Yong-Fan Chen, and Ying-Cheng Chen. Enhanced all-optical switching with double slow light pulses. *Phys. Rev. A*, 86:063836, Dec 2012.

[90] J Hwang, M Pototschnig, R Lettow, G Zumofen, A Renn, S Götzinger, and V Sandoghdar. A single-molecule optical transistor. *Nature*, 460(7251):76–80, July 2009.

[91] Thibault Peyronel, Ofer Firstenberg, Qi-Yu Liang, Sebastian Hofferberth, Alexey V Gorshkov, Thomas Pohl, Mikhail D Lukin, and Vladan Vuletić. Quantum nonlinear optics with single photons enabled by strongly interacting atoms. *Nature*, 488(7409):57–60, August 2012.

[92] Y O Dudin and A Kuzmich. Strongly interacting Rydberg excitations of a cold atomic gas. *Science*, 336(6083):887–9, May 2012.

[93] H. Gorniaczyk, C. Tresp, J. Schmidt, H. Fedder, and S. Hofferberth. Single-photon transistor mediated by interstate rydberg interactions. *Phys. Rev. Lett.*, 113:053601, Jul 2014.

[94] Daniel Tiarks, Simon Baur, Katharina Schneider, Stephan Dürr, and Gerhard Rempe. Single-photon transistor using a förster resonance. *Phys. Rev. Lett.*, 113:053602, Jul 2014.

[95] Darrick E. Chang, Anders S. Sørensen, Eugene A. Demler, and Mikhail D. Lukin. A single-photon transistor using nanoscale surface plasmons. *Nature Phys.*, 3(11):807–812, August 2007.

[96] M. Gullans, D. E. Chang, F. H. L. Koppens, F. J. García de Abajo, and M. D. Lukin. Single-photon nonlinear optics with graphene plasmons. *Phys. Rev. Lett.*, 111:247401, Dec 2013.

[97] M. Bajcsy, S. Hofferberth, V. Balic, T. Peyronel, M. Hafezi, A. S. Zibrov, V. Vuletic, and M. D. Lukin. Efficient all-optical switching using slow light within a hollow fiber. *Phys. Rev. Lett.*, 102:203902, May 2009.

[98] Vivek Venkataraman, Kasturi Saha, Pablo Londero, and Alexander L. Gaeta. Few-photon all-optical modulation in a photonic band-gap fiber. *Phys. Rev. Lett.*, 107:193902, Nov 2011.

[99] Pavel Kolchin, Rupert F. Oulton, and Xiang Zhang. Nonlinear quantum optics in a waveguide: Distinct single photons strongly interacting at the single atom level. *Phys. Rev. Lett.*, 106:113601, Mar 2011.

[100] Danny O'Shea, Christian Junge, Jürgen Volz, and Arno Rauschenbeutel. Fiber-optical switch controlled by a single atom. *Phys. Rev. Lett.*, 111:193601, Nov 2013.

[101] J D Thompson, B M Zwickl, A M Jayich, Florian Marquardt, S M Girvin, and J G E Harris. Strong dispersive coupling of a high-finesse cavity to a micromechanical membrane. *Nature*, 452(7183):72–75, March 2008.

[102] E. Verhagen, S. Delglise, S. Weis, A. Schliesser, and T. J. Kippenberg. Quantum-coherent coupling of a mechanical oscillator to an optical cavity mode. *Nature*, 482(7383):63–7, February 2012.

[103] Simon Gröblacher, Klemens Hammerer, Michael R Vanner, and Markus Aspelmeyer. Observation of strong coupling between a micromechanical resonator and an optical cavity field. *Nature*, 460(7256):724–7, August 2009.

[104] Jiang Qian, A. A. Clerk, K. Hammerer, and Florian Marquardt. Quantum signatures of the optomechanical instability. *Phys. Rev. Lett.*, 109:253601, Dec 2012.

[105] P. Kómár, S. D. Bennett, K. Stannigel, S. J. M. Habraken, P. Rabl, P. Zoller, and M. D. Lukin. Single-photon nonlinearities in two-mode optomechanics. *Phys. Rev. A*, 87:013839, Jan 2013.

[106] Xin-You Lu, Wei-Min Zhang, Sahel Ashhab, Ying Wu, and Franco Nori. *Sci. Rep.*, 3:2943, 2013.

[107] Xunnong Xu and Jacob M. Taylor. Squeezing in a coupled two-mode optomechanical system for force sensing below the standard quantum limit. *Phys. Rev. A*, 90:043848, Oct 2014.

[108] Jasper Chan, Matt Eichenfield, Ryan Camacho, and Oskar Painter. Optical and mechanical design of a "zipper" photonic crystaloptomechanical cavity. *Opt. Express*, 17(5):3802–3817, Mar 2009.

[109] Jasper Chan, Amir H. Safavi-Naeini, Jeff T. Hill, Sen Meenehan, and Oskar Painter. Optimized optomechanical crystal cavity with acoustic radiation shield. *Applied Physics Letters*, 101(8):–, 2012.

[110] J. Gomis-Bresco, D. Navarro-Urrios, M. Oudich, S. El-Jallal, A. Griol, D. Puerto, E. Chavez, Y. Pennec, B. Djafari-Rouhani, F. Alzina, A. Martnez, and C.M. Sotomayor Torres. A one-dimensional optomechanical crystal with a complete phononic band gap. *Nat Commun*, 5:4452, Jul 2014.

[111] Amir H. Safavi-Naeini, Jeff T. Hill, Seán Meenehan, Jasper Chan, Simon Gröblacher, and Oskar Painter. Two-dimensional phononic-photonic band gap optomechanical crystal cavity. *Phys. Rev. Lett.*, 112:153603, Apr 2014.

[112] Hiroshi Sekoguchi, Yasushi Takahashi, Takashi Asano, and Susumu Noda. Photonic crystal nanocavity with a q-factor of 9 million. *Opt. Express*, 22(1):916–924, Jan 2014.

[113] T. P. Purdy, P.-L. Yu, R. W. Peterson, N. S. Kampel, and C. A. Regal. Strong optomechanical squeezing of light. *Phys. Rev. X*, 3:031012, Sep 2013.

[114] Amir H. Safavi-Naeini, Simon Groblacher, Jeff T. Hill, Jasper Chan, Markus Aspelmeyer, and Oskar Painter. Squeezed light from a silicon micromechanical resonator. *Nature*, 500(7461):185–189, 08 2013.

[115] P.-L. Yu, K. Cicak, N. S. Kampel, Y. Tsaturyan, T. P. Purdy, R. W. Simmonds, and C. A. Regal. A phononic bandgap shield for high-q membrane microresonators. *Applied Physics Letters*, 104(2), 2014.

[116] Jasper Chan, Matt Eichenfield, Ryan Camacho, and Oskar Painter. Optical and mechanical design of a "zipper" photonic crystal optomechanical cavity. *Opt. Express*, 17(5):3802–3817, Mar 2009.

[117] Surabhi Joshi, Sherman Hung, and Srikar Vengallatore. Design strategies for controlling damping in micromechanical and nanomechanical resonators. *EPJ Techniques and Instrumentation*, 1(1):1–14, 2014.

[118] K. Y. Yasumura, T. D. Stowe, E. M. Chow, T. Pfafman, T. W. Kenny, B. C. Stipe, and D. Rugar. Quality factors in micron- and submicron-thick cantilevers. *Journal of Microelectromechanical Systems*, 9(1):117–125, March 2000.

[119] Zhili Hao, Ahmet Erbil, and Farrokh Ayazi. An analytical model for support loss in micromachined beam resonators with in-plane flexural vibrations. *Sensors and Actuators A: Physical*, 109(1?2):156 – 164, 2003.

[120] S. A. Chandorkar, M. Agarwal, R. Melamud, R. N. Candler, K. E. Goodson, and T. W. Kenny. Limits of quality factor in bulk-mode micromechanical resonators. In *Micro Electro Mechanical Systems, 2008. MEMS 2008. IEEE 21st International Conference on Micro Electro Mechanical Systems*, pages 74–77, Jan 2008.

[121] Jin Hwan Ko, Joonho Jeong, Jinbok Choi, and Maenghyo Cho. Quality factor in clamping loss of nanocantilever resonators. *Applied Physics Letters*, 98(17), 2011.

[122] Clarence Zener. Internal friction in solids ii. general theory of thermoelastic internal friction. *Phys. Rev.*, 53:90–99, Jan 1938.

[123] V. T. Srikar and S. D. Senturia. Thermoelastic damping in fine-grained polysilicon flexural beam resonators. *Journal of Microelectromechanical Systems*, 11(5):499–504, Oct 2002.

[124] Ron Lifshitz and M. L. Roukes. Thermoelastic damping in micro- and nanomechanical systems. *Phys. Rev. B*, 61:5600–5609, Feb 2000.

[125] Ivan S. Grudinin, Andrey B. Matsko, and Lute Maleki. Brillouin lasing with a caf_2 whispering gallery mode resonator. *Phys. Rev. Lett.*, 102:043902, Jan 2009.

[126] Ivan S. Grudinin, Hansuek Lee, O. Painter, and Kerry J. Vahala. Phonon laser action in a tunable two-level system. *Phys. Rev. Lett.*, 104:083901, Feb 2010.

[127] Gaurav Bahl, Kyu Hyun Kim, Wonsuk Lee, Jing Liu, Xudong Fan, and Tal Carmon. Brillouin cavity optomechanics with microfluidic devices. *Nat Commun*, 4, 06 2013.

[128] Gaurav Bahl, Matthew Tomes, Florian Marquardt, and Tal Carmon. Observation of spontaneous brillouin cooling. *Nat Phys*, 8(3):203–207, 03 2012.

[129] Hannes Pichler, Tomás Ramos, Andrew J. Daley, and Peter Zoller. Quantum optics of chiral spin networks. *Phys. Rev. A*, 91:042116, Apr 2015.

[130] Tomás Ramos, Benoît Vermersch, Philipp Hauke, Hannes Pichler, and Peter Zoller. Non-markovian dynamics in chiral quantum networks with spins and photons. *Phys. Rev. A*, 93:062104, Jun 2016.

[131] Benot Vermersch, Toms Ramos, Philipp Hauke, and Peter Zoller. e-print arXiv:1603.09097, 2016.

[132] Jasper Chan, Amir H. Safavi-Naeini, Jeff T. Hill, Sen Meenehan, and Oskar Painter. Optimized optomechanical crystal cavity with acoustic radiation shield. *Applied Physics Letters*, 101(8), 2012.

[133] Supriyo Datta. *Electronic Transport in Mesoscopic Systems*. Cambridge University Press, 1997.

[134] Ulrich Weiss. *Quantum Dissipative Systems*. Word Scientific, 4th edition, 2012.

[135] Sasikanth Manipatruni, Jacob T. Robinson, and Michal Lipson. Optical nonreciprocity in optomechanical structures. *Phys. Rev. Lett.*, 102:213903, May 2009.

[136] Mohammad Hafezi and Peter Rabl. Optomechanically induced non-reciprocity in microring resonators. *Opt. Express*, 20(7):7672–7684, Mar 2012.

[137] Chun-Hua Dong, Zhen Shen, Chang-Ling Zou, Yan-Lei Zhang, Wei Fu, and Guang-Can Guo. Brillouin-scattering-induced transparency and non-reciprocal light storage. *Nat Commun*, 6, 02 2015.

[138] JunHwan Kim, Mark C. Kuzyk, Kewen Han, Hailin Wang, and Gaurav Bahl. Non-reciprocal brillouin scattering induced transparency. *Nat Phys*, 11(3):275–280, 03 2015.

[139] Zhen Shen, Yan-Lei Zhang, Yuan Chen, Chang-Ling Zou, Yun-Feng Xiao, Xu-Bo Zou, Fang-Wen Sun, Guang-Can Guo, and Chun-Hua Dong. Experimental realization of optomechanically induced non-reciprocity. *Nat Photon*, advance online publication:–, 08 2016.

[140] Pieter Kok, W. J. Munro, Kae Nemoto, T. C. Ralph, Jonathan P. Dowling, and G. J. Milburn. Linear optical quantum computing with photonic qubits. *Rev. Mod. Phys.*, 79:135–174, Jan 2007.

[141] Jeremy L. O'Brien. Optical quantum computing. *Science*, 318(5856):1567–1570, 2007.

[142] M. Hafezi, S. Mittal, J. Fan, A. Migdall, and J. M. Taylor. Imaging topological edge states in silicon photonics. *Nat Photon*, 7(12):1001–1005, 12 2013.

[143] R. G. Smith. Optical power handling capacity of low loss optical fibers as determined by stimulated raman and brillouin scattering. *Appl. Opt.*, 11(11):2489–2494, Nov 1972.

[144] E.P. Ippen and R.H. Stolen. Stimulated brillouin scattering in optical fibers. *Applied Physics Letters*, 21(11):539–541, 1972.

[145] Utku Kemiktarak, Michael Metcalfe, Mathieu Durand, and John Lawall. Mechanically compliant grating reflectors for optomechanics. *Applied Physics Letters*, 100(6), 2012.

[146] Simone De Liberato, Neill Lambert, and Franco Nori. Quantum noise in photothermal cooling. *Physical Review A*, 83(3):033809, March 2011.